5.2. Posters

P01 THE MECHANISM OF ELECTROPHORETIC DEPOSITION OF SILICA LAYERS ON THE IRON SURFACES

ROBERT BÍLEK, PETR PTÁČEK
and JAROMÍR HAVLICA
[a]*Brno University of Technology, Faculty of Chemistry, Institute of Material Chemistry, Purkyňova 118, 621 00 Brno, Czech Republic, bilek-r@fch.vutbr.cz*

Abstract

A series of experiments oriented on deposition of the silica particles on steel surface in water containing medium were carried out. Sodium ions stabilized silica sol was used as a source of colloidal silica particles with diameter in range 9–10 nm. Influence of electrolyte compositions and mechanism of the deposition were investigated. Thick of the silica layer is function of deposition time and applied potential gradient. Migration of silica particles in heterogeneous system may be changed also via changes of their zeta potential.

Introduction

The utilization of some steels is limited in aggressive media, such as corrosive gases or liquids, etc., due to degradation of their material properties[1]. Corrosion resistance of metal may be improved by deposition of silica layer via sol-gel process. Thin film may be easily prepared by dip--coating, but thicker coatings, which are necessary for some applications, cannot be prepared by this simple method. On the other side, the electrophoretic deposition allows producing thicker coatings with enhanced corrosion resistance. The protective character of EPD coatings depends on the electrical conditions during formation of film. High current densities may be lead to corrosion of the metal substrate used as electrode[2].

EPD is combination of two processes: electrophoresis and deposition. Electrophoresis discovered in 1807 by F. S. Reis is motion of solid particles in electric field generated in liquid media. Deposition is based on the coagulation of particles to dense layer[3].

Experimental

The colloidal silica particles were deposited on the surface of carbonless ferrite steel from hydrosol of SiO_2. Commercially produced silica sol Tosil (Koma) with 30 mass % of SiO_2 was used as a source of silica particles with suitable diameter about 10 nm. A series of deposition experiments were carried out for potential gradients 0.19; 0.22; 0.25; 0.28; 0.31; 0.34; 0.37; 0.5 V cm^{-1}. Increasing mass of the deposit during experiment was continuously monitored in time by weighting. Configuration of deposition equipment is schematically illustrated in Fig. 1.

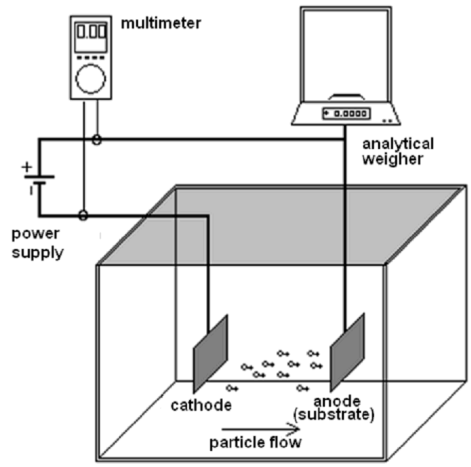

Fig. 1. **Schematic drawing of electrophoretic deposition cell showing the process**

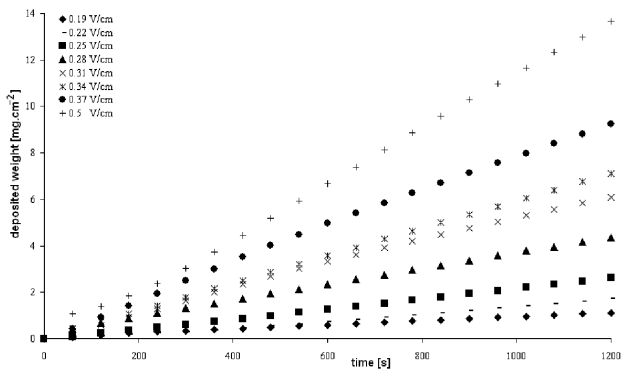

Fig. 2. **EPD kinetics at variable voltage condition**

Results

As may be observe in Fig. 2., growth mass of the silica deposited on the steel substrate is proportional with time. In the same time period, the weight of SiO_2 increases with the gradient of potential. The growth of layer may be described by Eq. 2, which was derived in this work, from general mass flow Eq. 1.

$$J_x = u_x \cdot c \tag{1}$$

$$\frac{1}{S}\frac{\mathrm{d}m}{\mathrm{d}t} = K\left(\frac{E}{L} - B\right) \tag{2}$$

Where J_x is flow of particles with velocity u_x along of x axis and c is concentration of sol. S in Eq. 2 represents area, m weight of deposited SiO_2, t time, E applied potential and L distance between the electrodes, respectively.

The constant K from Eq. 2 was determined by extrapolation (Fig. 3.) of slopes k from equation of lines plotted in Fig. 2. The value of K ($2.93 \cdot 10^{-2}$ g s^{-1} cm^{-1} V^{-1}) corresponds to mass of silica deposited on cm^2 of area at 1 s. The value of B ($1.72 \cdot 10^{-1}$ V cm^{-1}) means potential gradient which is needed to start of particle motion.

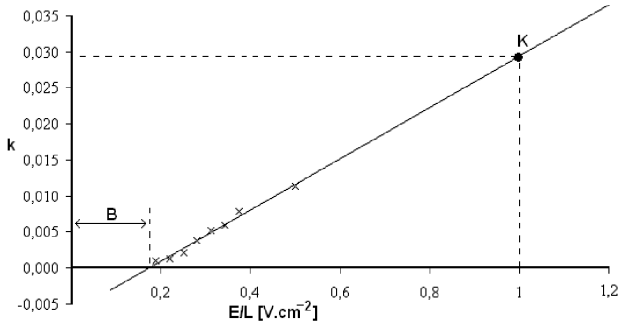

Fig. 3. **Graphic expression of constants K and B from Eq. 2**

Conclusion

Mass of silica deposited on the steel substrate increases with time proportionally. In the same time period, the weight of SiO_2 increases with the gradient of potential. Higher gradients cause to corrosion of steel substrates and releasing gas negatively influences results. Velocity of deposition particles may be changed via potential ζ by addition of electrolytes.

REFERENCES

1. Guglielmi M.: Journal of Sol-Gel Science Technology *8*, 443 (1997).
2. Castro Y., Ferrari B., Moreno R., Durán A.: Surface & Coatings Technology *191*, 228 (2005).
3. Sarkar P.: P. S. Nicholson, Journal of the American Ceramic Society *79*, 1987 (1996).

P02 THE COMPARISON OF DEACIDIFICATION OF THE PRE-AGED DEGRADED NEWSPRINT PAPER AND NEW NEWSPRINT PAPER

MARTINA CEDZOVÁ, MILAN VRŠKA, and GABRIELA SZEIFFOVÁ

Faculty of Chemical and Food Technology of the Slovak University of Technology, Department of Chemical Technology of Wood, Pulp and Paper, Radlinského 9, 812 37 Bratislava, Slovakia, martina.cedzova@stuba.sk

Introduction

In spite of the fact that deacidification processes are aimed at deacidifying degraded papers, old books and archive documents[4,5], testing of deacidification treatment efficiency for mechanical permanence improvement has been applied usually for a new acid paper[1,2,3]. A range of deacidification processes covering preventive deacidification of new acid documents is significantly lower.

The appreciable differences of the degraded paper in comparison with the new one are as follows: lower cellulose degree of polymerization, lower pH, lower tensile strength and folding endurance, lightness/brightness and higher concentration of carbonyl groups, radicals, organic acids, etc. Due to the considerable structural, chemical and physical differences the response of the new non-degraded and degraded cellulose materials to modification processes can be different.

The aim of this work lies in quantifying the differences in the efficiency of stabilisation of new and pre-aged degraded lignocellulose materials.

Experimental

Two different samples of paper were used: new newsprint paper with the pH value 5.7 and pre-aged degraded newsprint paper, with the pH value 4.6. Pre-aged degraded newsprint paper was prepared by accelerated aging in a closed reactor at 105 °C during 5 days.

Both specimens were modified by Bookkeeper dispersion[6,7] of MgO at a concentration of 4.3 g dm^{-3} with a particle size below 1 μm in the dispersing blend of C_5–C_{18} perfluoroalkanes and less than 0.1% perfluorinated Mg-soap surfactant.

The paper samples were deacidified by two sides spraying and by 1-minute immersion at laboratory temperature.

The treated samples were artificially aged by heating at 105 °C according to ISO 5630/1 (1994) for 6, 12 and 24 days.

The samples were characterized by changes in optical, mechanical and chemical properties. Surface pH[8], alkaline reserve[9] and tensile strength[10] were measured.

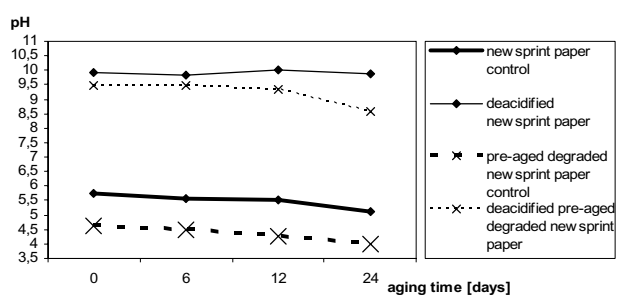

Fig. 1. **Comparison of the effect of deacidification by dispersion MgO[6,7] by two-side spraying of paper on pH of the pre-aged degraded newsprint paper and new newsprint paper**

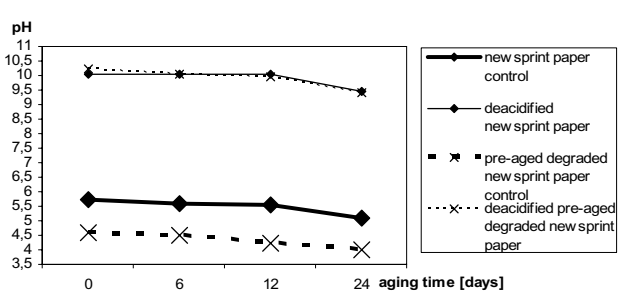

Fig. 2. **Comparison of the effect of deacidification by dispersion MgO[6,7] by immersing on the pH of the pre-aged degraded newsprint paper and new newsprint paper**

Table I
Comparison of an impact of impregnation mode (immersion, spraying) of pre-aged degraded and new newsprint paper on alkaline reserve

Sample	Alkaline reserve [% $CaCO_3$]				Average alkaline reserve*	Standard deviation
	Aging time 0 days	Aging time 6 days	Aging time 12 days	Aging time 24 days		
New newsprint paper control	0.2	0.2	0.1	0.1	0.2	±0.05
Deacidified new newsprint sprayed paper	1.1	1.9	2	1.5	1.6	±0.32
Deacidified new newsprint immersed paper	2.2	2.7	2.6	2.2	2.4	±0.23
Pre-aged degraded paper control	0.2	0.1	0.2	0.1	0.1	±0.04
Deacidified pre-aged degraded sprayed paper	1.1	1.3	1.2	0.6	1.1	±0.27
Deacidified pre-aged degraded immersed paper	3.3	2.7	3.1	2.6	2.9	±0.29

Table II
Comparison of efficiency of a given parameter before aging and after 12-days pre-aged degraded and new newsprint paper treated by means of spraying or immersion. S-efficiency of a given property (pH, alkaline reserve (A.R.), tensile strength (l_t), brightness (B)) expressed as a ratio of determined corresponding values of pre-aged degraded and new newsprint paper

Sample Efficiency * of a given property	Aging time [days]	Deacidified new newsprint sprayed paper	Deacidified pre-aged degraded sprayed paper	Deacidified new newsprint immersed paper	Deacidified pre-aged degraded immersed paper
s_{pH}	0	1.7	1.8	1.8	1.9
	12	1.8	1.9	1.8	2
$s_{A.R.}$	0	1.1	1.1	2.2	3.3
	12	2	1.2	2.6	3.1
s_{lt}	0	0.9	1.1	1	1
	12	1	1	1	1.1
s_B	0	1	1	1	1
	12	1	1	1	1

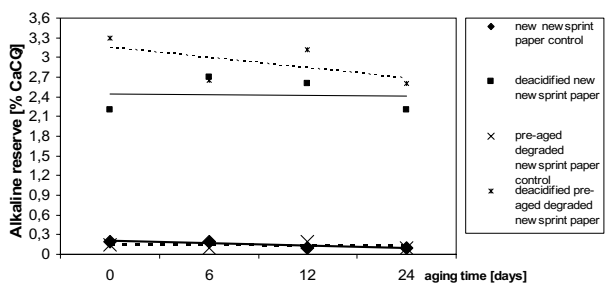

Fig. 3. **Comparison of the effect of deacidification by dispersion $MgO^{6,7}$ by immersing on alkaline reserve of the pre-aged degraded newsprint paper and new newsprint paper**

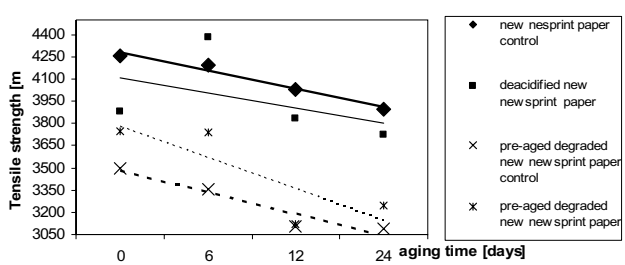

Fig. 4. **Comparison of the effect of deacidification by dispersion $MgO^{6,7}$ by two-side spraying of paper on tensile strength of the pre-aged degraded newsprint paper and new newsprint paper**

Results and discussion

As shown in Fig. 1. and 2., pH of deacidified samples varies in the range from 8.5 to 10.2. Stability of the pH value is for deacidified paper within accelerated aging of the paper sample impregnated by immersion is higher than that of the paper deacidified by spraying.

Alkaline reserve was found as being sufficient after applying the both modes of impregnantion. Alkaline reserve of the samples treated by immersion is a substantially (two times) higher than that for two-side sprayed samples (Table I).

A standard deviation of alkaline reserve during aging lies in the range from ±0.1 to ±0.29.

Tensile strength enhancement was documented in case of degraded paper (Fig. 4.). Tensile strength efficiency for 12-days pre-aged degraded paper exceeds that for new newsprint paper one (Table II).

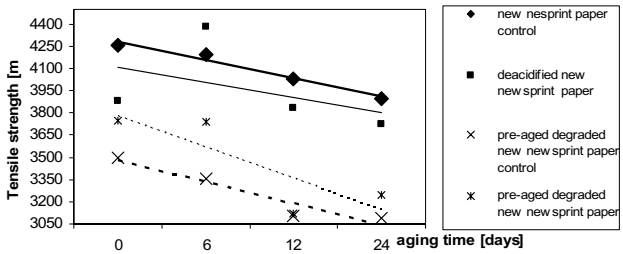

Fig. 5. **Comparison of the effect of deacidification by dispersion MgO[6,7] by immersing on tensile strength of the pre-aged degraded newsprint paper and new newsprint paper**

Efficiency of pH stabilization, lightness/brightness and tensile strength (Table II) is higher for degraded paper when compared with non-degraded sample. A better performance in terms of pH stabilization and alkaline reserve was reached using spraying technology as well as in case of short-term immersion, the latter mode of treatment to be more effective. In general, a conclusion can be formulated stating that the efficiency of the measured parameters is higher after 12 days than those determined at the time 0.

Conclusion

The goal of the contribution was to compare deacidification efficiency for pre-aged degraded newsprint paper and new newsprint paper with pH 5.7, both treated by short-term immersion and two sides spraying. Pre-aged degraded newsprint paper was prepared by accelerated aging in sealed reactor at 105 °C during 5 days with pH 4.6.

Efficiency for pH stabilization, alkaline reserve and tensile strength was determined higher for degraded newsprint paper. The efficiency of pH stabilization and alkaline reserve was found to be sufficient and maintaining also following an accelerated aging. Treatment by an immersion technique was more advantageous for both kinds of paper. The investigation of deacidification efficiency differences for pre-aged degraded and new newsprint paper is still in progress.

Stemming from up-to-now obtained results it follows that deacidification efficiency testing of both new and pre-aged degraded newsprint test paper is a necessity.

The authors express their thanks to the Ministry of Education of the Slovak Republic - project KNIHA.SK 661/2003 and Science and Technology Assistance Agency (Slovakia) – the contract No. APVT- 20-034202.

REFERENCES

1. Malesic J., Kolar J., Strlic M.: Restaurator *23*, 145 (2002).
2. Lewis J., Walker A.: *Infosave project repor*t. The Council for Museums, Archives and Libraries. London, 2003.
3. Kidder L., Boone T., Russick S.: *Bookkeeper spray for use in single item treatments*. Paper Delivered at the Annual Meeting of the American Institute for Conservation (AIC). Arlington, Virginia U.S.A. 1998.
4. Havermans J.: *Deacidification using the Bookkeeper process*, TNO Report, TNO Institute of Industrial Technology, Netherlands 1997.
5. Lienardy A.: *Evaluation of seven mass deacidification treatments*, Institut Royal du Patrimoine artistique (IRPA). Brusel 1992.
6. Buchanan S. et al.: *Technical evalution team report for the Preservation Directorate*, Library of Congress Washington 1994.
7. Zumbühl S., Wuelfert S.: Studies in Conservation *46*, 169 (2001).
8. STN 50 0374: Určenie povrchového pH papiera a buničiny. 1996.
9. STN ISO 10716: Papier a lepenka: Stanovenie alkalickej rezervy. 1994.
10. ISO 1924-1: 1. časť: Metóda s konštantnou rýchlosťou zaťažovania. 1992.

P03 ENHANCEMENT OF MECHANICAL PROPERTIES OF PP-HMDSO/HMDSZ FILMS BY MEANS OF THERMAL ANNEALING

JAN ČECH, PAVEL SŤAHEL, MARTIN ŠÍRA, VILMA BURŠÍKOVÁ, ZDENĚK NAVRÁTIL, DAVID TRUNEC and ANTONÍN BRABLEC
Department of Physical Electronics, Masaryk University, Kotlářská 2, 611 37 Brno, Czech Republic, cech@physics.muni.cz

Introduction

The plasma-enhanced chemical vapour deposition technique using barrier discharges at atmospheric pressure becomes a promising technique for depositions of plasma polymer (pp) thin films. Even though the films have good properties as homogeneity, good adhesion to substrates, high fracture toughness, their polymer-like nature results in relatively low hardness. This disadvantage could be surpassed by after-deposition thermal annealing of the films.

Experimental

The atmospheric pressure glow discharge was generated between two plane metal electrodes covered with glass as the dielectric barrier, with the frequency of 6 kHz and the power density 10 W cm^{-3}. The type of discharge mode (i. e. homogeneous or filamentary) was determined from the current-voltage measurements. The films were deposited from the mixture of hexamethyldisiloxane (HMDSO) or hexamethyldisilazane (HMDSZ) with nitrogen on the silicon wafers of 10 cm in diameter. Thermal desorption spectroscopy (TDS) in the range of 50–1000 °C and annealing tests were used to study the thermal stability of the coatings. The studied samples were placed into vacuum chamber and were heated with constant heating rate of 10 °C min^{-1}. The time evolution

of 8 specific masses during the heating was monitored by mass spectrometer Pfeiffer Vacuum Prisma 80. The thermal desorption spectra were fitted by Gaussian curves, leaving all the parameters free. The film composition was studied by infrared transmission spectroscopy (IR) using NICOLET Impact 400 spectrometer. The relative transmittance was determined as T/T_s, where T is transmittance of the film-substrate system and T_s is transmittance of substrate. The mechanical properties of the films were studied by means of the depth sensing indentation technique using a Fischerscope H100 tester in as-deposited and annealed state.

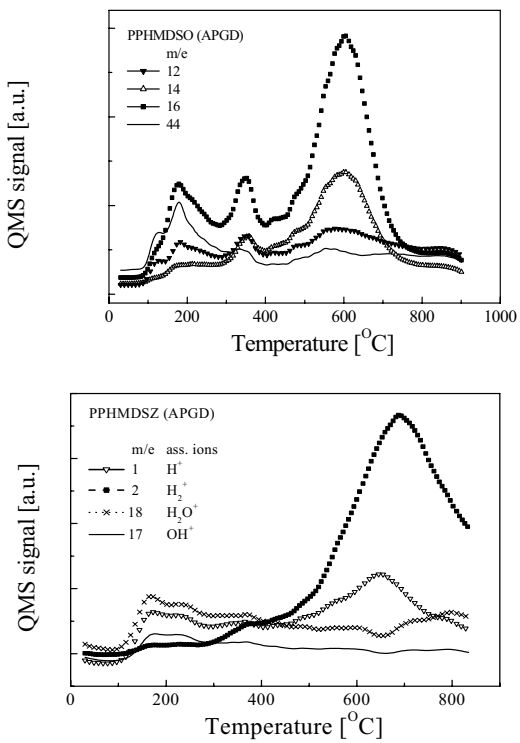

Fig. 1. **TDS spectra for PPHMDSO (left) and PPHMDSZ (right) films**

Results and discussion

Fig. 1. shows thermal desorption spectra for PPHMDSO film (on the left side) deposited from the mixture of nitrogen and HMDSO and for PPHMDSZ film (on the right) deposited from mixture of nitrogen and HMDSZ. The films were deposited in atmospheric pressure glow discharge. The films were stable approximately up to 150 °C. Achieving this value the thermal desorption of hydrogen, water and hydroxyl groups begun. Three significant TDS peaks associated to dehydration of the films were observed at around 200, 380 and 600 °C.

In order to reveal the changes in the structure of PPHMDSO and PPHMDSZ films the FTIR analysis was used. Previous XPS analysis showed, that the as-deposited films contain of about 40 atomic percentage of carbon, 30 atomic percentage of oxygen, 14 atomic percentage of silicon and 16 atomic percentage of nitrogen. The annealing effects on PPHMDSO and PPHMDSZ films are illustrated in Fig. 2. The TDS and FTIR results are in good agreement. Thermally induced changes were observed around wavenumbers 1550 and 1660 cm^{-1} assigned to C=N bonds. These peaks almost disappeared in annealed state in of polymer films. In contrary to this effect peaks attributed to Si-O-Si bonds are more intensive in annealed state (around 450 cm^{-1}, 800 cm^{-1} and 1080 cm^{-1}). This is due to release of –H and –OH and creation of additional Si–O–Si bonds. This substitution of polymer-like bonds with Si–O–Si groups results in the hardening of the coatings. The hardness of coatings increased in one order of magnitude. In as-deposited state it was about 0.3 GPa and in annealed state increased up to 5 GPa. After annealing the intensity of the peak at 2930 cm^{-1} attributed to sp^2-CH complexes significantly increased. This fact can be explained by conversion of sp^3-CH to sp^2-CH due to hydrogen release from sp^3-CH complexes.

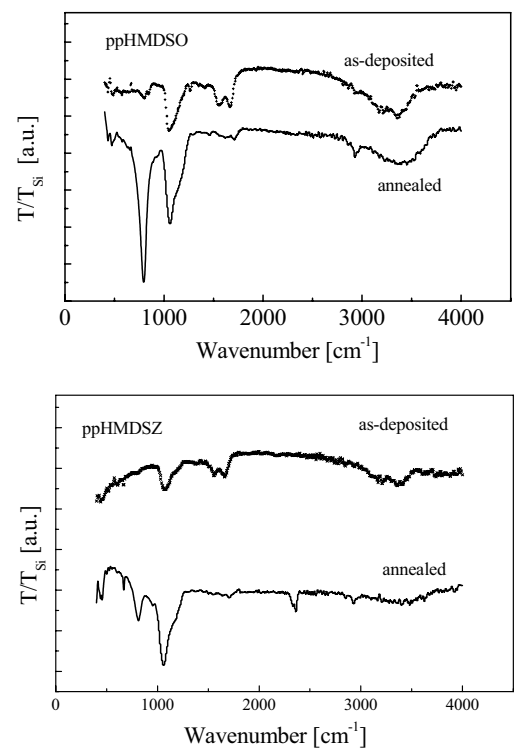

Fig. 2. **Comparison of the FTIR spectra of pp-HMDSO (left) and pp-HMDSZ (right) film before and after annealing**

Conclusion

The PPHMDSO and PPHMDSZ films were able to withstand the annealing up to 1000 °C without delamination. The observed hardening of coatings we put in correlation with the decrease of hydrogen and nitrogen in films observed using TDS and complementary increase of Si–O–Si groups.

This research has been supported by The Scientific Foundation of the Czech Republic under contracts No.202/

02/0880, 202/02/P097 and by The Ministry of Education of the Czech Republic under contract MSM:143100003.

REFERENCES

1. Gherardi N., Martin S., Massines F.: J. Phys. D.: Appl. Phys. *33*, 104 (2000).
2. Sawada Y., Ogawa S., Kogoma M.: J. Phys. D.: Appl. Phys. *28*, 1661 (1995).
3. Prat R., Koh Y. J., Babukutty Y., Kogoma M., Okazaki M.: Polymer *41*, 7355 (2000).
4. Brandenburg R., Kozlov K. V., Massines F., Michel P., Wagner H. E.: Hakone VII. Proc. p. *93*, Greifswald, 2000.

P04 PLASMA POLYMER FILMS PREPARED IN RF INDUCTIVE COUPLING SYSTEM

VLADIMIR CECH, JAN VANEK, JAN STUDYNKA and RADEK PRIKRYL
Institute of Materials Chemistry, Brno University of Technology, Purkynova 118, 612 00 Brno, Czech Republic, cech@fch.vutbr.cz

Introduction

We would like to demonstrate a possibility to deposit plasma polymer films of high reproducibility and controlled physicochemical properties. Plasma polymer films were prepared by plasma-enhanced chemical vapor deposition (PE CVD) employing an RF helical coupling system[1] operated at continuous or pulsed regime. The effective power (W_{eff}) of pulsed plasma was controlled by changing the ratio of the time when plasma is switched on (t_{on}) to the time when plasma is switched off (t_{off}), $W_{eff} = W_{total} \times t_{on}/(t_{on}+t_{off})$, where W_{total} = 50 W.

Experimental

Vinyltriethoxysilane (VTES) was used as the monomer. Thin films were deposited on silicon wafers or special microscope slides without flaws pretreated by Ar plasma (10 sccm, 10 Pa, 25 W) for 10 min. Employing a mechanical manipulator the pretreated substrate was placed into the plasma zone after plasma reached the steady state monitored by mass spectroscopy. The film thickness was measured by a Profiler Talystep (Taylor-Hobson) or a spectroscopic phase-modulated ellipsometer UVISEL (Jobin Yvon).

Results and discussion

Elemental composition of pp-VTES films (Fig. 1.) was determined from XPS and RBS spectra. The element ratio between carbon and silicon atoms evidenced an abrupt increase of organic character for the material prepared at higher power. The FTIR analysis of pp-VTES films confirmed a distinct chemical structure of films deposited at different powers. Films prepared at low power were formed by siloxane network with ethoxy side groups. Those films deposited at higher power were constructed from carbon network with hydroxyl and carbonyl side groups.

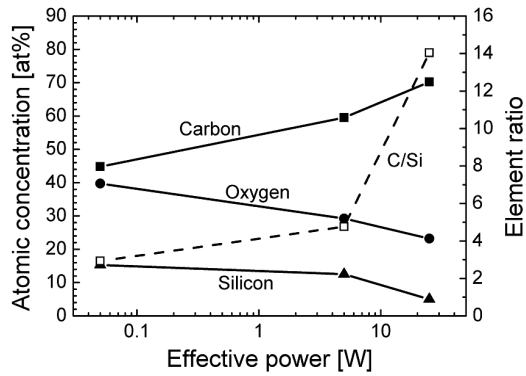

Fig. 1. **Elemental composition of pp-VTES films as a function of the effective power**

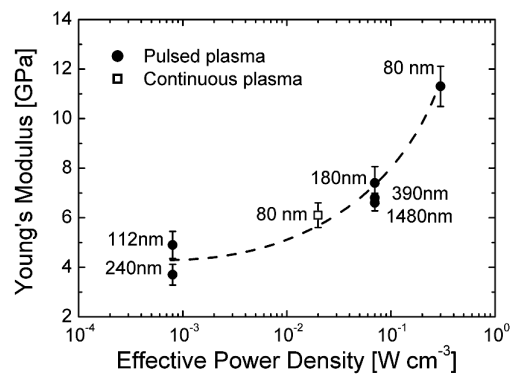

Fig. 2. **Elastic modulus of the plasma polymer controlled by the power density**

The Young's modulus and the hardness of the films were determined[2] from load-displacement curves obtained using a Hysitron Triboscope attached to a DI Dimension 3100 AFM and equipped with a three-sided pyramid Berkovich indenter. The elastic modulus, E, was estimated by averaging the values measured up to 10 % of the film thickness, where the measurements are not influenced by the substrate. The Poisson's ratio used was 0.3. The Young's modulus of pp-VTES film as a function of the effective power is depicted in Fig. 2. In spite of different film thicknesses, it is evident that the modulus increases with increasing power density from 3.7 GPa to 11.3 GPa. This change represents an enlargement of the modulus by 205 %. Young's modulus degreases with the film thickness for both used power densities. It could be a consequence of lower material compaction at the upper part of the film.

The depth profile of the hardness for pp-VTES films shows, that the hardness decreased from the film surface to the bulk value within the range of 20–30 nm for most of samples. This phenomenon could be a consequence of post-deposition oxidation, at the film surface stored in the open air, increasing the cross-linking of plasma polymer.

The ratios of *H/E* for the bulk and maximum data are 0.19 and 0.30 respectively. For crystalline materials *H/E* depends strongly on the microstructure, but in amorphous materials the reason for the proportionality between *H* and *E* is not quite clear. According to ref.[3], the proportionality between *H* and *E* can be related to the mean compressive elastic strain $\varepsilon_y = H/2E$ around the indenter. Thus, the high values for pp-VTES films signify higher mean compressive elastic strain with respect to other amorphous materials ($H/E = 0.06–0.11$). This interpretation corresponds with the elastic behavior of our material under a loading-unloading cycle.

A phase-modulated ellipsometer was used to characterize optical constants of pp-VTES films in the spectral range 240–830 nm. A model of a single homogeneous film on the semi-infinite silicon substrate was used for the calculation of the film thickness, refractive index and extinction coefficient.

A microscratch tester and an optical polarizing microscopy enabled to analyze a scratch path together with normal and lateral force recordings. Plasma-polymerized and polycondensed films (prepared from same monomer) were tested under dry and wet conditions with respect to film adhesion. While interfacial adhesion of polycondensed films immersed into cold and boiling water decreased with time, the adhesion of plasma-polymerized films was unvarying, Fig. 3. Therefore, interfacial hydrolytic stability of plasma-polymerized films was very good, probably due to a higher density of siloxane bonds at the glass/film interface and/or a higher crosslinking of plasma polymer.

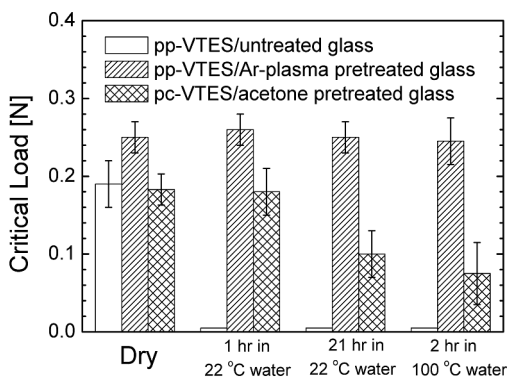

Fig. 3. **Interfacial adhesion of plasma-polymerized and polycondensed films under dry and wet conditions**

Conclusion

Plasma polymer films of vinyltriethoxysilane were deposited on planar substrates by PE CVD. The physicochemical properties of plasma polymer films can be controlled by deposition conditions. Increasing the effective power from 0.05 to 25 W the physicochemical properties of pp-VTES films varied as follows:

– Adhesion (Critical load: 0.3–0.4 N)
– Elastic modulus: 3.7–11.3 GPa
– Hardness: 0.7–2.1 GPa
– Refractive index: 1.47 to 1.58 (633 nm)
– Organic/inorganic character (C/Si ratio: 2.9–14.0)

The Czech Ministry of Education supported this work, contract No. OC 527.110 and OC P12.001. The authors thank J. Zemek (XPS), V. Perina (RBS), L. Zajickova (Ellipsometry), A.A. Goruppa, Ms. S. Behzadi and F.R. Jones (Nanoindentation).

REFERENCES

1. Cech V., Prikryl R., Balkova R., Vanek J., Grycova A.: J. Adhesion Sci. Technol. *17*, 1299 (2003).
2. Oliver W. C., Pharr G. M.: J. Mater. Res. *7*, 1564 (1992).
3. Sanchez-Lopez T. C., Donnet C., Loubet J. L., Belin M., Grill A., Patel V., Jahnes C.: Diam. Rel. Mater. *10*, 1063 (2001).

P05 SYNTHESIS OF ETTRINGITE FROM AMMONIUM ALUMINUM SULFATE

VÍTĚZSLAV FRANK and JAROMÍR HAVLICA
Brno University of Technology, Faculty of Chemistry, Department of Materials Chemistry, Purkyňova 118, 612 00 Brno, frank@fch.vutbr.cz

Introduction

Ettringite is a mineral with general formula $Ca_6Al_2(SO_4)_3(OH)_{12}.(26–32)H_2O$, shortly $C_6AS_3H_{32}$ or AF_t respectively. The AF_t designation was first suggested by Smolczyk in 1961 (ref.[1]). Ettringite is formed in setting cement, in hardening concrete (delayed ettringite formation, DEF) or is prepared by various methods. Naturally ettringite was formed by underground hydrothermal processes thousands years ago. It is found in Ireland and Jordan.

Ettringite forms hexagonal prismatic crystals. According to the structure model, the crystals are based on columns of cations of the composition $\{Ca_3[Al(OH)_6]._{12}H_2O\}^{3+}$ (ref.[2]). The channels contain the SO_4^{2-} ions and the remaining water molecules.

Ettringite occurs in various forms, often as spherical clusters of ettringite crystals, felt-like or parallel needles of differing sizes. If ettringite crystallizes without spatial obstruction, e. g. in pores in concrete, then it has typical needle-shaped crystal habit. Ettringite stability was found from pH values 10.5 to 12 (ref.[3]).

Experimental

Ettringite was prepared from commercial produced burnt lime and saturated solution of technical ammonium aluminium sulphate (alum). Ammonium aluminium sulphate is produced by DIAMO, Straz pod Ralskem as product from uranium mining improvement.

At first was the suspension of lime prepared with using of fresh water. The suspension was mixed 5 minutes. Then

solution of ammonium aluminium sulphate was added. The system was mixed during reaction. The last step was filtration. Filtrate was preserved with 1 mol dm^{-3} HCl. Solid product was dried in air atmosphere. Dry solid product was analysed by XRD and its morphology was studied by SEM.

In filtrate there is ammoniacal nitrogen. The amount of this one was determined by Nesslerization method, titrimetric method and indophenol method. Due to present of interferences in samples (especially Ca^{2+} and Al^{3+} ions coming from starting materials) the preliminary distillation step is required. Obtained results were compared with allowed limits of European Union Law related to maximum amount of ammoniacal nitrogen in water[4,5]. Technology of filtrate processing was proposed.

Preliminary distillation step: pH of diluted filtrate was adjusted to 9.5 by 6 mol dm^{-3} NaOH. The steam out distillation apparatus was used for the distillation. Distillate was collected in boric acid (20 g H_3BO_3 in 1 dm^3).

Nesslerization method: absorbance of samples was measured by a spectrophotometer UNICAM UV530 at 400 nm for 1 cm light path. It is convenient to prepare calibration curve[6].

Titrimetric method: diluted distillate was titrated with standard 0,02 mol dm^{-3} H_2SO_4 until mixed indicator. The indicator was turned from light green to light grey.

Indophenol method: for ammonia determination was used manual photometer Photometer PC 22. The instrument works with two kinds of tablets (Ammonia no. 1 and 2). Reagents in tablets react with sample in cuvete. Intensity of turning colour is measured and depends on amount of present ammonia.

Results and discussion

XRD analysis showed that in solid products there are two phases – ettringite and gypsum. Gypsum is a minority phase. Ettringite crystals are little and look like small needles. Particles form very often aggregate. The size and shape of crystals depend on concentration of starting sulphate solution and on amount of used water (for lime suspension).

Results of analysis show that concentration of present ammoniacal nitrogen is higher then the concentration limit of waste water in European Union Law. That is why it was

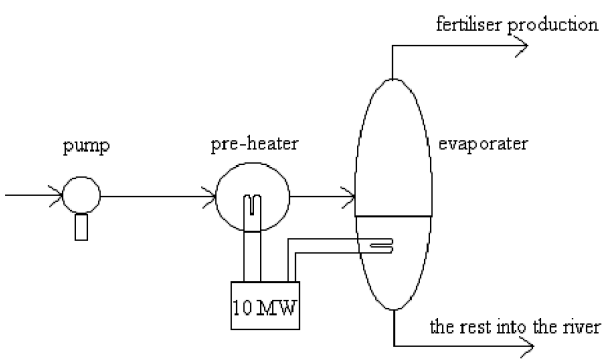

Fig. 1. **Water steam heating scheme**

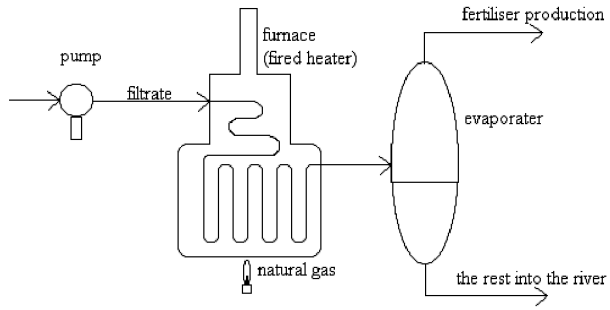

Fig. 2. **Natural gas combustion scheme**

devised a way to decrease of ammonium amount. Performed experiments showed that the best way is distillation. The distillation is convenient for sufficient decrease of ammonium concentration in filtrate. Two possible technological schemes were proposed. These are shown in Fig. 1. and 2. It was proposed that evaporated ammonia may be used for a fertiliser production (e. g. $(NH_4)_2SO_4$).

REFERENCES

1. Gougar M. L. D., Scheetz B. E. and Roy D. M.: Waste Manag. *16*, 295 (1996).
2. Stark J., Bollmann K.: Nordic Concrete Research. *5* (1999).
3. Gabrisova A., Havlica J. and Sahu S.: Cem. Con. Res. *21*, 1023 (1991).
4. Directive 2000/60/EC of the European Parliament and of the Council of 23 October 2000 establishing a framework for Community action in the field of water policy.
5. Directive 98/15/EEC, amending Directive 91/271/EEC: The Urban Waste-water Treatment.
6. ČSN 83 0530: Chemický a fyzikální rozbor povrchové vody.

P06 MODELING OF SURFACE OF CARBON FIBERS

JAN GRÉGR[a], MARTIN SLAVÍK[a]
and VLADIMÍR KOVAČIČ[b]
Technical University of Liberec, Hálkova 6, 461 17 Liberec, Czech Republic, [a]Department of Chemistry, Faculty of Education, jan.gregr@vslib.cz, [b]Department of Textile Materials, Faculty of Textile Engineering

Introduction

The carbon fibers are the strongest and the stiffest reinforcements for composite materials. Transfer of carbon fiber's high value of elasticity modulus to final composite is dependent on the size of fiber surface. A lots of articles describe properties and treatment of carbon fibers, a fewer part of them is interested in surface energetic. Allington[1] used molecular modeling to explanation of functional groups

influence to composites adhesion. His results are in agreement with results from experimental inversed phase gas chromatography (IGC). IGC is not problem-free for practical composite applications due to surface characterization related to vacuum. Moreover this procedure cannot explain adhesion improvements of standard treated carbon fibers after exposition to ammonia[2]. We therefore suppose a rather big importance of high energy surface carbons located on the "edge" of graphen band for composite adhesion. That is the place where are functional groups easily created.

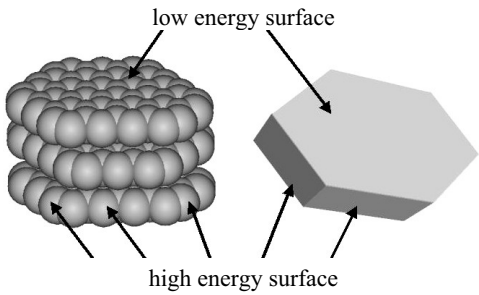

Fig. 1. **High and low energy surface of graphite**

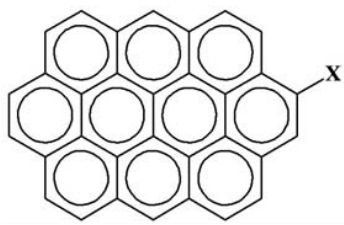

Fig. 2. **Formulae of model compounds**
X = H, OH, NH_2, COOH, $CONH_2$

We tried simpler model explanation. Surface adhesion is proportional to number of van der Waals interactions and ability to form covalent bond between fiber surface and matrix. Dispersive van der Waals forces are characterized by surface area and molecular volume, inductive van der Waals forces by α-polarizability, dipole interactions by dipole moment and ability to form covalent bond by reaction Gibbs energy of relevant reaction.

Experimental

Experiments were made with carbon fibers IMS Tenax – fibers were: 1. heated in argon to 2200 °C; 2. heated up to 600 °C; 3. anodic oxidized 4. treated with NH_3; 5. anodic covered by polyaniline.

Surface energy was studied by wetting of modified fibers with model liquids – contact angle of water, glycerole and ethylene glycol on fiber surface was measured.

For molecular modeling were used software Chem3D, semi-empirical calculations were performed with CS MOPAC Pro, and AM1, MNDO, MNDO/3, PM3 methods.

Results

Table I
Change of surface energy of carbon fibers by various treatment

Treatment	Surface energy [mJ m^{-2}]	Treatment	Surface energy [mJ m^{-2}]
0. none	49.1	3. anodic oxidation	57.9
1. 2200 °C in Ar	29.0	4. NH_3	54.9
2. 250 °C in air	47.2	5. polyaniline	56.6

Table II
Effect of functional group on dispersive and inductive van der Waals forces
(SEV – Connolly solvent excluded volume, SAS – Connolly solvent accessible area, MS – Connolly molecular area, α-polarizability; Å = 0.1 nm)

	–H	–OH	$–NH_2$	–COOH	$–CONH_2$
SEV [$Å^3$ mol^{-1}]	290.618	294.636	297.107	310.025	312.279
SAS [$Å^2$ mol^{-1}]	486.733	492.137	495.243	514.366	519.737
MS [$Å^2$ mol^{-1}]	326.476	330.667	333.255	347.226	349.649
α [$Å^3$ mol^{-1}]	42.6797	42.9118	44.2283	44.8964	58.6871

Table III
Effect of functional groups on surface polarity (dipole moment [Db])

Method/func. group	–H	–OH	$–NH_2$	–COOH	$–CONH_2$
AM1	0.006	1.077	2.135	2.541	3.709
MNDO/3	0.002	1.380	1.686	3.003	4.133
MNDO	0.004	1.058	1.984	2.458	3.611
PM3	0.005	1.054	2.276	2.312	3.729

Discussion

Dispersive and inductive van der Waals forces are minimally influenced with functional groups existed on carbon fibers. Significant differences among different functional groups were computed for surface polarity and reaction Gibbs energy (ability to form a bond with epoxy-group).

Heating in argon to 2200 °C lead to complex removing of functional groups from carbon fiber surface; heating to 250 °C reveal decrease in number of strong acidic carboxy-groups; anode oxidation show on the contrary increase in number of carboxy- groups; treatment with ammonia cause partial change of –OH and –COOH groups to $–NH_2$ and $–CONH_2$ groups; fibers covered by polyaniline exhibit totally different surface properties. Now we are able to explain increase or decrease in adhesive properties of carbon fibers by comparing results obtained with molecular mechanics to surface energy of treated surfaces.

Conclusions

Properties (included in Table II characterizing van der Waals interactions) of functional groups presented on carbon fiber surface computed via molecular modeling are tightly tied with shear properties of composites. We suppose that the main role have polar interactions and ability to form covalent bond with matrix molecules.

REFERENCES:

1. Allington R. D., et all.: Composites; Part A *35*, 1161 (2004).
2. Severini F., Formaro L., Pegoraro M., Posca L.: Carbon, *40*, 735 (2002).

P07 TITANIUM COMPLEX HAVING TWO PHENOXY-IMINE CHELATE LIGANDS FOR LIVING ETHYLENE POLYMERIZATION

SOŇA HERMANOVÁ, JAN MERNA,
JAROSLAV CIHLÁŘ and MILOSLAV KUČERA
Institute of Material Science, Brno University of Technology, Purkyňova 118, 612 00 Brno hermanova-s@fch.vutbr.cz

Introduction

Living olefin polymerization catalysts enable preparation of precisely controlled polymers such as monodisperse polymers, macromonomers and block copolymers. In this report phenoxy-imine complex bis [N-(3-*tert*-butylsalicylidene)-2,3,4,5,6-pentafluoroanilinato] titanium(IV)dichloride was in combination with methylalumoxane (MAO) as a co-catalyst examined for ethylene polymerization.

Experimental part

All manipulations of air- and moisture-sensitive materials were carried out under nitrogen atmosphere, using either a dual vacuum/nitrogen line and standard Schlenk techniques or a high vacuum line. Ethylene (99.8 %, Siad) and nitrogen (99.999 %, Siad) were purified by passing through 4A molecular sieves and supported Cu columns. Solvents (toluene, hexane, THF, dichloromethane and diethyl ether) were obtained from Sigma-Aldrich and Penta Chrudim and purified according to the usual procedures[1].

Bis[N-(3-*tert*-butylsalicylidene)-2,3,4,5,6-pentafluoroanilinato]titanium(IV)dichloride (1) was synthesized according to the previously described procedure[2].

Co-catalyst methylalumoxane (MAO) was purchased from Crompton GmbH (10 % wt in toluene) and remaining trimethylaluminium was evaporated in vacuo prior to use.

Ligand and complex analyses ^{1}H NMR spectra were recorded on Bruker Avance 300 spectrometer.

Molecular weights (M_n and M_w) of polyethylenes and polydispersities (M_w/M_n) were determined by high temperature gel-permeation chromatograph (Polymer Laboratories) at 140 °C using polystyrene calibration. Melting temperatures (T_m) of polymer were determined by DSC upon heating sample to 160 °C at heating rate of 10 °C min^{-1}.

Results and discussion

The complex (1) was prepared as a reddish brown solid in 57 % yield.

^{1}H NMR ($CDCl_3$) δ 1.29 (s, 18H, ^{t}Bu), 6.95 (t, J = 7.6 Hz, 1.75 Hz, 2H, aromatic H), 7.10 (dd, J = 7.6, 1.75 Hz, 2H, aromatic H), 7.58 (dd, J = 7.6, 1.75 Hz, 2H, aromatic H), 8.15 (s, 2H, CH = N).

Ethylene polymerizations with phenoxy-imine titanium complex (1) using MAO as a co-catalyst were carried out at 30 °C under pressure 110 kPa. The results are collected in Table I. Polyethylene produced after 0.5 min polymerization time possessed narrow distribution of molecular masses M_w/M_n = 1.12. GPC peak of this polyethylene had the monomodal shape and is shown at Fig. 1. This result suggested that the polymerization proceeded in a living fashion. Since the activity of complex (1)/MAO for ethylene polymerization is high, long polymerization time caused broadening of distribution of molecular masses, probably mainly because of nonhomogenity of polymerization system. The dependence

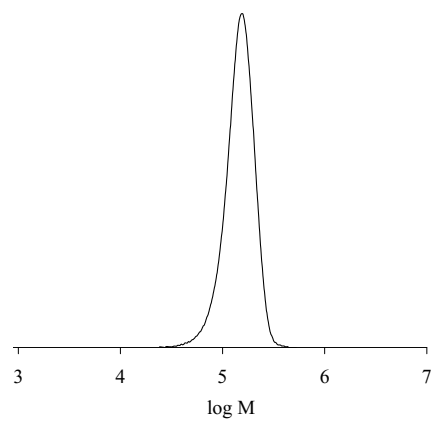

Fig. 1. **GPC profile of polyethylene P1, M_n = 138 400, M_w/M_n = 1.12**

Table I
Results of Ethylene Polymerization with bis [N-(3-*tert*-butylsalicylidene)-2,3,4,5,6-pentafluoroanilinato]titanium(IV) dichloride/MAO

Entry	Time [min]	Polymer yield [g]	Activity[a]	M_n[b] [×10^{-3}]	M_w/M_n[b]	T_m [°C]
1	0.5	0.14	140	138.40	1.12	135
2	1	0.24	240	150.55	1.43	135
3	1.5	0.34	340	181.90	1.53	135
4	2.5	0.45	450	663	1.97	137
5	5	0.69	690	412.35	2.30	135
6	10	1.50	1500	441.80	9.16	137

Conditions: MAO (1.2 mmol), catalyst (1μmol), 30 °C, ethylene 110 kPa, 100 ml toluene
[a]Activity kg PE·mol(Ti)$^{-1}$ · atm^{-1}, [b] Determined by GPC using PS calibration

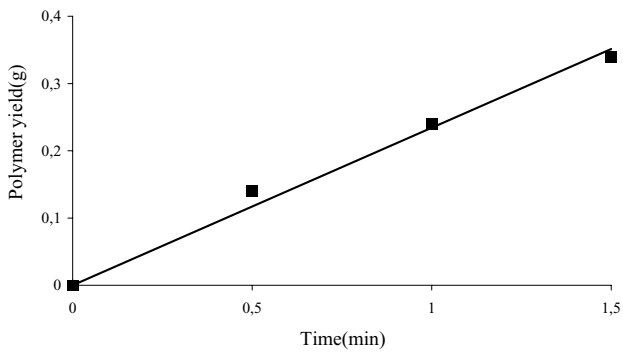

Fig. 2. **Polymer yield as a function of polymerization time**

of polymer yield on polymerization time was nearly linear (Fig. 2.), but a linear relationship between M_n and polymerization time was not found.

Melting temperatures (T_m) of produced polyethylenes were from 135 to 137 °C.

Conclusion

The catalytic property of titanium complex (1)/MAO for the polymerization of ethylene was described. The highly active complex promoted living polymerization of ethylene at 30 °C and at little polymerization time.

Acknowledgement is given to COST D.17.10 Project and to Project MSM0021630501for financial support of this work.

REFERENCES

1. Fujita T., Mitani M.: J. Am. Chem. Soc. *124*, 3327 (2002).
2. Errington R. J.: *Advanced Practical Inorganic and Metalorganic Chemistry*. Blackie Academic&Professional, London 1997.

P08 POSSIBILITY OF METAKAOLINE APPLICATION INTO THE GLASS FIBER REINFORCED CONCRETE COMPOSITE

RADEK HOLEŠINSKÝ, JINDRA DROTTNEROVÁ and JOSEF KRÁTKÝ
Výzkumný ústav stavebních hmot, a. s., Hněvkovského 65, 617 00 Brno, Czech Republic, holesinsky@vustah.cz

Introduction

The aim of the experimental work is to verify the possibility of the metakaolin application into the glass fiber reinforced concrete (GFRC) composite materials[1]. Metakaolin belongs to the synthetic pozzolana and its preparation is based on the calcinations of clay mineral in the temperature range form 600 to 800 °C. An advantage of metakaolin usage is that the micro structure of GFRC matrix is positively influenced by lower production of portlandite.

Currently, microsilica is predominantly used as an admixture into the GFRC composite materials in the Czech Republic. There is a hypothesis that microsilica, however, could be replaced with metakaolin, which is supposed to have similar resulting properties as microsilica and moreover is cheaper. Therefore it is essential to verify this hypothesis by the experimental work that would prove the metakaolin effect on resultant parameters of the GFRC composite materials.

Experimental part

To demonstrate the hypothesis mention above, a large variety of both commercial (e. g. AGS Mineraux and Imerys) and pilot plant produced samples of metakaolin were chosen. In total 8 samples of metakaolin were examined to test the dosages in amount of 5, 10 and 15 wt % (measured from the content of cement).

Considering the large number of measured values results of only two samples (MetaStar 501 – commercial and K21

– pilot plant produced) of metakaolins are presented. All measured parameters were compared with standardly produced GFRC composite materials that content microsilica (SVB standard). In some cases the comparison was supplemented by parameters of GFRC without admixture.

Defining the basic mechanic properties

For the purpose to define the basic mechanic properties, the test GFRC boards (sized 500 × 500 × 10 mm) containing different sample of metakaolin were produced. After unframing the test board was placed into the wet storage and kept there for 28 days. Then the test board was cut into 16 test elements sized 247.5 × 50 × 10 mm. These test elements were used to define bulk density, absorbability, impact strength and flexural strength. Measured results are displayed in Table I.

Table I
Basic mechanic properties

Sample	Absorbability [%]	Bulk density [kg m^{-3}]	Flexural strength [MPa]	Impact strength [MPa]
MS 501 – 5 %	8.77	2007.7	13.44	10.64
MS 501 – 10 %	8.88	1993.8	8.88	10.00
MS 501 – 15 %	10.52	1916.2	12.90	10.38
K21 – 5 %	8.06	2029.9	13.78	8.82
K21 – 10 %	7.77	2033.1	14.89	8.37
K21 – 15 %	8.91	1981.8	13.16	8.67
Standard SVB	8.88	2039.8	12.09	8.84

Generally, the results of absorbability test are identical to the result of SVB standard, except the sample with higher dosage of commercial metakaolin. The bulk density test shows that the increased dosage of metakaolin causes the slight decrease of bulk density. On the other hand, the increased dosage of metakaolin tends to raise the flexural strength of pilot plant metakaolin. The sample with commercial metakaolin, however, shows the growth of impact strength.

Durability test

For verifying the long-term progression of the GFRC composite materials parameters, an accelerating durability test was carried out. The methodology of the accelerating durability test stems from technical norms[2,3]. The accelerating test involves cyclic changes of the dominating factors that have an influence on the mechanic properties of the GFRC composite materials during the season of year. The test is based on principle that the test boards are periodically exposed to heat, wet and freeze. Duration and the number of periods within one cycle are presented in Table II.

Table II
Methodology of the durability test

Phase	Time	Parameters	Number of repetition in one cycle
Sprinkling	170 min.	2.5 dm^{-3} m^{-2} min^{-1}	18
Pause	10 min.	–	18
Radiant heat	170 min.	IR lamp (capacity 2400 W m^{-2})	18
Pause	10 min.	–	18
Freezing	240 min.	–20 °C ± 2 °C	1
Defrosting	120 min.	+20 °C ± 2 °C	1

The test elements, for the durability test in this case, were prepared in the same way as has been mentioned in previous paragraphs. The mechanic parameters of these test elements were evaluated after 50 cycles. The achieved results are shown in Table III.

Table III
Mechanic properties after the durability test

Sample	Absorbability [%]	Bulk density [kg m^{-3}]	Flexural strength [MPa]	Impact strength [MPa]
MS 501 – 5 %	6.36	2082.2	13.63	6.47
MS 501 – 10 %	6.12	2082.6	12.16	6.78
MS 501 – 15 %	7.34	1998.8	12.26	7.74
K21 – 5 %	5.93	2094.4	15.98	8.74
K21 – 10 %	5.93	2060.5	16.26	9.2
K21 – 15 %	6.34	2020.4	14.38	8.14
Standard SVB	7.15	2113.2	16.00	6.26

The measured results highlight the significant distinctions in the flexural strength and impact strength between the commercial and pilot plant produced samples of metakaolin. The sample with dosage of 10 % of pilot plant produced metakaolin indicates higher impact strength than the SVB standard or the sample of commercial metakaolin. Concerning other mechanic parameters, they are comparable to those of SVB standard except the lowering of bulk density.

The study of the GRFC composite materials' behaviour under the influence of the aggressive environment

Two aggressive environments were prepared to study the behaviour of the GRFC composite materials with metakaolin as an admixture. The first one was Na_2SO_4 solution and the second one was NaCl solution, both solutions containing 4.4 % of given salts. The test elements were soused into these solutions. And again the mechanic properties were the subject of this study. The measurement of this test was staggered into three phases. The first phase of measuring was done after 7 days of keeping test elements in solutions. The

second measuring was realized after 28 days and the last one was carried out after 90 days. The achieved results are summarized in the following Tables IV and V.

Table IV
Evolution of flexural strengths in NaCl solution

Sample	Storage period 7 days	28 days	90 days
MS 501 – 5 %	15.77	13.09	14.89
MS 501 – 10 %	11.85	14.14	15.12
MS 501 – 15 %	16.37	13.25	12.64
K21 – 5 %	15.67	13.62	11.26
K21 – 10 %	10.59	12.18	15.03
K21 – 15 %	18.21	15.27	16.72
Standard SVB	14.48	17.25	17.02

Table V
Evolution of flexural strengths in Na_2SO_4 solution

Sample	Storage period 7 days	28 days	90 days
MS 501 – 5 %	17.24	15.67	14.74
MS 501 – 10 %	13.64	18.73	16.01
MS 501 – 15 %	14.16	13.72	14.16
K21 – 5 %	10.68	12.8	13.7
K21 – 10 %	14.55	17.09	13.83
K21 – 15 %	14.42	17.54	16.47
Standard SVB	11.25	12.1	14.48

Conclusion

The experimental work confirmed that the GRFC composite materials with metakaolin admixture after 28 days of aging have the similar results of mechanical parameters as SVB standard with microsilica as an admixture.

The durability test revealed differences in measured results between commercial and pilot plant produced metakaolins.

Nevertheless, the above mentioned hypothesis was verified. which means that microsilica as an admixture in the glass fiber reinforced concrete composite materials could be replaced by metakaolin.

This work was financially supported by Ministry of Industry and Trade within the grant project no FK-K3/043.

REFERENCES

1. Čechmánek R.: 7th Conference: Ecology and new building materials and products, Telč, 2003, p. 138.
2. ČSN EN 492: Technical specifications and testing method for fibre cement roof board and fitting.
3. ČSN EN 494: Technical specifications and testing method for fibre cement corrugated roof board and fitting.

P10 USE OF BACTERIAL SYSTEMS TO PRODUCTION AND BIODEGRADATION OF BIOMATERIAL COMPONENTS: A SCREENING STUDY

JANA HRDLIČKOVÁ, IVANA MÁROVÁ, LIBOR BABÁK, RADKA KOČÍ and TEREZA VIDLÁKOVÁ
Department of Food Chemistry and Biotechnology, Faculty of Chemistry, Technical University Brno, Purkyňova 118, 612 00 Brno, Czech Republic, hrdlickova@fch.vutbr.cz

The term 'biomaterials' includes chemically unrelated products that are synthesised by microorganisms under different environmental conditions. One important family of biomaterials is bioplastics. These are polyesters that are widely distributed in nature and accumulate intracellularly in microorganisms in the form of storage granules. These polymers are usually built from hydroxy-acyl-CoA derivatives via different metabolic pathways. Depending on their microbial origin, bioplastics differ in their monomer composition, macromolecular structure and physical properties. A number of bacteria including *Alcaligenes*, *Pseudomonas*, recombinant *Escherichia coli* and methylotrophs have been used for the production of PHAs and high productivities have been achieved. Selection of microorganism for the production of PHA should be based on several factors including the cell's ability to utilise an inexpensive carbon source, growth rate, polymer synthesis rate, and the maximum extent of polymer accumulation.

Most of PHA are biodegradable and biocompatible, which makes them extremely interesting from the biotechnological point of view. Under condition of nutrient limitation, these materials can be depolymerised and utilized by microorganisms as energy source. Degradability of polymeric materials is generally a function of the structure, the presence of degradative microbial population and the environment conditions. We have only recently begun to understand the complex nature of interactions between the microflora and deterioration of polymeric materials.

Methods

Strains. For production of polyhydroxyalcanoates bacteria *Wautersia eurotropha* CCM 3726 (= *Alcaligenes eurotrophus*) was used. For degradation of polyurethans a mixed culture of *Thermophillus* sp. was tested.

Cultivation. W. eurotropha was cultivated in NB 1 medium at 30 °C. *Thermophillus sp.* were cultivated in synthetic medium at 65 °C under permanent shaking.

Quantification of polyhydroxyalkanoates. After the fermentation is over, the cells containing PHA were separated from medium by centrifugation. The harvested cells are then lysed for recovery of PHAs. Analysis of PHA in bacteria using GC/MS was performed. This method involves simultaneous extraction and methanolysis of PHA in mild acid or alkaline conditions.

Analysis of polyurethans degradation. *Thermophillus* culture was cultivated with 1 g sample of several polyurethans for 4 weeks. In regular intervals biomass and total organic mass were determined. After cultivation, surface microscopy and water content in polyurethans was tested.

Results

In pilot experiments cultivation conditions suitlable for maximal production of PHA were tested. While *W. eurotropha* requires the limitation of an essential nutrient, optimal concentrations of nitrogen and phosphorous for the synthesis of PHA were tested. Further, analysis of PHA using gas chromatography was optimized and GC/MS analysis of produced polymers was tested.

Degradation of polyurethans was tested using mixed culture of *Thermophillus* sp. After 4 weeks of cultivation polyurethane co-polymers exhibited some surface changes according to type of polymer. Hydratation was slightly changed too.

This work was supported by project MSM 0021630501 of Czech Ministry of Education.

REFERENCES

1. Qun Yan, Guocheng Du, Jian Chen: Process Biochemistry *39*, 69, (2003).
2. Tsuje T., Tahala K., Ishizaki A.: J. Ferment. Bioeng. *24*, 545 (2001).
3. Gu J. D.: Int. Biodeter. Biodegrad. *52*, 69 (2003).

P10 SURFACE FREE ENERGY COMPARISON BY DIFFERENT CONTACT ANGLE INTERPRETATIONS

ZUZANA JAKUBÍKOVÁ, MILAN MIKULA and BRANISLAV PROSNAN

Department of Graphic Arts Technology and Applied Photochemistry, Faculty of Chemical and Food Technology, Slovak University of Technology, Radlinského 9, SK-812 37 Bratislava, zuzana.jakubikova@stuba.sk

Introduction

Contact angle measurement is a powerful method to estimate the surface free energy of solid surfaces in pure and applied science. This measurement is easily performed by establishing the tangent angle of a liquid drop resting on a solid surface. Several contact angle interpretations are nowadays known and used. Every of these approaches are based on different interpretation for determining a solid surface free energy. The most often methods used are Owens-Wendt--Kaelble approach and van Oss-Chaudury-Good acid-base approach. Both are based on measurements with liquids of known surface energy and its components. *Owens-Wendt--Kaelble approach* (OWK) assumes the presence of two components such as dispersion σ^d and hydrogen bonding forces so called polar component σ^p:

$$\sigma = \sigma^d + \sigma^p \quad (1).$$

To calculate components following equation is used (S – solid, L – liquid):

$$\sigma_L(1+\cos\theta) = 2(\sigma_S^d\sigma_L^d)^{1/2} + 2(\sigma_S^p\sigma_L^p)^{1/2} \quad (2).$$

Acid-base van Oss-Chaudury-Good approach (A-B) considers perceived acid-base interactions at the interface and divides the surface energy into different components such as so-called Lifshitz-van der Waals (LW) which represents disperse part, acid (+) and base (–) components which represents polar part of surface energy. To calculate components following equation is used (S – solid, L – liquid):

$$\sigma_L(1+\cos\theta) = 2(\sigma_L^{LW}\sigma_S^{LW})^{1/2} + 2(\sigma_L^+\sigma_S^-)^{1/2} + 2(\sigma_L-\sigma_S^+)^{1/2} \quad (3)$$

and the polar component is

$$\sigma^P = 2(\sigma_S^+\sigma_S^-)^{1/2} \quad (4).$$

Calculation according to OWK method requires the usage of at least two known liquids and A-B method the usage of at least three known liquids. Considering the wide range of liquid variation appropriate set of liquids is very important[1].

Experimental

Four different surfaces (polypropylene PP, corona treated PP, SiO_x, paper – offset, coated, glossy, 130 g m^{-2}) and seven different liquids (Table I) were used to measure contact angles. Contact angle measurements were performed on a device SEE System (Surface Energy Evaluation System) with CCD camera. The final value of an angle represents mean value of 5 angle measurements of 5 drops of a liquid. Surface energy and its components were calculated using all possible liquids couples and triplets according to OWK and A-B methods. The effort was to determine the appropriate liquid combinations to obtain reasonable surface energy values.

Table I
List of used testing liquids

Testing liquid	Surface energy σ [mJ m^{-2}] total	polar	disperse	acid (+)	base (–)
water	72.8	51.0	21.8	25.5	25.5
glycerol	64.0	30.0	34.0	3.92	57.4
ethylene glycol	48.0	19.0	29.0	1.92	47
formamide	58.0	19.0	39.0	2.28	39.6
aniline	43.4	10.3	33.1	–	–
benzyl alcohol	38.9	9.9	29.0	–	–
bromo naphthalene	44.4	0.0	44.4	0	0

Results and discussion

As has been earlier mentioned Owens-Wendt and acid--base methods involve the usage of proper liquid combinations. We calculated the determinants 2×2 for Owens-Wendt and 3×3 for acid-base from Eq. 2 and 3 and compared them with the surface energy values and their components. The determinant for two liquid combination is calculated according the following

$$D_{\mathrm{OWK}} = \begin{vmatrix} \sqrt{\sigma_{\mathrm{L1}}^{\mathrm{d}}} & \sqrt{\sigma_{\mathrm{L1}}^{\mathrm{p}}} \\ \sqrt{\sigma_{\mathrm{L2}}^{\mathrm{d}}} & \sqrt{\sigma_{\mathrm{L2}}^{\mathrm{p}}} \end{vmatrix} \tag{5}$$

and for three liquids

$$D_{\mathrm{A-B}} = \begin{vmatrix} \sqrt{\sigma_{\mathrm{L1}}^{\mathrm{LW}}} & \sqrt{\sigma_{\mathrm{L1}}^{+}} & \sqrt{\sigma_{\mathrm{L1}}^{-}} \\ \sqrt{\sigma_{\mathrm{L2}}^{\mathrm{LW}}} & \sqrt{\sigma_{\mathrm{L2}}^{+}} & \sqrt{\sigma_{\mathrm{L2}}^{-}} \\ \sqrt{\sigma_{\mathrm{L3}}^{\mathrm{LW}}} & \sqrt{\sigma_{\mathrm{L3}}^{+}} & \sqrt{\sigma_{\mathrm{L3}}^{-}} \end{vmatrix} \tag{6}$$

where 1, 2, 3 represent different liquids. The other method of determining the proper liquid combination was suggested by C. Della Volpe et al.[1] Tables II and III compare values of disperse and polar components and total surface energy values with determinants for four different surfaces. According to these values we selected several liquids combinations (Table IV) for both OWK and A-B methods that gave reasonable results. We assumed that determinant for OWK approach should be greater than 12 and for A-B approach greater than 160. The determinant limit for the A-B approach could be even lower but there were no liquid combinations with the determinant value in the interval of 40–160. The final values of total surface energy and its components (Table V) represent the average of values calculated for selected liquid combinations.

Comparing the values of surface energies and components seem both methods to be convenient when measuring non-polar surfaces, in our case PP (Table V). More significant differences are for more polar surfaces (corona treated PP, SiO_x and paper). The A-B method prefers disperse (LW) part of surface energy – is higher compare to disperse component calculated according to OWK method. The total surface energies are sufficiently comparable for both methods. The OWK approach seems more all-purpose considering variety of possible surfaces. On the other hand, the A-B approach provides the possibility to characterize the surface acid or base character. The usage of a totally disperse liquid (bromo

Table II
Calculated total surface energy and its components (mJ m^{-2}) using A-B approach. $D_{\mathrm{A-B}}$ – determinant according to equation (6), disp. – disperse component, polar – polar component, total – total surface energy

Liquid combination	PP			PP treated			
	disp.	polar	total	disp.	polar	total	$D_{\mathrm{A-B}}$
water-formamide-bromo naphthalene	36.2	1.2	37.4	41.4	1.4	42.8	160.9
water-ethylene glycol-bromo naphthalene	36.2	0	36.2	41.4	2.5	43.9	184.1
water-glycerol-bromo naphthalene	36.2	0	36.2	41.4	4.7	46.1	188.3
water-glycerol-formamide	13.1	2.6	15.7	27.6	13.5	41.1	40.4
water-glycerol-ethylene glycol	26.9	0.5	27.4	0.2	68	68.2	5.5
water-formamide-ethylene glycol	11.6	2.8	14.4	36.3	5.7	42	34.8
glycerol-formamide-ethylene glycol	12.5	0.2	12.7	30.5	6.2	36.7	4.2
glycerol-formamide-bromo naphthalene	36.2	340.2	376.4	41.4	96.3	137.7	6.8
glycerol-ethylene glycol-bromo naphthalene	36.2	0	36.2	41.4	6	47.4	20.5
formamide-ethylene glycol-bromo naphthalene	36.2	77	113.2	41.4	4	45.4	10.9

Liquid combination	SiO_x			Paper			
	disp.	polar	total	disp.	polar	total	$D_{\mathrm{A-B}}$
water-formamide-bromo naphthalene	41.1	12.5	41.1	12.5	41.1	12.5	160.9
water-ethylene glycol-bromo naphthalene	41.1	3.9	41.1	3.9	41.1	3.9	184.1
water-glycerol-bromo naphthalene	41.1	14.5	41.1	14.5	41.1	14.5	188.3
water-glycerol-formamide	33	20.8	33	20.8	33	20.8	40.4
water-glycerol-ethylene glycol	379.9	454	379.9	454	379.9	454	5.5
water-formamide-ethylene glycol	83.5	23.1	83.5	23.1	83.5	23.1	34.8
glycerol-formamide-ethylene glycol	48	92.2	48	92.2	48	92.2	4.2
glycerol-formamide-bromo naphthalene	41.1	17.2	41.1	17.2	41.1	17.2	6.8
glycerol-ethylene glycol-bromo naphthalene	41.1	75.3	41.1	75.3	41.1	75.3	20.5
formamide-ethylene glycol-bromo naphthalene	41.1	113.4	41.1	113.4	41.1	113.4	10.9

Table III
Calculated total surface energy and its components (mJ m^{-2}) using OWK approach. D_{OWK} – determinant according to equation (5), disp. – disperse component, polar – polar component, total – total surface energy

Liquid combination	PP			PP treated			
	disp.	polar	total	disp.	polar	total	D_{OWK}
water-glycerol	35.3	0.1	35.4	10.2	34.4	44.6	16.1
water-ethylene glycol	18.3	1.8	20.1	5.2	41.9	47.1	18.1
water-formamide	41.4	0	41.4	27.1	20.7	47.8	24.2
water-aniline	45.3	0.1	45.4	22.1	23.8	45.9	26.1
water-benzyl alcohol	46.9	0.1	47	16.3	28.3	44.6	23.8
water-bromo naphthalene	36.2	0	36.2	41.4	14.1	55.5	47.6
glycerol-etylenglykol	0.1	39.4	39.5	0	85.1	85.1	4.1
glycerol-formamide	48.8	0.7	49.5	55.7	1.8	57.5	8.8
glycerol-aniline	51.4	1.1	52.5	30.9	11.2	42.1	12.8
glycerol-benzyl alcohol	55.1	1.8	56.9	20.8	19.5	40.3	11.1
glycerol-bromo naphthalene	36.2	0	36.2	41.4	5.9	47.3	36.5
ethylene glycol-formamide	163.6	84.2	247.8	192.9	62.2	255.1	3.7
ethylene glycol-aniline	86.1	23.5	109.6	52.5	0.1	52.6	7.8
ethylene glycol-benzyl alcohol	99.8	32.7	132.5	38.2	2.7	40.9	6.5
ethylene glycol-bromo naphthalene	36.2	0.7	36.9	41.4	1.8	43.2	29
formamide-aniline	54.2	2	56.2	13	46.9	59.9	5
formamide-benzyl alcohol	64.1	5.4	69.5	0.5	120.3	120.8	3.8
formamide-bromo naphthalene	36.2	0.3	36.5	41.4	7.8	49.2	29
aniline-benzyl alcohol	26.3	6.7	33	182	118.1	300.1	0.8
aniline-bromo naphthalene	36.2	1	37.2	41.4	3.2	44.6	21.4
benzyl alcohol-bromo naphthalene	36.2	1.2	37.4	41.4	1.5	42.9	21

Liquid combination	SiO_x			Paper			
	disp.	polar	total	disp.	polar	total	D_{OWK}
water-glycerol	10.6	52	10.6	52	10.6	52	16.1
water-ethylene glycol	4.6	62.9	4.6	62.9	4.6	62.9	18.1
water-formamide	19.6	41.6	19.6	41.6	19.6	41.6	24.2
water-aniline	12	50.1	12	50.1	12	50.1	26.1
water – benzyl alcohol	7.2	57.6	7.2	57.6	7.2	57.6	23.8
water-bromo naphthalene	41.1	26.5	41.1	26.5	41.1	26.5	47.6
glycerol-etylenglykol	0.2	125.6	0.2	125.6	0.2	125.6	4.1
glycerol-formamide	32.8	21	32.8	21	32.8	21	8.8
glycerol-aniline	12.8	47.2	12.8	47.2	12.8	47.2	12.8
glycerol-benzyl alcohol	5.3	67.5	5.3	67.5	5.3	67.5	11.1
glycerol-bromo naphthalene	41.1	14.8	41.1	14.8	41.1	14.8	36.5
ethylene glycol-formamide	123.6	9.9	123.6	9.9	123.6	9.9	3.7
ethylene glycol-aniline	23.3	21.4	23.3	21.4	23.3	21.4	7.8
ethylene glycol-benzyl alcohol	11	42.1	11	42.1	11	42.1	6.5
ethylene glycol-bromo naphthalene	41.1	7.1	41.1	7.1	41.1	7.1	29
formamide-aniline	1.9	116.9	1.9	116.9	1.9	116.9	5
formamide-benzyl alcohol	4.8	253.8	4.8	253.8	4.8	253.8	3.8
formamide-bromo naphthalene	41.1	13	41.1	13	41.1	13	29
aniline-benzyl alcohol	186.5	125.6	186.5	125.6	186.5	125.6	0.8
aniline-bromo naphthalene	41.1	3.2	41.1	3.2	41.1	3.2	21.4
benzyl alcohol-bromo naphthalene	41.1	1.4	41.1	1.4	41.1	1.4	21

naphthalene) in testing liquid couples or triplets leads to the same value of disperse component for both evaluating methods (Tables II and III). Similar results were obtained by Kwok with bromo naphthalene[2] and by C. Della Volpe et al.[1] with diiodomethane which is also a totally disperse liquid.

Table IV
Selected liquid couples and triplets according to determinants to calculate the surface energy and its components

Liquid couples	
water-glycerol	glycerol-bromo naphthalene
water-ethylene glycol	ethylene glycol-bromo naphthalene
water-formamide	formamide-bromo naphthalene
water-aniline	aniline-bromo naphthalene
water-benzyl alcohol	benzyl alcohol-bromo naphthalene
water-bromo naphthalene	glycerol-aniline

Liquid triplets
water-formamide-bromo naphthalene
water-ethylene glycol-bromo naphthalene
water-glycerol-bromo naphthalene

Table V
Calculated total surface energy (mJ m^{-2}) and its components using selected liquid combinations

Acid-base van Oss-Chaudury-Good approach					
Surface	disperse	polar	acid (+)	base (–)	total
PP	36.2	0.4	0.14	0.33	36.6
PP treated	41.4	2.9	0.11	25.10	44.3
SiO_x	41.1	10.3	0.83	41.86	51.4
paper	43.0	5.2	0.47	26.38	48.2

Owens-Wendt-Kaelble approach					
Surface	disperse	polar	acid (+)	base (–)	total
PP	35.1	0.5	–	–	35.6
PP treated	27.7	15.0	–	–	42.7
SiO_x	24.1	29.0	–	–	53.1
paper	30.4	13.7	–	–	44.1

Conclusion

To consider proposed determinant limit values as generally valid requires to test more solid surfaces and liquid combinations. However, we assumed that calculating the determinants could be one of the options, how to choose the proper liquid combinations. More general-purpose contact angle interpretation method seems OWK approach but A-B approach provides the possibility to determine the acid and base character of solid surfaces.

We thank the Slovak Grant Agency VEGA (project VEGA 1/2454/05) and Science and Technology Assistance Agency (contract APVT-20-034202) for financial support.

REFERENCES

1. Della Volpe C., Maniglio D., Siboni S., Morra M.: J. Adhesion Sci. Technol. *17*, 1477 (2003).
2. Kwok D. Y.: Colloids and Surfaces A: Physicochemical and Engineering Aspects *156*, 191 (1999).

P11 CRYSTAL MORPHOLOGY OF STRONTIUM DOPED ETTRINGITE

SVATOPLUK KOKRHEL[a], JIŘINA MATĚJKOVÁ[a] and JAROMÍR HAVLICA[b]
[a]*Institute of Scientific Instruments AS CR, Královopolská 147, 612 64 Brno, Czech Republic,* [b]*Faculty of Chemistry BUT, Purkyňova 118, 612 00 Brno, Czech Republic*

Introduction

Presented work is focused on the influence of strontium substitution into ettringite structure on the crystal morphology. The evolution of ettringite morphology and its derivates determines kinetics parameters of products decomposition and it has a strong impact on mechanical properties of potential composites.

Experimental

Substituted ettringite phases were prepared in according with reactions described by Eq.1

$$(6\text{-}x)Ca(OH)_2 + xSr(OH)_2 + Al_2(SO_4)_3.18H_2O + 8H_2O \rightarrow \rightarrow Ca_{6-x}Sr_xAl_2(SO_4)_3(OH)_{12}.26H_2O \quad (1)$$

Resulting products were determined by X-ray powder diffraction, TG-DTA and ICP-OES analysis[1].

Crystal morphologies were studied on FE SEM – JSM 6700F JEOL. Conductivity of the sample surface was provided by sputtering of a 50 nm gold film. A semi-quantitative EDX analysis was measured on INCA analyzer made by Oxford Instruments Ltd.

Results and discussion

Phase $Ca_5SrAl_2(SO_4)_3(OH)_{12}.26H_2O$ was identified by elementary analysis as solid solution with formula $Ca_{5.3}Sr_{0.7}Al_2(SO_4)_3(OH)_{12}.26H_2O$. Needle hexagonal crystals with a diameter of 50–200 nm and a length of 1–2 μm were observed. (Fig. 1. and Fig. 2.)

The morphology of ettringite crystals is dependent on conditions and the rate of its precipitation[2]. The precipitation of the microcrystal ettringite is caused by increased value of pH of the mother solution and faster ettringite kinetic formation.

The presence of the strontium ions in needle crystals was verified by EDX analysis. An area of 600 by 1200 nm was analyzed, where only needle crystals of ettringite were

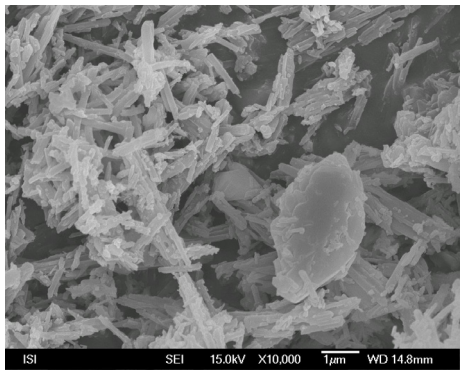

Fig. 1. **Crystals of modified ettringite $Ca_{5.3}Sr_{0.7}Al_2(SO_4)_3(OH)_{12}.26H_2O$ and celestite at magnifications 10 000**

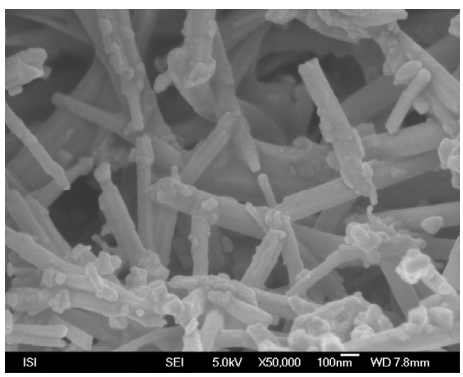

Fig. 2. **Crystals of modified ettringite $Ca_{5.3}Sr_{0.7}Al_2(SO_4)_3(OH)_{12}.26H_2O$ at magnifications 50 000**

presented. The analysis in the configuration used is semi quantitative. The EDX analysis proved that needle crystal similar to the ettringite contained atoms of calcium, strontium, aluminum and sulfur.

Conclusions

The EDX analysis used here above is a semi quantitative method however result demonstrates presence of solid solution of modified ettringite and increasing amount of strontium ions in the crystal lattice. This fact opens possibility to using of ettringite in separation/solidification technologies.

REFERENCE

1. Kokrhel S., PhD thesis, Faculty of Chemistry BUT Brno, Czech Republic (2004).
2. Havlica J., Sahu S.: Cem. Concr. Res. *22*, 661 (1992).

P12 MANUFACTURING OF CARBON NANOFIBER WEBS FROM ELECTROSPUN NANOFIBER PRECURSORS

EVA KOŠŤÁKOVÁ[a], JAN GRÉGR[b] and JANA MÜLLEROVÁ[b]

[a]*Department of Nonwovens, Faculty of Textile Engineering, Technical University of Liberec, Hálkova 6, 461 17 Liberec, Czech Republic, eva.kostakova@vslib.cz,* [b]*Department of Chemistry, Faculty of Education, Technical University of Liberec, Hálkova 6, 46117 Liberec, Czech Republic*

Introduction

Nanofibers are generally fibers of diameter smaller than 1 μm. This article is focused on nanofibers produced during electrospinning process[1]. Modification of the method with higher efficiency of nanofiber production has been developed recently at TUL and patented[2].

First experiments of carbonization of electrospun nanofibers have been realized in last years. Electrospun nanofiber materials made from non-aqueous solutions are used as a precursor for carbonization in majority of articles: e. g. polyacrylonitril[3,4], polybenzimidazol[5,6]. Only one article being engaged in carbonization water-soluble polymer – polyvinyl alcohol nanofibers was published on web[7].

Polyvinyl alcohol unfix physically fixed water in the course at heating, a decomposition reactions occur at the temperature over 200 °C (ref.[8]). Primarily polyens arise, thus water peels by degradation of hydroxyl (OH) groups and hydrogen from carbon chain of macromolecule. This reaction manifests itself by gradual yellowing, browning and then blackening of fibers. If there is faster heating, it leads to decomposition to acetaldehyde and crotonaldehyde

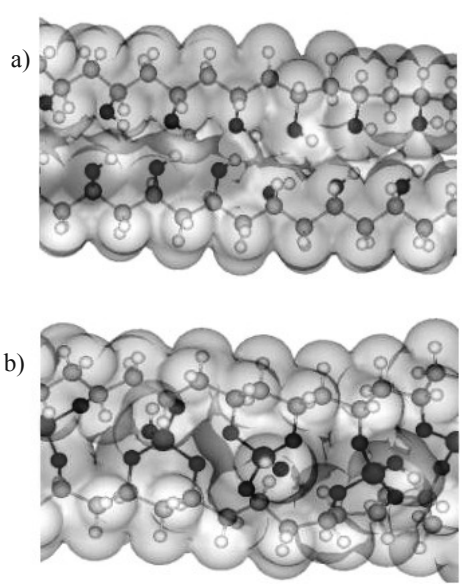

Fig. 1. **Van der Waals surface of two chains of polyvinyl alcohol a), Van der Waals surface of two polyvinyl alcohol chains cross-linked (dehydration) by phosphoric acid b)**

and whole original structure of chains can be damaged (destroyed). Polyen chains can their self each other join by means of Diels-Alder addition at careful heating and eventual catalysis, or their take place to intramolecular cycling. Created unsaturated cyclic compounds are already considerably more stable against additional increasing of temperature. An aromatization of these cycles comes into being at temperature above 450 °C, thus a basic graphite structure arises. Remains of water in the structure accelerate decomposition of structure to volatile aldehydes, accordingly usage of flame retardant catalysts is convenient for acquirement of the biggest possible carbonization gain.

Experimental part

During our experiments, we have elected following operation: (i) a producing of electrospun nanofiber web, (ii) an impregnation of web by means of combustion retarder, (iii) stabilization – dehydration at temperature and (iv) carbonization.

The nanofiber materials used in these experiments were produced at TUL and had these parameters: PVA (polyvinylalcohol) with addition of glyoxal and phosphoric acid for later cross-linking at 140 °C for 10 minutes; random orientation of fibers; surface density 5 g m^{-2}; average diameter of fibers 236 ± 79 nm. We have tested more then twenty different samples, which were created with different temperature cycles (regimes) up to 215 °C in laboratory drier with different concentrations of combustion retarders – phosphoric acid (H_3PO_4) in water solution and also we used no aqueous solutions: H_3PO_4 in ethyl alcohol, butyl alcohol and isopropyl alcohol, and $(NH_4)H_2PO_4$ in ethyl alcohol.

Carbonization of samples was accomplished in a special oven (HIP) at these conditions: inert nitrogen atmosphere, maximal temperature 1100 °C, pressure inside 5 bars, rate of temperature's growth 5 °C $min.^{-1}$.

We have studied result dehydrated nanofiber materials by means of infrared spectroscopy and DSC, we have prepared images by means of scanning electron microscope (SEM) and we have tested a result samples in the course of combustion. After carbonization, we have used the same methods for studying a result samples.

Results and conclusions

Impregnation by means of water solution: Results showed us the best samples were stabilized by regime a up to 200 °C, water solution of 1.25 % and 2.5 % by volume of H_3PO_4. These samples were after stabilization completely black, they did not burn with flame and damaging, DSC outputs did not show any changes, infrared spectrum showed a decline of OH and CH groups and creating of conjugated double C=C bonds. However the sticking of nanofibers after dehydration is visible from SEM pictures (see Fig. 2.). Impregnation by means of alcohol solutions (the best was usage of butyl alcohol) brought better results respecting the structure of resulting carbonized samples. Of course we want to produce the carbon nanofibers with large surface area, because we supposed that our carbonized electrospun polyvinylalcohol nanofiber materials could be used as adsorbent or catalysts because of the high surface density of the resulting carbon nanofiber materials. We are determined to continue the research in the branch, use other special method for detection of surface and material composition of the nanofibers after the method of carbonization.

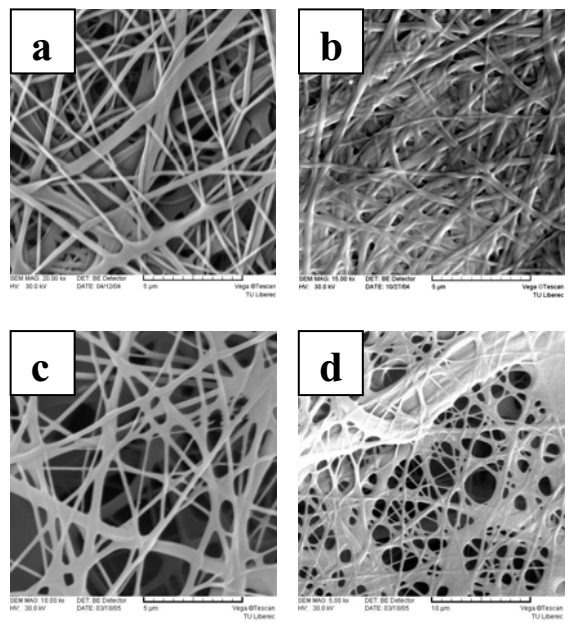

Fig. 2. **SEM images: a) Polyvinyl alcohol nanofibers; b) carbonized nanofiber webs after impregnation of 1.25 % of H_3PO_4 in water solution; (c and d) PVA nanofibers dipped to alcohols and drying at normal temperature – c) Butyl alcohol; d) Isopropyl alcohol. The scale is 5 μm at the pictures a), b) and c), 10 μm at the picture d)**

REFERENCES

1. Forhams A.: US Patent, *1*, 975, 504 (1934).
2. Jirsák O. et al.: CZ patent 2003–2414 (2003).
3. Wang Y., Furlan R., Ramos I., Santiago-Aviles J.: IEEE Transactions on Nanotechnology, *2*, 39 (2003).
4. Wang Y., Santiago S., Santiago-Aviles J. J.: Synthetic metals, *138*, 423 (2003).
5. Kim Ch., Kim Y.: Solid State Communications, *132*, 567 (2004).
6. Kim Ch., Park S., Lee W., Yang K.: Electrochimica Acta, *50*, 877 (2004).
7. Fong H.: Electrospinning and polymer nanofibers, 2004, Avaliable from: http://webpages.sdsmt.edu/~hfong/1.1.html.
8. Smolinski R.: Dissertation, University of Dortmund, Germany, 2003.

P13 FRAGILITY AND FRAGMENTATION OF BASALT FIBERS

JAN GRÉGR[b], VLADIMÍR KOVAČIČ[a] and JIŘÍ MILITKÝ[a]
[a]*Department of Textile Materials, Faculty of Textile Engineering, Technical University of Liberec, Hálkova 6, 461 17 Liberec, Czech Republic, vladimir.kovacic@vslib.cz,* [b]*Department of Chemistry, Faculty of Education, Technical University of Liberec, Hálkova 6, 461 17 Liberec, Czech Republic*

Introduction

Basalt fibers are modern reinforcing fibers suited for polymer composites. We compared basalt and glass fibers in its fragility and fragmentation – two important properties for safe handling with these fibers.

Experimental

We studied four type of basalt fibers – Old Ukraine, Basaltex, MDI experimental fibers and Kamennyj Vek. We measured fragility of fibers – ratio of critical loop diameter D and fiber diameter d. Critical loop diameter was measured by deformation of basalt loop under microscope to failure.

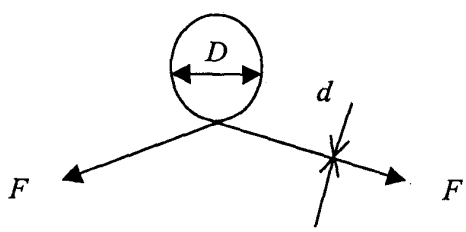

Fig. 1. **Fragility loop test for fibers**

The fragmentation was realized by the abrasion on the propeller type abrader. It was proved by microscopic analysis that basalt fibers are not split and the fragments have the cylindrical shape. Fiber fragments were analyzed by the image analysis, system LUCIA M.

Results

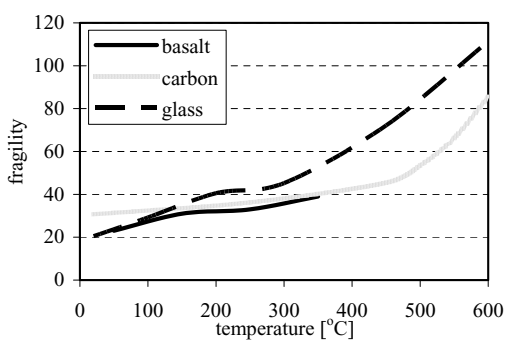

Fig. 2. **Comparison of fragility of basalt, carbon and glass fibers after high temperature treatment**

Table I
Fragility of basalt fibers at room temperature

Fiber	Fragility	Confidence limits	Fiber	Fragility	Confidence limits
Kam. Vek.2	11.94	0.68	Basaltex.275	14.69	0.52
Kam. Vek.4	13.37	0.72	Basaltex.330	9.91	0.69
Basaltex.150	14.74	0.47	MDI 2	16.71	0.88

Basic statistical characteristics of basalt fiber fragments

Table II
Length of fragments

Fibers	Basaltex	Kamennyj Vek	Old Ukraine
mean value [μm]	206.09	254.12	230.51
standard deviation	155.59	171.13	142.46
skewness	1.40	1.06	0.97
kurtosis	5.19	3.77	3.97

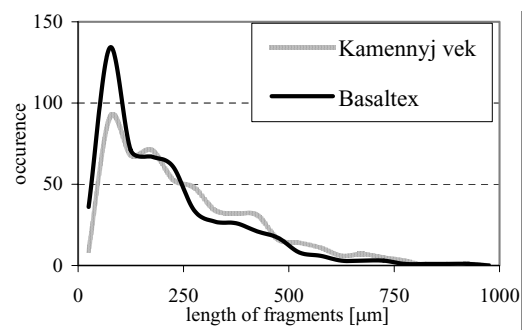

Fig. 3. **Probability of fragments lengths**

Table III
Diameters of fragments

Fibers	Basaltex	Kamennyj Vek	Old Ukraine
mean value [μm]	11.52	12.37	11.08
standard deviation	1.37	1.04	2.12
skewness	0.09	–0.21	0.64
kurtosis	2.43	2.11	2.92

Statistical parameters of fragments lengths shows that the distribution of fiber fragments is unimodal and positively skewed. Because the mean value of fiber fragment diameter is the same as diameter of no splitted fibers during the process of abrasion. It is known, that from point of view of cancer hazard the length/diameter ratio R is very important. For basalt fiber fragments is ratio:
Basaltex: 17.89 Kamennyj vek: 20.55 Old Ukraine 20.80

Mass of individual fragments is in range 8–300 ng (mean value $65 \cdot 10^{-9}$ g).

Conclusions

According to WHO, risk of cancer is for ceramic fibers with diameter lesser 3 μm, length higher 5 μm and length/diameter ratio higher 5 : 1. Basalt particle are fortunately too thick to be inspirable, but the handling of basalt fibers must be carried out with care.

This article was elaborated with support of grant No 106/05/0817 – Grant Agency Academy of Science, Czech Republic.

P14 DIFFERENT METHODS USED FOR SUPERPLASTICIZER CONTENT ANALYSIS

JOSEF KRÁTKÝ[a], JIŘÍ BRANDŠTETR[a], PAVEL ŠILER[a], EVA MAKALOUŠKOVÁ[a] and RADEK HOLEŠINSKÝ[b]
[a]*Department of Materials Chemistry, Faculty of Chemistry, Brno University of Technology, Purkyňova 118, 612 00 Brno, kratky@fch.vutbr.cz,* [b]*Výzkumný ústav stavebních hmot, a. s., JSC., Hněvkovského 65, 617 00 Brno*

Introduction

For the manufacture of the tailored concretes, the chemical modifying admixtures are used for many years. Ones of the important chemical modifying admixtures are *superplasticizers* (SP), synthetic water soluble polymers facilitating the dispersion of the mineral particles, which leads to the improved workability of the pastes and the reduction of the required amount of the mixing water[1]. Superplasticizers are used to reach and maintain the desired workability level (consistency) of the concrete, to significantly lower the water/binder ratio in mortars and concrete, to produce self-compacting and self-levelling concretes, shotcretes and other high performance concretes. More than a half century, three types of the superplasticizers was used: lignosulfonates, sulphonated naphtalene formaldehyde condensate (PNS) and sulphonated melamine formaldehyde condensate (PMS). In the last decade, the assortment was extended by the introduction of the very effective SP based on polycarboxylates (PCP). The branched structures of which are quite different from former PNS and PMS based SP[2,3].

The dominant mechanism of the particle repulsion depends on the SP composition and molecule shape. The PNS and PMS type SP mode of the particle repulsion is based primarily on the reaction of the $–OSO_2^-$ groups firstly with the positively charged surface of tricalciumaluminate ($3CaO \cdot Al_2O_3$, C_3A) or brownmilleritte ($4CaO \cdot Al_2O_3 \cdot Fe_2O_3$, C_4AF). The remaining free $–OSO_2^-$ groups bring about the electrostatic repulsion between particles with adsorbed SP molecules and negatively charged tricalciumsilicate ($3CaO \cdot SiO_2$, C_3S) or dicalciumsilicate ($2CaO \cdot SiO_2$, C_2S). PCP based SP react with the grain surface via $–COO^-$ groups and usually have long side chains, which causes the steric repulsion between mineral particles[4]. It is important to understand how superplasticizers are adsorbed on each constituent of the concrete mixture for better control over the fluidity of cement paste and concrete.

Presented work is aimed on comparison of two different methods, which can be used to determine the SP content in the solution. These techniques are useful to determine the SP remaining in the liquid phase after the adsorption of the SP on the solid particles surface. To separate the liquid phase from the reacting solid constituents of the paste, membrane filtration was used with subsequent determination of the SP content by ultraviolet and visible spectrophotometry (UV/VIS)[5,6]. The other compared technique is based on the measuring of the heat evolved during the oxidation of the SP by the $KMnO_4$ solution in acid media. Among other methods total organic carbon (TOC) determination is routinely used.

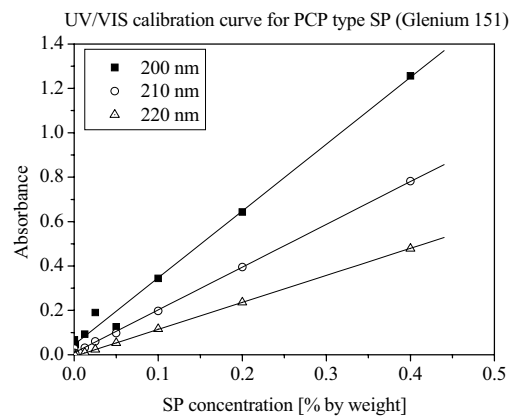

Fig. 1. **UV/VIS calibration curve for PCP type SP, measured at 200, 210 and 220 nm wavelength**

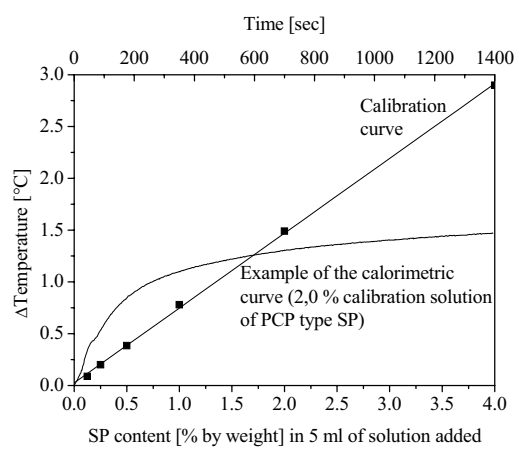

Fig. 2. **Solution calorimetry calibration curve for PCP type SP; bottom coordinates shows the dependence between temperature change and SP concentration, top coordinates document the course of the calorimetric curve for reaction of SP (in 5 cm³ of solution)**

Experimental

The calibration solutions of the different SP (containing up to SP 4 % by weight) were filtered by the 0.22 μm membrane filter. After the filtration, the *UV absorbance* was measured using three wavelengths 200, 210 and 220 nm on Varian Cary50 UV/VIS spectrometer. *Solution calorimetry*[7] method is based on the measurement of the temperature change after the addition of 5.0 cm^3 SP solution into the mixture of the 50.0 g of 0.2 M $KMnO_4$ and 50.0 g of the mixture of diluted sulphuric and phosphoric acids (70 g 96% H_2SO_4 and 90 g 85% H_3PO_3 diluted to 500 cm^3). The examples of the results are shown on Fig. 1. and 2.

Conclusions

1. The UV/VIS spectrophotometry can be used to determine the concentrations of PCP and PNS based SP in solutions. The proper wavelengths for the particular SP were determined. The solid particles must be carefully separated to assure the accuracy of the measurement.
2. The solution calorimetry method[7] can be suitably used to determine higher concentrations of PCP based SP. The PNS and PMS SP, due to their different chemical nature with aromatic rings, produce much less heat of the oxidation. The method is less sensitive to the content of the solid particles in the measured solution.

The authors wish to thank the Grant Agency of the Czech Republic for funding this research through the grant no. 104/05/P046.

REFERENCES

1. Aitcin P.-C., Jolicoeur C., MacGregor J. G.: *Concrete International: Design and Construction 5*, 45 (1994).
2. Spiratos M. P., Mailvaganam N., Malhotra V. M., Jolicoeur C.: S*uperplasticizers for Concrete*. Supplementary Cementing Materials for Sustainable Development Inc. Ottawa 2003.
3. Brandštetr J., Krátký J., Szklorzová H.: Silika *7*, 214 (2003).
4. Uchikawa H., Hanehara S., Sawaki D.: Cement and Concrete Research *1*, 37 (1997).
5. Yoshioka K., Tazawa E.-I., Kawai K., Enohata T.: Cement and Concrete Research *10*, 1507 (2002).
6. Termkhajornkit P., Nawa T.: Cement and Concrete Research *6*, 1017 (2004).
7. Brandštetr J., Krátký J., Havlica J., Pospíšil O.: Silika *22*, 177 (2002).

P15 FUNGICIDE TREATED POLYMERS USED IN TEXTILE INDUSTRY AND TESTING THEREOF

FRANTIŠEK KUČERA, JIŘINA OMELKOVÁ and ILONA HRONKOVÁ
Faculty of Chemistry, Brno University of Technology, Purkyňova 118, 612 00 Brno

Introduction

Fungi and mushrooms may destroy a whole range of products and performances. Therefore various fungicides are used for protection as external paint, in agriculture it protects seed for sowing at stocking etc. They are also used to protect crop to sponge and mildew infections and marine loads. Broad range of fungicidal agents has been found and sorted according to series of criteria. They could be sorted to several groups by the structure of additive compounds: substitute benzenes, thiokarbamate substances contain metals (copper, cadmium), organometallic, other organics fungicides.

Work is focused on testing of effectiveness of two chosen fungicidal agents in polyurethane coating, which are used for textile surface adjustment. Textiles modified by coating of polyurethane polymer are used as protective clothes, tent sail, in military etc. By most applications may the products be stored damp after being used, which may cause the growth of mildew and devaluation. Fungi and mildew may cause allergic reaction on human skin and other illnesses. Using of fungicidal agent can decrease the of possibility rise of fungi and prevent at suitable conditions for their rise. Comparison of effectiveness of couple of fungi ride agent. Second goal was to determinate the lowest suitable concentration of fungicidal agent used in polyurethane coating.

Materials

Agent A285 – is liquid fungicide, (iodine solution of alkyl ester carboxylic acids) with content 15 wt % of active substances in aqueous solution, without odor, non corrosive, non-metallic fungicidal extracts. It is intended for PVC, wooden compound and polyolefine. It is suitable for polyurethane coating, because it is thermal stable up to 200 °C.

Agent A3 – (Bayer AG, Germany), N-(dichlorfluormethylthio)phthalimide, white powder characteristic sulphur odor and it is used for fungicide coating plastics for technical applications.

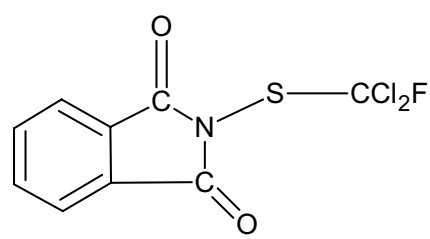

N-(dichlorfluormethylthio) phthalimide

Fungi – common, in nature prolific fungi were used to testing. Spats of fungi can attack clothes stored in dampness. Cultures fungi originate from the Collections of microorganisms MU Brno:

F 431 *Penicillium rogneforti*
F 445 *Rhizopus stolonifer*
F 8189 *Aspergillus niger*
F 314 *Botrytis cinerea*
F 503 *Fusarium avenaceum*
F 443 *Mucor plumbeus*

Textile – polyester fabrics MAYTEX (Liptovsky Mikulas, SR), specific weight 70–76 g m^{-2}.

Experimental part

The effectiveness of single fungicidal agent was tested with their solutions in acetone. Antifungal effect was monitored after application of agents to the coating textile with specific amount of fungicidal agent. The optimalization of fungicide concentration in product was carried out.

Specimen preparation:

Prepared solution (Agent A285, Agent A3 or acetone – blank experiment) was pipetted 0.1 cm^3 into prepared sampling seats. The quantity of A285 was calculated on the content of an active fungicidal substance of concentration. For checking the effectiveness of fungicidal reagent was the test performed twice. Samples were observed in seven – day intervals as long as it happened to observable changes. Reproduce of effectives of fungicidal activity on the concentration of fungicidal agent was determined to optimalization of ratio effect, price of treatment.

Table I
Stock solution for experiment 1

Fungicide agent	Weight of fungicide agent [g]	Volume of acetone [ml]
Agent A285	0.3891	1.0
Agent A3	0.0526	1.0
acetone	0.0000	1.0

Table II
Composition of blend mixture for preparation coating with fungicide reagent for experiment 2

Fungicide reagent	Weight of fungicide reagent [g]	Desmodur [g]	Estane [g]	Concentration of active component [wt %]
Agent A285	1.7578	0.9	29.7	0.81
Agent A3	0.1666	0.9	30.2	0.53
–	0.0000	0.9	30.1	0.00

Polyester polyole Estane 5735P was dissolved in acetone to 25% solution in closed vessel by mixing for 24 hours. Isocyanate Desmodur L75 in concentration from 4 to 15 wt % was added to the prepared solution of store. The prepared solution of polyurethane system was applied to textile using coating machine Inotex LZ-01. The couples of coated textile were over using hot-air gun Steinel Thermocontrol at temperature 110–130 °C.

Table III
Composition of preparation coating with fungicide, reagent for experiment 2 with Agent A285 of different specific concentrations for experiment 3

Concentration of fungicide agent	Weight of fungicide reagent [g]	Desmodur [g]	Estane [g]
1 wt%	0.1864	0.9	30.30
3 wt%	0.5543	0.9	29.18
5 wt%	0.9010	0.9	31.46
7 wt%	1.7723	0.9	29.17

Methods for effectiveness of fungicidal additives testing

The experiment classification was compiled by time monitoring the growing range of fungi and metering sizes of inhibition zone. A distance of fungus from the edgings of sample place was measured repeat by and resulting distance was obtained as an arithmetic mean of measured values. Classification is shown on applied Fig. 1.

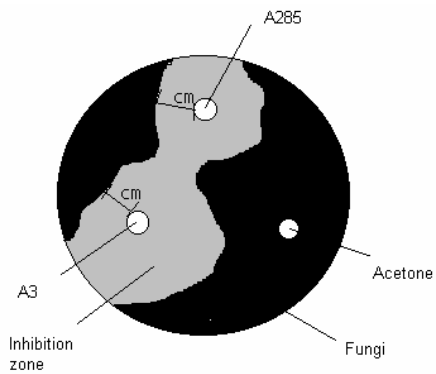

Fig. 1. **Method of testing of fungicidal agents**

Results and discussion

The growth of fungi was watched in several – day intervals. Perceptible difference among sizes of inhibitive zones of used fungicidal agent was observed in seventh day. Quarters, to which was poured pure acetone, there are rot totally scrubby. Blank experiment was done for confirmation that only acetone can not caused any fungicidal influence. Inhibition zone of Agent A3 is smaller than inhibitory zone arisen out Agent A285 at of all six used fungi.

Table IV
Experiment 1 – testing of fungicidal reagents dissolved in acetone – 7th day of observation

Agent	Fungi					
	F 431	F 443	F 445	F 8189	F 314	F 503
Agent A285	3.0	1.8	1.0	3.5	0.5	1.5
Agent A3	0.5	0.3	–	0.5	–	0.2
Acetone	0	0	0	0	0	0
	Size of the inhibition zone [cm]					

Table V
Experiment 2 – testing reagent in coating – 9th day observation

Agent	Fungi					
	F 431	F 443	F 445	F 8189	F 314	F 503
Agent I	0.1	0.1	–	0.3	–	0.2
Agent II	0.3	0.1	–	0.3	–	–
Acetone	0	0	0	0	0	0
	Size of the inhibition zone [cm]					

The effectiveness of agents in coating is less perceptible compare with higher concentration of pure fungicidal agent. Their mobility of coating is in coating affected by cross linked polyurethane matrix. Textile with untreated coating was covered by fungi in all experiments. Textiles powered by coating with agent damage only fungi F 314 and F 445 when fungi overgrew the whole Petri dish.

The concentration influence of Agent A285 was monitored on size of inhibitory zone for each fungus. From results of experiments 2 and 3 is evident that in the case of Agent A285 is more effective fungicidal reagent than in the case of Agent A3. Therefore other experiments were performed only with Agent A285.

Table VI
Experiment 3 – various specific concentrations of Agent A285 in coating – 2nd day of observation

wt %	Fungi		
	F 8189	F 431	F 443
1 wt %	1.0	1.5	0
3 wt %	1.5	1.5	0
5 wt %	2.0	2.0	0
7 wt %	2.0	2.0	0.5
	Size of the inhibition zone [cm]		

Three incident fungi were performed for experiment. From 1 wt % used reagent is his influence observable already. 100% effectiveness is reached from 5 wt % and higher. Mounting concentration of the used fungicidal reagent does not changed over 5 wt % the effectiveness and concentration 5 wt % can be selected as optimal.

Conclusion

Confrontation of two chosen fungicidal reagents I and II was performed in experiment 1. Agent A285 is more effective in the most tests at comparable concentrations of active substances. Comparison of fungicidal reagents in coating was performed in experiment 2. Agent A285 is again more effective from measured inhibitory zones. Therefore the influence of concentration of Agent A285 on the size of inhibitory zone was watched for the single cultures fungi. Concentration 5 wt % was intended as optimum specific concentration. Fungi grow the edgings of textile at lower concentration and she didn't cause visible changes in sizes of the inhibitory zone at higher concentration the solution.

REFERENCES

1. Pritchard G.: *Plastics additives*, Champan & Hall, London (1998).
2. Kostolaninova V.: *Textile and Chemistry* (1992).
3. Flink E. W.: *Fungicides, biocides and preservatives for Industrial and Agricultural Applications*, New Jersey (1987).

P16 THERMAL STABILITY OF $SIO_XC_YH_Z$ FILMS PREPARED BY PECVD

ZUZANA KUČEROVÁ[a], VILMA BURŠÍKOVÁ[a], LENKA ZAJÍČKOVÁ[a], JANA FRANCLOVÁ[a] and VRATISLAV PEŘINA[b]

[a]*Department of Physical Electronics, Faculty of Science, Masaryk University, Kotlarska 2, 611 37 Brno, zus@physics.muni.cz,* [b]*Institute of Nuclear Physics, Czech Academy of Sciences, 250 68 Rez.*

Annealing experiments carried out on a plasma polymerised organosilicon coatings revealed certain changes in film structure and composition. These changes includes mainly water and hydrogen desorption, which leads to a removal of SiH and SiOH bonds from the films and to the significant increase in silicon-oxygen bonds. These results were obtained by RBS/ERDA analysis, FTIR spectroscopy and TDS analysis. Annealed films were determined by various characterisation methods (optical properties by the means of spectroscopic ellipsometry, mechanical properties by depth sensing indentation test) in order to find out how the film properties are influenced by the thermaly effected structural changes.

Introduction

Compared to other deposition techniques the main advantage of the plasma enhanced CVD (PECVD) seems to be the low temperature of the discharge (even below 100 °C). This fact makes PECVD a very powerfull tool especially for coatings of polymer materials. Nevertheless, this is not the only benefit of PECVD. It also enables to change the deposition conditions in a wide range and to prepare films of desired properties. The mechanical behaviour of films prepared by PECVD are, in general, significantly better than their counterparts fabricated by other methods, e. g. physical vapour deposition. Even more important is the fact, that PECVD seems to be a good choice from the environmental point of view as it does not produce any toxical byproducts. In case of protective coatings the thermomechanical stability plays a crucial role for their technological applications. In the present work, a large set of coatings were prepared from HMDSO/O_2 mixtures at a wide range of deposition condition in order to study their properties and thermomechanical stability.

Experimental

Thin films were prepared on silicon substrates from hexamethyldisiloxane HMDSO ($Si_2OC_6H_{18}$) and HMDSO/O_2 mixtures by PECVD in reactor with parallel plate electrodes. The r. f. generator PG 501 (13.56 MHz) was capacitively coupled to the bottom electrode serving also as a substrate holder. Due to the coupling and different mobility of electrons and ions its potential was a sum of r. f.voltage and d. c. self-bias. Before every deposition the substrates were treated 5 min in argon or oxygen discharges using the power of 100 W. For the deposition the flow rate of HMDSO (Q_{HMDSO}) was fixed at 4 sccm and the flow rate of O_2 (Q_{O2}) varied from 0 to 45 sccm. Deposition time was 7 min. The gasses were fed into the reactor through the upper grounded showerhead electrode. The pressure in the reactor was in the range from 1 to 32 Pa depending on the oxygen flow rate. The r.f. power used for the deposition varied from 100 to 450 W. The films were annealed for 60 min in a laboratory furnace Classic Clare 4.0 evacuated by turbomolecular pump. A new as-deposited film was always used for every given maximum annealing temperature that varied in the range from 100 to 500 °C.

Results and discussion

F i l m c o m p o s i t i o n

According to results of combined Rutheford Backscattering Spectroscopy and Elastic Recall Detection Analysis (RBS+ERDA), the prepared films should be described as $SiO_xC_yH_z$. Atomic percentages varied with deposition conditions from polymer films, which can be prepared at low powers and at low Q_{O2} (e.g. $SiO_{0.7}C_{1.2}H_{3.4}$, for P = 100 W and pure HMDSO) to SiO_2-like films prepared at higher powers and with higher amount of O_2 e. g. $SiO_{2.1}C_{0.2}H_{1.1}$ for P = 450 W and Q_{O2} = 45 sccm). The temperature induced changes in atomic composition carried out using RBS+ERDA in case of annealed films are summarized in Table I. The O/Si ratio shows similar behaviour at all deposition conditions. The O/Si ratios in case of films annealed up to 300 °C are significantly lower, than those in case of as-deposited films. On the other hand, at 500 °C slightly increased. This could be explained with the help of thermal desorption spectroscopy measurements (TDS). From Fig. 1. could be seen that the main outflux from the film is caused by water up to the temperature of 320 °C. There the water outflux reaches its peak and rapidly decreases. At the higher temperatures the hydrogen desorption took place from the film.

Table I
Dependence of the atomic composition on the deposition conditions and on the annealing temperature

	100 W			450 W		
			20 sccm			
T [°C]	0	300	500	0	300	500
O/Si	1.99	1.68	1.71	1.84	1.79	1.99
C/Si	0.85	0.81	0.64	0.55	0.57	0.57
H/Si	2.31	1.88	1.57	1.60	1.37	1.01
(O+H)/Si	4.31	3.56	3.27	3.45	3.17	3.00
			45 sccm			
O/Si	1.92	1.68	1.90	2.12	1.92	1.93
C/Si	0.66	0.57	0.51	0.24	0.29	0.21
H/Si	1.26	1.33	1.32	1.12	0.81	0.55
(O+H)/Si	3.17	3.10	3.22	3.24	2.75	2.49

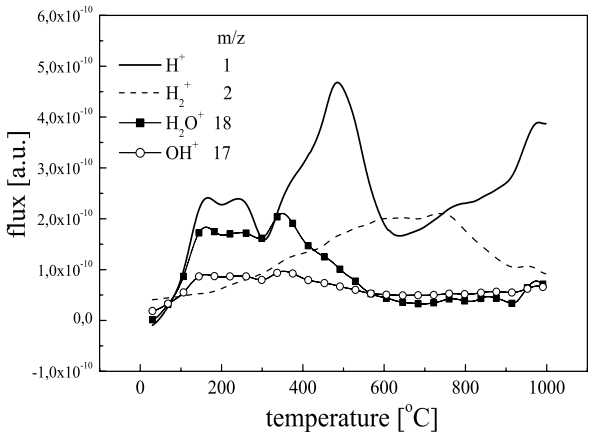

Fig. 1. **Thermal desorption from the film prepared at P = 450 W, Q_{O2} = 20 sccm**

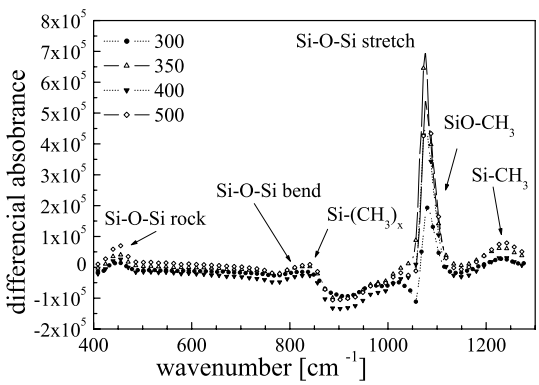

Fig. 2. **Differential absorbance of annealed films with respect to as-deposited film (P = 450 W, Q_{O2} = 45 sccm)**

In the FTIR spectra of as-deposited film peaks correlated to –OH bonds were revealed. Namely Si–OH at aprox 920 cm^{-1} and broad bands centred at the wavenumber of 3650 cm^{-1} correlated with bending of OH in Si–OH, ovelaped by broad band of H–OH centred at the 3450 cm^{-1}. These peaks are not observed in the spectra of annealed film which is in good agreement with above discussed RBS+ERDA and TDS results. The same applyes to the Si-H stretching peak between 2100 and 2300 cm^{-1}. Further three main peaks associated with Si–O–Si bond may be spotted. It is the rocking, bending and network vibration (stretching) at the wawenumbers of 450 cm^{-1}, 830 cm^{-1} and 1070 cm^{-1}, respectively. These peaks exhibit an increase with the insreasing temperature which also correlates with the RBE results. In order to visualize the changes in spectra of annealed samples, the spectrum of the as-deposited film was subtracted from the spectra of annealed samples. These differential absorbance is plotted on Fig. 2. Si–CH_x correlated peaks (i. e. Si–CH_3 rock. and Si–CH_3 stretch. at approx. 790–815 cm^{-1}, Si–$(CH_3)_3$ rock. at approx. 840 cm^{-1} and Si–$(CH_3)_2$ rock. at 870–890 cm^{-1} as well as symetric deformation of Si–$(CH_3)_{1,2,3}$ at the 1250 cm^{-1}) are not influenced by thermal annealing very much. Therfore it seems that the water desorption happens to be the main effect of thermal annealing on $SiO_xC_yH_z$ and an equation 1. could be written.

$$\equiv Si–OH + HO–Si\equiv \rightarrow \equiv Si–O–Si\equiv + H_2O \qquad (1)$$

F i l m p r o p e r t i e s

Optical properties of as-deposited as well as annealed films were studied as a function of oxygen flow rate and of power. Refractive index is increasing with increasing power for all oxygen flow rates used and this tendency is observed also on annealed films. Dependence of refractive index (λ = 633 nm) on oxygen flow rate is plotted on Fig. 3. The more inorganic the film is, the lower refractive index. Although plotted just for the r. f. power of 200 W, same tendencies were observed also at the other powers, even if the differences are more significant at the lower powers. Annealed films also exhibited changes in refractive index.

The refractive index decresed with increasing annealing temperature. The difference in refractive index of as-deposited and annealed sample was again more significant for films prepared at lower powers.

The mechanical properties of as-deposited films were significantely improved by the thermal annealing. As-deposited film were brittle, due to the high amount of hydroxyl groups bonded to silicon. After removal of these groups fracture thoughness of annealed films was higher and even increased with increasing temperature as well as hardness, elastic modulus.

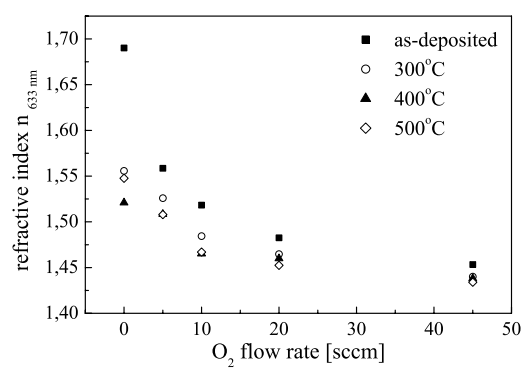

Fig. 3. **Dependence of refractive index at wavelength of λ = 633 nm on oxygen flow rate**

Conclusion

A large series of $SiO_xC_yH_z$ coatings were prepared in the wide range of deposition conditions from HMDSO and HMDSO/O_2 mixtures. This set of coatings underwent a thermal annealing in temperature range from 100 °C to 500 °C in order to study their composition and structure. Annealed films were studied by various characterization methods and correlations between thermally effective changes and film properties were found. RBS and FTIR experiments revealed increase in Si–O–Si bonds and the decrease of –OH bonds that mean water desorption from films. It leads to decrease of refractive index and to improvement of mechanical properties.

This work was supported by grant of Ministry of Education MSM 0021622411 by the ASCR project K1010104.

REFERENCES

1. Zajíčková L., Buršíková V., Peřina V., Macková A., Subedi D., Janča J. and Smirnov S.: Surface and Coatings Tech., *449*, (2001).
2. Franclová J., Kučerová Z., Buršíková V., Zajíčková, Peřina V.: Czech Journal of Physics *54*, C847 (2004).

P17 INFLUENCE OF WASTE, SECONDARY AND NATURAL RAW MATERIALS ON TECHNOLOGICAL PROPERTIES OF PORTLAND CEMENT

RADOVAN NEČAS, HALINA SZKLORZOVÁ, THEODOR STANĚK and VLADIMÍR TĚHNÍK
Výzkumný ústav stavebních hmot, a. s., Hněvkovského 65, 617 00 Brno, Czech Republic, necas@vustah.cz

Introduction

Materials applicable as components into cement blends can be various industrial wastes or non-traditional natural raw materials, which have never been used for this purpose before or have never been used in any other branch so far and show favorable influence on properties of final cement mixture. When applied they either give some specific features to cement and mortar (e. g. latent hydraulic – pozzolana activity, improvement of rheology, consistency and workability, compaction of microstructure and thus improvement of water impermeability and resistance to chemical corrosion and strength enhancement) or reduce the consumption of Portland clinker in cement blends. Out of waste materials, these can be various fly ashes, fluidized bed coal combustion wastes, slag, mine refuses, sludge, tailing rocks, mine spoils, and other rocks and minerals hard to utilize, received as side products at rocks and minerals mining and treatment[1].

The aim of this work was to compare the properties of blended cements with those of pure Portland cement. Consistency of cement pastes, setting process, development of hydration heat, and strength of cement mortar were subjects of the measurements and observations. Results of this work indicate possibility of utilization of some non-traditional materials as components for cement binders.

Results and discussion

Based on analyses carried out to characterize particular samples of non-traditional materials[2] (chemical analysis, petrographic description, X-ray diffraction analysis, differential thermal analysis, sieve analysis, density and specific surface assessment, determination of latent (pozzolana) hydraulic activity and for slag determination of glassiness), 26 samples in total were selected for further experiments. These samples were ground to the residue of 2 % on sieve with mesh of 0.090 mm and mixed with cement CEM I 42.5R Hranice in a ratio of 1/3 by weight, respectively. The mixtures were examined to obtain following technological properties such as consistency, the start and period of setting, the setting process measured by Tussenbrock method, and hydration process, recorded on adiabatic and differential calorimeters. The compressive and flexural strengths of the specimens were measured.

Heat generation during hydration process of cement blends

We are able to predict the development of strength in cement, concrete, and mortar according to the amount of heat generated during hydration process. The optimization of hydration heat generated during setting is very important in massive constructions, where the insufficient heat transfer can cause overheating, followed by fracture of construction. The heat, generated during hydration processes of the samples was determined from two different ways of measurement:
The first one uses *adiabatic calorimeter*, which records changes of the temperature as consequence of chemical reactions running in cement and mortar mixtures during hydration process. Sample of fresh cement mixture is placed into a reaction container equipped with a moisture-proof lid and this is placed into a metal box with wire winding for heat induction. The temperature sensor is placed into the sample. All measurements were carried out in isoperibolical mode at constant temperature of the metal box of 35 °C for 24 hours. The maximum temperature of hydration, $T_{max.}$ in °C, and time of hydration, $t_{max.}$ in hours, are used for the hydration heat evaluation.
The second way uses *differential calorimeter*, which complements the above described method and enables to observe thermal effects, appearing immediately after the mixing of cement with water within the first seconds until a few hours. The increase of temperature at very early stage of reaction is caused by dissolving clinker minerals and setting regulator (gypsum) and their interaction, which gives formation of hydration products, e. g. ettringite.

Sample of cement and required amount of water are placed into thermally isolated (adiabatic) container with standard and the whole system is left for temperature stabilization. Water is mixed into the sample after stabilization and the temperature difference between the sample and the standard during reaction is measured.

The hydration process is characterized by hydration curve or it is evaluated by temperature difference, ΔT_{max}, in time, $t_{max.}$ in min.

The results of obtained technological properties are listed in Table I.

Index of hydraulic activity

The index of hydraulic activity was modified from the CSN EN 450 standard, which defines the index of hydraulic activity for fly ash in concrete as the ratio of compressive strength of specimen prepared from 75 wt. % of reference cement and 25 wt. % of fly ash to compressive strength of

Table I
Technological properties of selected non-traditional materials

Sample	Mix.	Setting [h:min] beg./end.	Standard Consist. [w/c]	Adiabat. calorimetr [°C/h]	Different. calorimeter [Δ°C/min]
Ref. CEM I 42.5 R Hranice	REF	2:40/5:00	0.27	62.53/7.2	2.025/6.0
Fly ash Dětmarovice	T-P1	4:10/5:10	0.27	51.86/8.6	1.925/6.0
Fly ash Mělník II	T-P5	4:00/5:30	0.28	50.17/8.5	2.075/4.5
Fly ash Prunéřov	T-P7	3:30/4:10	0.31	52.09/7.7	2.475/5.5
Fly ash Tušimice	T-P8	4:00/5:20	0.29	48.06/8.4	1.675/7.0
Fluidized ash Třinec lože	T-P9	3:30/5:30	0.35	50.83/7.8	2.200/4.5
Fluidized ash Třinec filtr	T-P10	4:00/5:40	0.32	49.51/8.0	2.125/5.5
Fluidized ash Tisová	T-P16	2:40/3:30	0.29	60.35/7.0	3.150/6.0
Granul. blast fur. slag NH	T-S1	3:50/4:50	0.27	53.17/7.8	1.900/5.0
Martin slag Třinec 4-8	T-S4	4:30/5:40	0.26	47.3/11.5	2.225/5.0
Martin slag Třinec 8-16	T-S5	4:10/5:10	0.26	49.6/10.2	2.100/6.0
Foundry slag Královopolská	T-S6	6:10/9:30	0.27	41.3/23.1	2.175/5.0
Heap slag Zetor	T-S7	3:50/5:10	0.30	54.46/7.9	1.975/4.5
Water treat.sludge Lachema	T-O1	4:40/6:40	0.32	49.59/9.0	2.375/5.0
Red mud Žiar nad Hronom	T-O2	2:20/3:50	0.30	51.24/6.5	3.125/4.5
Microsilica Šumperk	T-O4	3:10/4:20	0.43	53.99/6.9	1.650/5.5
Silica fume Mníšek p.Brdy	T-O5	4:00/6:40	0.60	51.47/7.7	1.00/10.5
Burnt shale Nové Strašecí	T-O6	5:50/7:30	0.30	53.54/9.7	2.325/4.0
Ni product. sludge Sereď	T-O9	3:00/5:00	0.27	53.59/7.5	2.150/5.5
Siliceous earth Borovany	T-H4	3:10/3:50	0.38	52.75/6.0	2.225/6.0
Arenaceous marl N.Strašecí	T-H5	2:40/4:30	0,33	52.75/6.8	2.550/4.5
Kaolin Nové Strašecí	T-H6	5:10/8:50	0.37	54.08/8.1	1.825/5.5
Shale Horní Benešov	T-H10	3:40/5:10	0.33	55.33/7.3	1.875/4.5
AndesiteVacíkov	T-H14	3:20/5:00	0.30	54.35/7.8	1.875/4.0
Zeolite Nižný Hrabovec	T-H15	2:20/4:40	0.37	45.17/6.2	2.800/6.0
Chert Nikolčice	T-H16	3:20/6:20	0.30	45.25/9.2	2.025/5.5
Pearlitic rhyolite Lehôtka	T-H17	3:00/5:10	0.30	54.01/7.9	1.950/5.0

standard mortar specimen prepared from only pure cement. The CEM I 42.5 is prescribed as standard.

For our purpose, the index of hydraulic activity for flexural strength and for other waste and non-traditional materials as components into cement blends has also been calculated. The results of the hydraulic activity indexes are exhibited in Fig. 1.

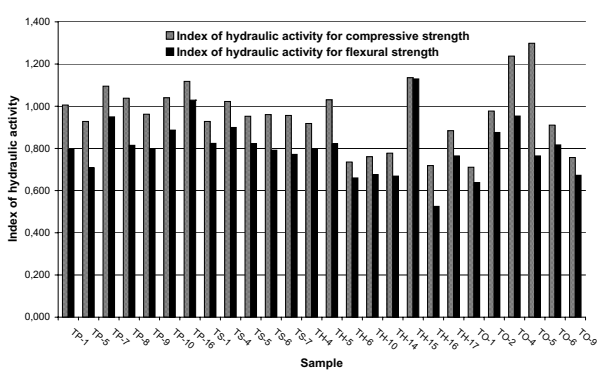

Fig. 1. **Index of hydraulic activity for compressive and flexural strength for samples aged 56 days**

Setting process by Tussenbrock

The principle of this method consists in determination of the consistency of setting cement paste in time by measurement of the depth of submersion of 6 probes of different diameter stabbing into it. The depth of submersion indicates the threshold of shearing stress (in kPa) which corresponds to the consistency achieved in the moment of measurement. The results of setting processes obtained from Tussenbrock measurement are shown in Fig. 2.

Conclusion

Based on experimental results obtained so far and presented, we can conclude that some of the tested non-traditional raw materials seem to be perspective as the components into cement blends. The examinations of other properties of prepared cement blends continue currently and lead to optimization of dosage of selected components into the cement mixtures.

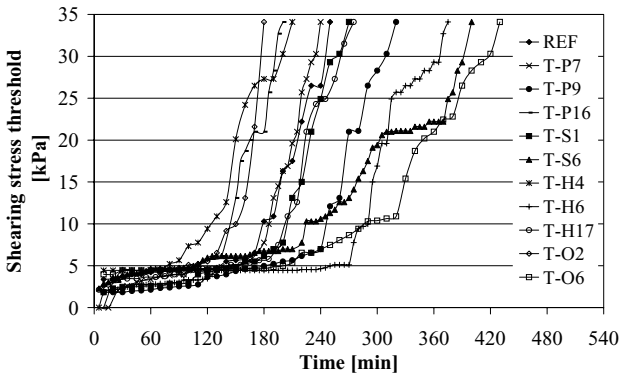

Fig. 2. **Change of consistency – setting process by Tussenbrock for selected samples**

This work was supported by the Ministry of Industry and Trade of Czech Republic, project No: FT-TA/020.

REFERENCES

1. Nečas R., Szklorzová H., Staněk T., Těhník V.: *Influence of Selected Non-traditiona Raw Materials on Technological Properties of Portland Cement*, IXth Conference "Ecology and New Building Materials and Products" – proceedings, VUSTAH, Telč, 2005
2. Staněk T., Nečas R.: *Properties of non-traditional raw materials and evaluating their applicability in cement production*. Annual report from the project being solved under the TANDEM program – project No. FT-TA/020, Brno (2004).

P18 PREPARATION OF WASTE RUBBER-GEOPOLYMER COMPOSITE MATERIAL

ONDŘEJ SKOBA[a], VRATISLAV BEDNAŘÍK[a], MILAN VONDRUŠKA[a], ROMAN SLAVÍK[a] and TOMÁŠ HANZLÍČEK[b]

[a]Tomas Bata University in Zlín, Department Of Environmental Protection Engineering, Náměstí T. G. M. 275, 762 72 Zlin, Czech Republic, skoba@ft.utb.cz, [b]Academy of Sciences of the Czech Republic, Institute of Rock Structure and Mechanics, V Holesovickach 41, 182 09 Prague, Czech Republic

Introduction

Per year amount of waste tyres in 2000 was more than 40 000 tons in Czech Republic[1] and more than 2 500 000 tons in EU[2]. Almost 40 % of them were deposited in landfills[1,2]. According to "EU directive 99/31/EC on the landfill of waste", landfilling of whole tyres has been prohibited since 2003 and landfilling of tyre-shreds will be prohibited from 2006. One of the possibilities of waste tyres reuse is their material recycling. The object of this work is to solidify waste tyre-shreds into geopolymeric matrix to gain technically applicable material.

Geopolymers are inorganic polymers. They are becoming very popular due to their properties. Geopolymers are fire-resistant (excellent fire resistance up to 1200 °C)[3], their compressive strength is about 20 MPa after only 4 hours of setting and between 80–100 MPa after complete hardening (about 1 month). Emissions of CO_2 during their manufacturing are five times lower compared to concrete[4].

The term geopolymer was first used by Davidovits[5] to describe family of silico-aluminate binders. These polymers consist of Al–O–Si framework that is similar to zeolites. The main difference between zeolites and geopolymers is amorphous or semicrystaline structure of geopolymers compared to highly crystalline structure of zeolites. The synthesis of geopolymers takes place by polycondensation of silico-aluminates. The reaction is co-polymeration of the individual alumino and silicate species, which are formed by dissolution of silica and alumina contained in source materials at a high pH in the presence of soluble alkali metal silicates[5,6].

Materials and methods

As a raw material for geopolymer synthesis was used clay, which is by-product from washing of glass sand. Sodium silicate, sodium hydroxide, distilled water and activated clay was mixed together in ratios according to literature[7,8]. Waste tyre-shreds from tyre retreading were used for experiments. Their particle size was between 10 μm–3 cm. Specimens made of either non-separeted tyre-shreds or tyre-shreds particles smaller than 0.9 mm were prepared. The content of tyre shreds in both cases varied from 0 to 40 % (v/v).

Reaction mixtures were poured into molds and closed into PE bags, where they were left for 7 days to harden. After that, the hardened specimens were took out and left for 3 days under laboratory conditions to dry.

Prepared specimens were used for leaching tests in distilled water and 0.1 M HCl. The liquid:solid ratio was 10 : 1 in both cases, the extraction period was 24 hours. The overview of the received leachates is shown in Table I.

Table I
Leachates of rubber-geopolymer composite specimens

Extraction liquid	Size of tyre-shreds	Symbol used for the leachetes
0.1 M HCl	Non separated	A
0.1 M HCl	Smaller than 0.9 mm	B
H_2O	Non separated	C
H_2O	Smaller than 0.9 mm	D

The leachates were characterized by measurement of conductivity and pH values and Zn content (AAS method; concentration of zinc in the leachate was measured due to the application of ZnO during the rubber production). The

specimens were assessed by water absorbability determination (weighing of dry and water saturated specimens).

Results

Values of pH are shown in Fig. 1. and ranges between 10.96 and 11.53 in case of leaching in distilled water and between 2.10 and 3.27 in case of leaching in 0.1 M HCl. There is no significant trend in dependence of pH on amount of tyre-shreds.

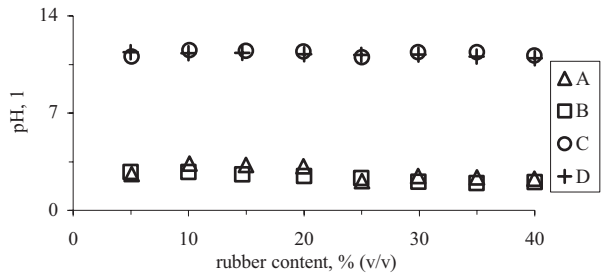

Fig. 1. **Dependence of pH values of specimen leachates on rubber content in the specimen**

Conductivity of leachates is shown in Fig. 2. While the conductivity of C leachates is decreasing with the higher amount of tyre-shreds (except sample with 5 vol. % of shreds), the other leachates (A, B, D) show no trend in dependence on amount of tyre-shreds. Conductivity ranges from 10.40 mS cm^{-1} to 13.5 mS cm^{-1} in 0.1 M HCl leachates and from 1.48 mS cm^{-1} to 4.18 mS cm^{-1} in distilled water leachates.

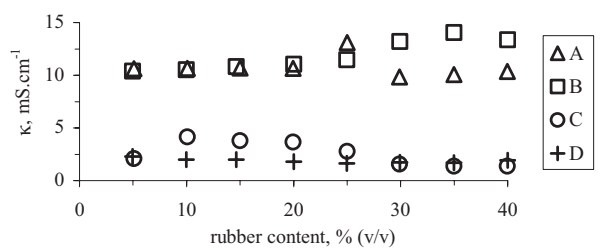

Fig. 2. **Dependence of conductivity values of specimen leachates on rubber content in the specimen**

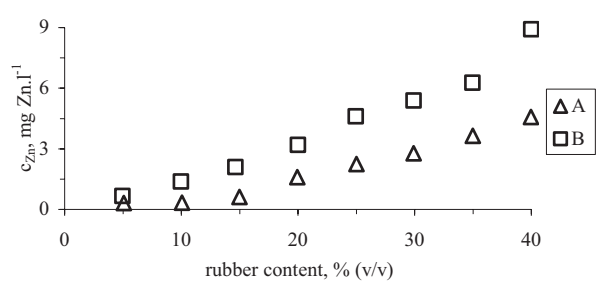

Fig. 3. **Dependence of Zn concentration in leachates on rubber content in the specimen**

Concentration of Zn in 0.1M HCl leachate is shown in Fig. 3. It increases with increasing rubber content from 0.318 mg dm^{-3} to 4.580 mg dm^{-3} for samples with non-separated tyre-shreds and from 0.664 mg dm^{-3} to 8.910 mg dm^{-3} for specimens with tyre-shreds with size under 0.9 mm.

Concentration of Zn in aqueous leachates was under the limit of detection, pH and conductivity values met the regulatory levels for inert waste.

Water absorbability decreases from 30 % (v/w) to 19 % (v/w) and is shown if Fig. 4.

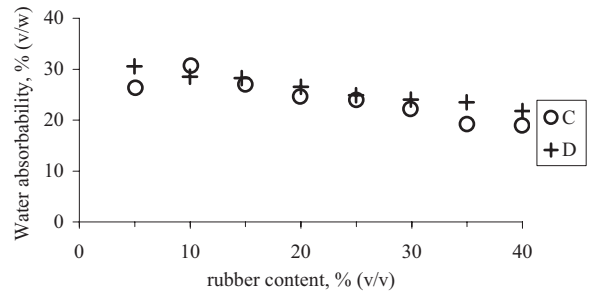

Fig. 4. **Dependence of water absorbability of specimens on rubber content in the specimen**

Samples with higher amount of tyre-shreds (35 and 40 vol. %) do not have smooth surface. It is caused by high viscosity of their mixture and consequently with their difficult transfer into the molds.

Conclusion

Specimens of rubber-geopolymer composite were prepared from tyre-shreds. Waste rubber in amount 5–30 vol. % can be used for manufacture of this composite material. Rubber content higher than 30 % (v/v) lowers workability of mixture during preparation and causes problems with molding. Prepared specimens were tested by leaching tests in water and in 0.1 M HCl. All the observed parameters met the regulatory levels for inert waste. The material is resistant to water and also to acid. It is assumed that the prepared composite rubber-geopolymer could be used in different technical applications.

Financial support for this study was provided by the Ministry of Education of Czech Republic (Project No. MSM 7088352101).

REFERENCES

1. ECO trend s. r. o.: *Research report*. Praha, Czech Republic, 2004.
2. Shulman V.: *11th Annual ETRA Conference on Tyre Recycling,* Brusels, 2004.
3. Davidovits J.: *Proceedings of Second International Conference Géopolymére '99* (Davidovits J., Davidovits R., James C., ed.), p. 165. Institut Géopolymére, Saint-Quentin 1999.
4. Davidovits J.: World Res. Rev. *6*, 263 (1994).

5. Davidovits J.: *Proceedings of First European Conference on Soft Mineralurgy* (Davidovits J., Orlinsky J., ed.), Vol. 1, p. 25. Geopolymer Institut, Compiegne 1988.
6. van Jaarsveld J. G. S., van Deventer J. S. J., Lorenzen L.: Miner. Eng. *10*, 659 (1997).
7. Davidovits J., Davidovits M., Davidovits N.: US patent 5,342,595.
8. Davidovits N., Davidovics M., Davidovits J.: US patent 4,888,311.

P19 PROOF OF SODALITE STRUCTURES IN GEOPOLYMERS

ROMAN SLAVÍK[a], VRATISLAV BEDNAŘÍK[a], MILAN VONDRUŠKA[a], ONDŘEJ SKOBA[a], and TOMÁŠ HANZLÍČEK[b]
[a]*Tomas Bata University in Zlin, Department of Environmental Protection Engineering, 762 72 Zlin, Czech Republic, slavik@post.cz,* [b]*Academy of Sciences of the Czech Republic, Institute of Rock Structure and Mechanics, V Holesovickach 41, 182 09 Prague, Czech Republic*

Introduction

Geopolymers are amorphous three-dimensional aluminosilicate materials with ceramic-like properties but which are synthesized and hardened at ambient pressure and temperature[1]. Polymerization occurs under highly alkaline conditions, when reactive aluminosilicate materials are rapidly dissolved and free [SiO_4] and [AlO_4] tetrahedral units are released into solution. During the reaction, water is gradually split out and the tetrahedral units are alternatively linked to polymeric precursors by sharing oxygen atoms between two tetrahedral units and thereby forming amorphous geopolymers[2]. It is known[1,2] that structure of some geopolymers is similar to that of sodalite, which is a natural zeolite with characteristic cubooctahedral unit.

Natural zeolite ultramarine has also sodalite structure and it is characteristic with its blue color. Presence of chromophore anionic radicals S_3^-, which are closed in cubooctahedral units of sodalite, causes the blue color of ultramarine. Presence of anionic chromophore radicals S_2^- cause yellow color and bring about green color of some types of ultramarine[3,4,5].

We suppose that addition of polysulphide solution to geopolymer should change its color if sodalite structure is present. The presented work is focused on verifying of this hypothesis.

Experimental

Preparation of polysulphide solution

Pulverous sulphur (p. a.) was added to the water solution of $Na_2S \cdot 9H_2O$ (p. a.) in molar ratio 4:1. Color of the solution has been changed from colorless to red-orange. The prepared polysulphide solution has been preserved in closed plastic bottle.

Preparation of Geopolymers

Two different geopolymers have been prepared from materials as follows: SiO_2 (Ultrasil VN3PD, Plastservis), Al_2O_3 (Brockmann's for chromatography, neutral), solid NaOH (p. a.), distilled water, water glass (composition is in Table I), raw clay material S-N (composition is in Table I).

Table I
Chemical composition of raw material S-N and water glass

Composition* of raw clay material S-N [%] (w/w)			
SiO_2	28.7	TiO_2	0.29
Al_2O_3	22.6	K_2O	0.16
Fe_2O_3	0.1	LOI	6.6
CaO	0.15	Total	88.45
Composition of water glass [%] (w/w)**			
SiO_2	31.22	Na_2O	10.96
H_2O	57.82		

* determined by XRF method
** data of the water glass producer

NaOH and distilled water were added into water glass solution at continual stirring. After NaOH dissolution, S–N was added to the mixture. The reaction mixture has been divided into two halves after stirring. They were labeled as *A* and *B*. 10 ml of polysulphide solution was added into mixture *A* and stirring continued for next 5 min. Both reaction mixtures *A* and *B* were poured into lockable plastic forms and were kept closed for 28 days. Visual observation of color changes was carried out once per day. After 28 days, the hardened specimen of mixture *B* was removed from form and was putted into polysulphide solution for 24 hours. After that, the both specimens *A* and *B* were evaluated by XRD and FTIR measurement.

The second geopolymer was prepared from mixture of SiO_2 and Al_2O_3, with molar ratio Si/Al = 1:1, instead of S-N. The other components and procedure steps was identical with previous preparation. Prepared specimens were labeled as *C* (polysulphide was added to the reaction mixture) and *D* (polysulphide was added to hardened specimen).

Results and discussion

Polysulphide solution applied into reaction mixture

After one day of hardening, no color change of geopolymer surface of the specimen *A* was observed. Surface of the specimen *A* was orange and was covered by thin polysulphide coating.

After 48 hours, a color change of specimen *A* surface was observed. After 28 days, specimen *A* was removed from the form, washed up by distilled water and dried up. During drying, a loss of color from surface was registered.

In case of specimen *C*, the surface got green color after two days. After 28 days, specimen *C* was removed from the form, washed up by distilled water and dried up. No loss of color was registered.

XRD analysis of the specimen *A* showed only characteristic peaks of quartz, which was presented in raw material S-N. No characteristic peaks were found in XRD record of specimen *C* at all. It is possible to assume, that prepared specimen *C* has an amorphous structure.

Characteristic vibrations of chromophore anionic radicals S_3^- and S_2^- were searched by measurement of FTIR spectra. It is known from literature, that chromophore anionic radical S_3^- has characteristic vibrations about 547 cm^{-1} and 582 cm^{-1}. However, S_2^- radical, which causes the green color of ultramarine, has not a characteristic vibration in FTIR spectra. This fact was confirmed by measurement of the FTIR spectra of prepared geopolymer specimens in the presented work.

Polysulphide solution applied on surface of geopolymer specimens

After application of polysulphide solution to specimen *B*, the change of surface color was observed within 30 min. After 24 hours, the surface of specimen *B* was blue-green. After removing of geopolymer specimen *B* from polysulphide solution and its washing in distilled water and drying up, decolorization was registered.

Application of polysulphide solution to specimen *D* caused a change of color after 24 hours. After removing of the specimen from polysulphide solution and its washing in distilled water and drying up, decolorization was registered.

Conclusion

Achieved results confirmed previous hypothesis about the possibility of using polysulphide solution as indicator of sodalite structures in prepared geopolymers. It was observed, that when sodalite structures are present, the reaction product changes its color. The polysulphide solution can be applied into reaction mixture or on surface of hardened geopolymer. The results of XRD measurements confirmed that geopolymers are amorphous materials. The characteristic vibrations of anionic radicals S_3^- in FTIR spectra were not found. In spite of this finding the change of color turn up and that means that anionic radicals S_2^- are probably present.

Financial support for this study was provided by the Ministry of Education of Czech Republic – Project: VZ MSM 7088352101.

REFERENCES

1. Davidovits J.: *Chemistry of geopolymeric systems, terminology*. Proc. of Second International Conference Géopolymére '99. (Davidovits J., Davidovits R., James C., ed.), Institut Géopolymére, Saint Quentin, France 1999.
2. Davidovits J.: J. Therm. Anal. *37*, 1633, (1991).
3. Booth D. G., Dann S. E., Weller M. T.: Dyes Pigments *58*, 73, (2003).
4. Remy H.: *Anorganicka chemie I.* SNTL, Praha 1971.
5. Kowalak S., Jankowska A.: Micropor. Mesopor. Mat. 61, 213, (2003).

P20 THE INFLUENCE OF SELECTED NON-TRADITIONAL RAW MATERIALS ON THE REACTIVITY OF RAW MEAL DURING PORTLAND CLINKER BURNING

THEODOR STANĚK, RADOVAN NEČAS and DALIBOR VŠIANSKÝ
Výzkumný ústav stavebních hmot, a. s., Hněvkovského 65, 617 00 Brno, Czech Republic, stanek@vustah.cz

Introduction

Demands on cement quality required from cement producers keep increasing throughout the world. The development in cement production is currently being affected by ecologic and economic aspects on one hand; on the other hand the customer requests for high quality of cement products come into account. The optimal utilization of primary raw material sources, usage of secondary raw materials and secondary energy sources under the achievement of high quality and durability of cement products present all together the main producers' efforts. From this point of view the pointing of non-traditional raw materials and considering the possibility of their alternation for natural sources to receive unchanged, possibly increased quality of final products seems to be very eligible.

Methods

Based on chemical and mineral analyses of 59 samples of non-traditional raw materials[1], several wastes, secondary and natural raw materials were selected, which appear applicable as components into cement raw meal for the Portland clinker burning. The list of selected materials is given in Table I.

From total amount of approx. 30–50 kg of the original material, smaller representative amount of 5–7 kg was separated by fourth. Moist and wet materials and sludge were dried at temperature of 50 or 105 °C, with respect to the chemical structure. Lumpy materials were ground to grain size under 1 cm. The amount of 100–200 g of each dry and ground raw material was used for preliminary analyses, and especially for calculation of chemical composition of raw meal.

Coarse raw materials were milled using laboratory ball mill to the fineness defined by the sieve residue with the sieve

Table I
The list of selected raw materials applicable as the cement raw meal component

Group	Raw material	Mark
Fly ash	Fly ash Dětmarovice	T-P1
	Fly ash Malešice	T-P3
	Fly ash Tušimice	T-P8
	Fluidized ash Třinec bed	T-P9
	Fluidized ash Třinec filter	T-P10
	Fluidized ash Olomouc	T-P15
Slag	Blast furnace granulated NH	T-S1
	Blast furnace non-granulated NH	T-S2
	Martin s.Třinec fraction 4-8mm	T-S4
	Martin s.Třinec fraction 8-16mm	T-S5
	Foundry slag Zetor	T-S7
	Heap slag Kladno	T-S9
Rocks	Limestone sludge Vitošov	T-H3
	Siliceous earth Borovany	T-H4
	Arenaceous marl Nové Strašecí	T-H5
	Glaukonitic clay Nové Strašecí	T-H7
	Kaolinitic sand Nové Strašecí	T-H9
	Shale Horní Benešov	T-H10
	Granodiorit powder Leskoun	T-H18
Other	Water treatment sludge Lachema	T-O1
	Red mud Žiar nad H.	T-O2
	Sugar refinery waste Cukrspol	T-O3
	Ni production sludge Sereď	T-O9

mesh 0.090 mm, which formed approx. 20 wt. %. Other fine raw materials were kept in original state.

The influence of particular raw material on the clinker formation rate was studied by the kinetic method of raw meal reactivity determination[2]. The method was modified in such way that the maximum affecting factors were eliminated. The following basic chemical parameters of the raw meal composition were invariable – lime saturation (SLP = 94), silicate modulus (Ms = 2.4), aluminate modulus (Ma = 1.6). However the required value of aluminate modulus in some cases and the silicate modulus in one case could not be achieved as the chemical composition of raw materials did not allow it. The particular raw materials, the influence of which was observed, were added into the mixtures in constant dosage of 15 wt. %. The influence of other chemically pure components ($CaCO_3$, Al_2O_3, SiO_2, and Fe_2O_3) was minimized by triturating to minus mesh 0.040 mm.

Results

The principle of the kinetic method is the accurate isothermal clinker burning[3] at the temperature of 1430 °C[3] followed by quantitative analysis of the clinker by microscopic method[4]. With use of the quantitative analysis the reaction rate constant *K* for the alite formation ($C+C_2S=C_3S$) can be calculated as well as the raw meal reactivity value *Rm*, which is the non-dimensional variable defined as the ratio of *K* reaction rate constant and the reaction rate constant of reference raw meal.

Thus the raw meal reactivity is the relative rate of isothermal clinker formation from the raw meal at the mean temperature of sintering zone in rotary kiln. It comprises the influence of all reactivity factors, which can be divided into non-effectible raw material source factors (mineral composition and microstructure of components, the content of secondary oxides, etc.) and effectible factors of raw meal preparation (composition, grain size, homogeneity).

The relative influence of the factors from the first group can be determined when standardizing the factors from the second group, that means by preparation of raw meals of the same chemical and granular composition. That is very hard to achieve in practice, and thus this standardization is carried out by calculation, based on the knowledge of mechanism and kinetics of clinker formation[5]. Using the standardization calculation together with phase analysis results from *Rm*

Table II
Sieve analyses of particular raw materials in wt. %

Group	Mark	Mesh in mm			Note
		0.063	0.090	0.125	
Fly ash	T-P1	18.4	9.1	3.9	original
	T-P3	14.6	6.2	2.5	original
	T-P8	33.0	19.8	9.6	milled
	T-P9	32.5	18.8	7.5	milled
	T-P10	26.8	14.2	6.8	milled
	T-P15	33.8	20.3	9.6	milled
Slag	T-S1	30.8	16.2	6.2	milled
	T-S2	32.1	17.8	8.2	milled
	T-S4	32.4	17.9	7.3	milled
	T-S5	33.6	19.2	8.5	milled
	T-S7	31.7	17.4	6.8	milled
	T-S9	24.9	11.0	3.8	milled
Rocks and mins.	T-H3	25.8	14.0	7.4	original
	T-H4	38.0	23.3	12.0	milled
	T-H5	30.1	16.1	6.9	milled
	T-H7	34.2	23.0	16.7	milled
	T-H9	35.0	19.8	6.4	milled
	T-H10	18.4	11.9	6.1	original
	T-H18	30.2	16.7	6.7	original
Other	T-O1	12.9	8.5	5.3	original
	T-O2	30.1	18.8	9.2	original
	T-O3	19.8	12.0	6.4	original
	T-O9	24.9	14.5	6.9	original

Table III
Selected results of analyses for the reactivity determinations and their final values

Raw meal	Phase content [vol. %]					$C_3S_{eq.}$	$C_2S_{eq.}$	Rm	Rs
	C_3S	C_2S	MH	C_{free}	pores				
SM-R-T-P1	50.6	26.3	17.8	5.3	23.8	73.0	9.2	0.70	0.47
SM-R-T-P3	32.3	41.5	19.2	7.0	22.6	61.8	19.0	0.32	0.15
SM-R-T-P8	33.5	40.8	19.8	5.9	27.7	58.4	21.8	0.41	0.59
SM-R-T-P9	47.6	28.4	20.1	4.0	20.9	64.5	15.4	0.86	0.86
SM-R-T-P10	32.7	38.3	21.1	7.8	25.1	65.6	13.3	0.28	0.25
SM-R-T-S1	40.3	34.4	19.6	5.7	24.7	64.3	16.1	0.52	0.49
SM-R-T-S2	47.0	26.7	20.3	6.0	26.3	72.3	7.4	0.58	0.63
SM-R-T-S4	51.2	24.4	20.5	4.0	27.1	68.1	11.4	0.92	0.94
SM-R-T-H3	52.7	25.8	17.7	3.7	21.7	68.3	14.0	1.00	1.04
SM-R-T-H4	38.8	34.7	19.2	7.3	23.4	69.6	11.2	0.38	0.55
SM-R-T-O2	48.5	30.0	17.5	4.0	31.1	65.4	17.1	0.87	1.31
SM-R-T-O3	44.7	31.4	19.0	4.8	37.9	65.0	16.0	0.69	0.73

Where: $C_3S_{eq} = 4{,}219 \times C_{free} + C_3S$ is calculated equilibrium content of alite
$C_2S_{eq} = 100 - C_3S_{eq} - C_3A - C_4AF$ is calculated equilibrium content of belite

determination and supplementing them with raw meal sieve analysis the relative value of reactivity of raw meal source *Rs* can be calculated[2].

When determining the reactivity in practice 4 tablets of the same weight of 0.06 g and the bulk density of 2.8 g cm^{-3}, were pressed out from each raw meal and the clinkers were burned out individually, isothermally, at the same conditions (1430 °C, 360 s) in an automatic kiln equipped with a manipulator[3]. Those four tablets of clinkers were compounded into one polished section for each raw meal for carrying out the microscope quantitative phase analysis by the method of point integration[4]. Next, the values of *Rm* and *Rs* were calculated from the results of quantitative phase analyses and sieve analyses of raw meals (see Table II). Selected final results are given in Table III. The value reactivity of raw material source *Rs* is crucial for the comparison of particular raw material reactivity. The value of raw meal reactivity *Rm* reflects the value of *Rs* and the raw meal preparation; in this case the various grain sizes play dominant factor for tested materials.

Conclusion

Presented results advert to utilization of non-traditional raw materials as components into cement raw meal from the point of view of their reactivity. For instance, the red mud Žiar nad Hronom possesses highest reactivity; also waste limestone sludge, Martin slag and a representative of fluidized bed coal combustion waste appear as highly reactive. The sugar refinery waste seems to be very interesting due to its high content of combustible substances, which could lead into lowering the dosage of fuels.

In the future, the research on the influence of those non-traditional materials on the Portland clinker burning, its properties, and the cement produced will continue.

This paper was elaborated with the financial support from the Ministry of Industry and Trade of Czech Republic, project No: FT-TA/020.

REFERENCES

1. Staněk T., Nečas R.: Annual report from the project being solved under the TANDEM program – project no. FT-TA/020, Research Institute of Building Materials, Brno (2004)
2. Chromý S.: Z-K-G *35*, 555 (1982).
3. Chromý S., Zavadil M.: Silikáty, *26*, 57 (1982).
4. Chromý S.: Silikáty *22*, 215 (1978).
5. Chromý S.: Z-K-G *35*, 204 (1982).

P21 SUPERPLASTICIZERS IN USE – FROM OLD TO NEW GENERATION

HALINA SZKLORZOVÁ[a], JIŘÍ BRANDŠTETR[b], RADOVAN NEČAS[a] and JOSEF KRÁTKÝ[a]
[a]Výzkumný ústav stavebních hmot, a. s., Hněvkovského 65, 617 00 Brno, Czech Republic, szklorzova@vustah.cz, [b]Faculty of Chemistry, Brno University of Technology, Purkyňova 118, 612 00 Brno, Czech Republic

Introduction

In recent technologies of cement and concrete composites, strong emphasis is laid on the final physico-chemical properties of hardened cement pastes, as well as on the properties of fresh mixture. Such properties, indicating its consistency and workability can all together be called the rheology of cement, concrete or mortar mixture. They can be successfully modified, currently, by very common and sometimes irreplaceable chemical admixtures, out of which the superplasticizers are the most widespread[1]. Together with mineral admixtures (blast furnace slag, microsilica, fly ash, pozzolana, microaggregates, etc.), they enable producing new, non-traditional types of concrete[2].

Although nowadays market is overfilled with different kinds of chemical admixtures for cement based concretes and mortars, the consumers' understanding of their effects and proper use is insufficient. Consequently, they come across many unexpected and undesirable resulting properties, caused by incompatibility of superplasticizer with some of the constituents of binder mixture, changing its setting time, etc. Therefore, the determination of optimal kind and dosage of plasticizing admixture for proper application in tailored composites is a very important task. The efficiency of various superplasticizers and their effect on properties of fresh and hardened cement can differ at various conditions radically. Since this can be studied mainly on the rheology of fresh paste, observing rheology changes, in cement pastes modified by various superplasticizers in time was the main subject of our study.

Functioning mechanism of superplasticizers

Superplasticizers bring about the dispergation of cement particle agglomerates. In this way they modify the consistency of fresh cement paste, making it more flowable, and hence workable. They also influence the start of setting significantly. The water/cement ratio can be reduced substancially and the compact dense structure of hardened concrete, water impermeable and resistant to chemical corrosion, of enhanced strength can be achieved[3].

Superplasticizers are organic macromolecules of different composition, structure and molecular weight. They are mostly the co-polymers with long branch chains and various functional groups. The sulfonate based superplasticizers cause the electrostatic effect of particle repulsion. After adsorbing to positively charged surface of tricalciumaluminate C_3A or tetracalciumaluminateferrit C_4AF by the $–SO_3H$ group, the other negatively charged $–SO_3H$ groups of the molecule cause the electrostatic repulsion with other negatively charged particles C_3S and C_2S. The polycarboxylate based superplasticizers induce mainly sterical repulsive forces among particles of cement. These macromolecules bear, apart from negatively charged and electrostatic repulsive forces inducing $–COO^–$ groups, also long branch chains, which, after adsorption to the cement particle surface, prevent particle agglomeration. Due to significantly higher efficiency the polycarboxylates enable to decrease their dosage to tenths of percentage.

The experiments

For the experiments, two types of Portland cement CEM I 42.5 R with significantly different moduli and mineral compositions were selected.

Superplasticizers used in this work were chosen to be of different chemical composition and producer:

– Naphtalensulfonate A
– Polycarboxylate A
– Naphtalensulfonate B
– Polycarboxylate B

Fresh mixtures were prepared by mixing cements and solutions of superplasticizers, and examined by methods of viscosity and minislump test determination in time. Different influence of superplasticizers on properties of fresh cement pastes was observed.

The viscosity of fresh cement paste

The viscosity can be defined generally as the rate of the resistance of liquid material toward the flow. The Brookfield DV-E viscometer, on which the measurement of plasticized cement suspensions was performed, is principally based on the rotation of spindle equipped with calibrated string in tested liquid (suspension).The viscosity is given by the rate of torsion of the string. The measuring of viscosity of cement suspension in time by this viscometer makes sense only before beginning of setting process (through dormant period) and in case of strongly diluted suspensions (high

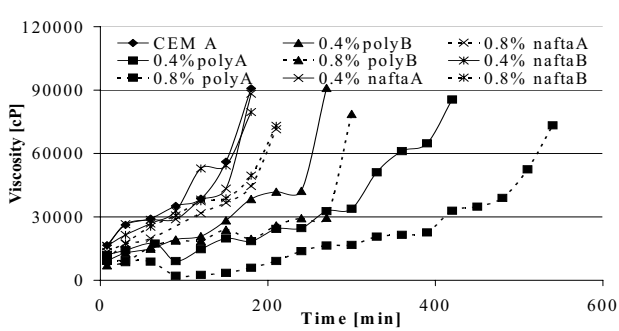

Fig. 1. The viscosity development of fresh cement suspensions prepared from CEM I 42.5 R Mokrá, modified by various supeplasticizers (w/c = 0.35)

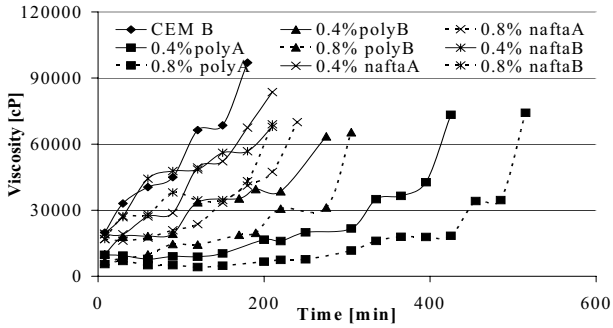

Fig. 2. **The viscosity development of fresh cement suspensions prepared from CEM I 42.5 R Čížkovice, modified by various supeplasticizers (w/c = 0.35)**

water/cement ratio), until the suspension holds plasticity and low viscosity. Once the initial set occurs, the suspension looses its plasticity and transforms into the stiff mixture of dense consistency. The spindle drives a channel in such dense mixture and moves ahead in it without overcoming the resistance of paste any more. The results of viscosity measurement in time of modified cement suspensions are shown in Fig. 1. and 2.

The minislump flow test

The minislump flow test of fresh cement paste was modified from the ČSN 72-2441 standard. Plasticized cement pastes, with the water/cement ratio of 0.40 were spread from the cone over the Haegermann table. Four diameters of the spread paste were taken and the average of these values was calculated. The measuring was repeated until no slump flow occurred. The cone with following diameters was used: bottom diameter = 10 cm; upper diameter = 7 cm, height = 6 cm. The results of slump test are given Fig. 3. and 4.

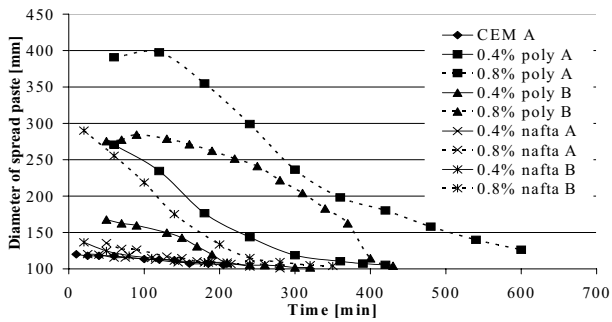

Fig. 3. **The minislump flow test of cement paste CEM I 42.5 R Mokrá modified by various superplasticizers (w/c = 0.40)**

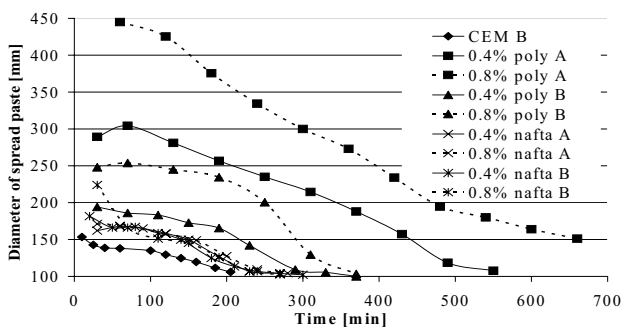

Fig. 4. **The minislump flow test of cement paste CEM I 42.5 R Čížkovice modified by various superplasticizers (w/c = 0.40)**

Conclusion

Modification of properties of cement pastes prepared from two kinds of portland cement by addition of various kinds and amount of superplasticizers was demonstrated. The results of viscosity and minislump flow test indicate that given superplasticizer affects properties of cement paste in similar way concerning dosage; increased dosage causes more intensive plasticizing effect. If the effects of various superplasticizers at the same dosage are compared, the different ways of their influence are notable; as well as the effect of one superplasticizer with two different cements. Another fact can not be omitted, that one kind of superplasticizer can react with given cement in different way, when the conditions and parameters are changed, especially water/cement ratio and temperature. Neglecting this fact we sometimes come across the undesirable results of the modification such as bleeding, decrease of strengths, etc.

The unfavorable and unexpectable influence has to be observed and minimized. The accurate water/cement ratio and other parameters need to be set for every superplasticized mixture. The pilot tests are recommended prior to every single application. Thus the purpose, for which superplasticizer is going to be used, and the properties of final product should be considered thoroughly before every application.

REFERENCES

1. Spiratos N., Jolicoeur C.: Proceedings of 6th CANMET/ACI International Conference on Superplasticizers and Other Chemical Admixtures in Concrete. Trends in Concrete Chemical Admixtures for the 21st Century. ACI SP 195, Nice 2000, p. 1–16.
2. Malhotra V. M., Ramachandran V. S., Jolicoeur C., Spiratos N.: *Superplasticizers- Properties and Application in Concrete.* CANMET, Ottawa 1998, p. 404
3. Aitcin P.-C.: *High-Performance Concrete*. E&FN SPON, London 1998.

P22 PLASMA SURFACE ACTIVATION OF POLYCARONATE USING ATMOSPHERIC PRESSURE GLOW DISCHARGE

MARTIN ŠÍRA, PAVEL SŤAHEL,
ZDENĚK NAVRÁTIL, FRANTIŠEK ZLÁMAL
and DAVID TRUNEC
Department of Physical Electronics, Masaryk University, Kotlářská 2, 611 37 Brno, Czech Republic,
pstahel@physics.muni.cz

Introduction

Polycarbonate is widely used material in different branches of industry. This thermoplastics material is used everywhere high impact resistance and transparency is required. However, surface properties of polycarbonate (e. g. wettablity and adhesion with deposited metallic or dielectric films) are not suitable for every application. Plasma surface treatment is very promising technique for adhesion improvement. Most of reported works with plasma activation of different polymers[1] especially polycarbonates were made in different types of low-pressure plasma[2,3]. The disadvantage of the low-pressure techniques is their demand of expensive vacuum pumping systems. Moreover, the difficulties in arranging the system for large area treatment have to be overcome. Recently, plasma activation of polymers at atmospheric pressure has become a promising technology due to its economical and ecological advantages.

Dielectric barrier discharges at atmospheric pressure are widely used in various applications such as depolution, ozone production, surface treatment and thin film deposition. Two modes of barrier discharge can occur: filamentary and glow. In the filamentary mode the treatment is not homogeneous so its application is limited for surface activation and plasma depositions. The atmospheric pressure glow discharge (APGD) allows homogenous treatment of the surface however this kind of discharge is possible to obtain only under certain specific conditions.

The main objective of this paper was to investigate the effect of the plasma surface treatment in APGD on the surface properties of polycarbonate.

Experimental

The atmospheric pressure glow discharge was generated in a reactor chamber between two brass electrodes. The upper electrode was covered by a dielectric (pyrex glass) 1 mm thick and the bottom one was covered with the polycarbonate sample. The discharge was generated in pure nitrogen or in pure nitrogen with small admixture of hydrogen (3 %). The bottom electrode was periodically moving with sample during the treatment to achieve higher homogeneity and to increase the treated area. The distance between electrodes was 1 mm. The operating frequency was kept at 10 kHz and the input power density was kept at 0.8 W cm^{-2} in all cases. The treatment time varied from 4 to 100 s.

So called Acid Base Regression method[4] was used to calculate the total surface free energy γ) and its components (Lifshitz-van der Walls γ^{LW}, acid-base γ^{AB}, acid part γ^{+} and base part γ^{-}) from contact angles measured by means of Surface Energy Evaluation System[5]. The topology of treated and untreated samples was studied by means of AFM and SEM and chemical changes were investigated by XPS.

The discharge properties were studied by means of the optical emission spectroscopy. The spectra emitted by the discharge were recorded with the Jobin-Yvon TRIAX 550 spectrometer with a CCD detector.

Results and discussion

Typical spectrum of the nitrogen discharge with 3% hydrogen admixture is displayed in Fig. 1. The spectrum consists only of the molecular bands of the second positive system of nitrogen ($C\ ^3\Pi_u \rightarrow B\ ^3\Pi_g$). Neither hydrogen atomic lines nor hydrogen molecular lines were registered, although the integration time was exaggeratedly raised. This is probably due to the complex structure of nitrogen molecule excited states, which absorbs the most of the supplied energy.

The surface free energy (SFE) of treated polycarbonate as a function of the plasma treatment time in nitrogen-hydrogen mixture is shown in Fig. 2. The total surface free energy γ) and also its components (γ^{LW} Lifshitz-van der Walls and

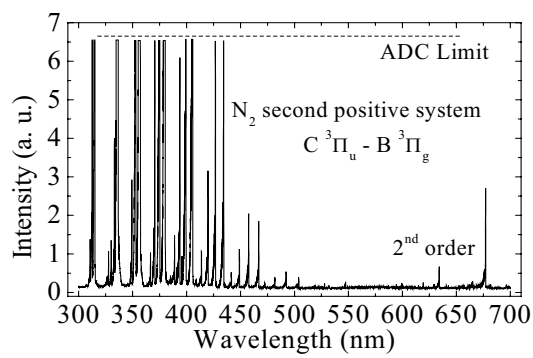

Fig. 1. **Overview spectrum of APG discharge in nitrogen with 3% hydrogen admixture. Whatever the hydrogen admixture was, only nitrogen emission was observed**

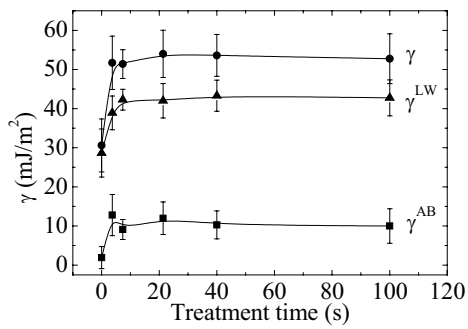

Fig. 2. **SFE of sample versus treatment time. γ is total surface free energy,) γ^{LW} is Lifshitz-van der Walls component and γ^{AB} is acid-base component**

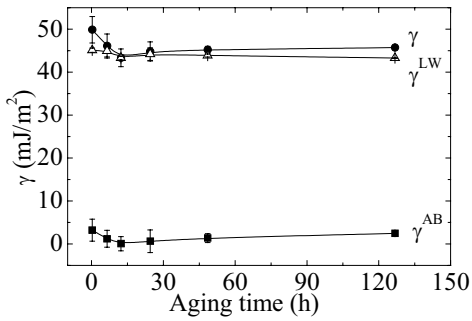

Fig. 3. **SFE of sample versus aging time. γ is total surface free energy, γ^{LW} is Lifshitz-van der Walls component and γ^{AB} is acid--base component. Plasma treatment time of sample was 100 s**

γ^{AB} acid-base component) rapidly increased during the first 7 s of treatment then reached saturation.

The time stability of treated samples was also investigated (see Fig. 3.). The total surface free energy and its components slightly decreased during the first 12 hours of the aging and remained constant. The stable value of SFE of aged sample was considerably higher then the value of SFE of untreated sample. We suppose the good stability is caused due to croslinking effect.

The surface atomic concentration of samples was measured by X-ray Photoelectron Spectroscopy using Mg K_α photon beams. The results are in Table I.

Table I
Atomic concentration of virgin sample and treated samples. Plasma treatment time of samples was 100 s

Sample	C [%]	O [%]	N [%]
virgin PC	83.2	16.8	0.0
PC treated in N_2	72.1	17.9	10.0
PC treated in N_2+H_2	68.1	16.9	15.0

Conclusion

Polycarbonate samples were activated in the atmospheric pressure glow discharge. The surface free energy of treated samples increased from 30 to 53 mJ m^{-2}. The treated samples showed out only low ageing effect. The saturated value of SFE of samples plasma treated in APGD was comparable with saturated value of SFE of samples treated in low-pressure discharges. The benefit of the technique based on APGD is short-process time and low aging effect in contrast to low-pressure techniques.

This work was supported by Grant Agency of Czech Republic No. 202/05/0777 and 202/02/D097.

REFERENCE

1. Lehotský M., Drnovská H., Lapčíková B., Barros-Timmons A. M., Trindade T., Zembala M., Lapčík Jr. L.: Colloids and Surfaces A: *222*,125 (2003).
2. Zajíčková L., Subedi D. P., Buršíková V., Veltruská K.: Acta Physica Slovaca *53*, 6, 489 (2003).
3. Klemberg-Sapieha J. E., Poitras D., Martinu L., Ymasaki N. L. S., Lantman C. W.: J. Vac. Sci. Technol *A15*, *3*, 985 (1997).
4. Navrátil Z., Buršíková V., Sťahel P., Šíra M., Zvěřina P.: Czech. J. Phys. *54*, C877 (2004).
5. http://www.seesystems.wz.cz.

P23 PUZZOLANIC ACTIVITY OF SECONDARY RAW MATERIALS

FRANTIŠEK ŠOUKAL and JAROMÍR HAVLICA
Department of Materials Engineering, Faculty of Chemistry, BUT, Purkyňova 118, 612 00 Brno, Czech Republic, soukal@fch.vutbr.cz

Introduction

During the cement and water reaction, the clinker minerals are hydrated to create hydration product. The reactions are accompanied by heat evolution in several stages. Some materials may be added to the cement in a certain amount without decreasing of the final material properties despite of they don't create a binder alone. This material property is known as puzzolanic activity. The reactions course in the cement-water system must be logically joined with the thermal effect. To enable measurement of the heat evolved by puzzolanic reactions, they have to be subjected to a calorimetric study. If compared the cement-water reaction heat with the heat evolved from the same mixture with addition of a puzzolan, there is an ability to determine the amount of heat belonging to puzzolanic reactions. It is necessary to use abundance of water to eliminate mixture dilution by puzzolan addition. Also there is a need to choose the appropriate amount of the puzzolan.

Experimental and results

200 g of portland clinker Mokrá 2004 and 20 g of the secondary raw material sample was mixed in a dish. The dry mixture was thoroughly homogenized and then 100 ml of distilled water was added. The mixture was blended for 120 s followed putting into the styrofoam dish and starting the calorimetric measurement. Obtained curves were numerically integrated to chosen temperature level. Values acquired by the curves integration were compared with the integral value of blank sample and their difference corresponds with puzzolanic activity of tested raw material.

Table I
Relative heats of the secondary raw materials

Label	Material	Location	Q_P	ΔQ	Q_{rel}
		HIGH TEMPERATURE FLY ASHES			
T-P1	Fly ash	Dětmarovice	239.83	42.07	0.213
T-P2	Fly ash	Chvaletice	211.40	18.38	0.095
T-P3	Fly ash	Malešice	213.59	15.83	0.080
T-P4	Fly ash	Mníšek	216.34	18.58	0.094
T-P5	Fly ash	Mělník II	225.02	27.26	0.138
T-P6	Fly ash	Opatovice	211.74	18.72	0.097
T-P7	Fly ash	Prunéřov	229.01	22.54	0.109
T-P8	Fly ash	Tušimice	180.49	–12.53	–0.065
		FLUID BED FLY ASHES			
T-P9	Fly ash	Třinec bed	224.42	26.66	0.135
T-P10	Fly ash	Třinec filter	243.21	45.45	0.230
T-P11	Fly ash	Hodonín bed	277.81	16.29	0.062
T-P12	Fly ash	Hodonín filter	260.51	–1.01	–0.004
T-P13	Fly ash	Ledvice bed	258.81	–2.71	–0.010
T-P14	Fly ash	Ledvice filter	228.93	–32.59	–0.125
T-P15	Fly ash	Olomouc	236.62	38.86	0.197
T-P16	Fly ash	Tisová	245.35	38.88	0.188
		SLAGS			
T-S1	GBFS	Nová huť Ostrava	139.28	–99.47	–0.417
T-S2	BFS,	Nová huť Ostrava	130.09	–108.66	–0.455
T-S3	Slag	ŽDB Bohumín	248.76	–12.76	–0.049
T-S4	GBFS	Třinecké železárny 4-8	189.19	–49.56	–0.208
T-S5	GBFS	Třinecké železárny 8-16	194.78	–43.97	–0.184
T-S6	Foundry slag	Foundry Královopolská	195.04	–11.43	–0.055
T-S7	Foundry slag	Foundry Zetor	161.37	–31.65	–0.164
T-S8	Slag	Štramberk	233.62	27.15	0.131
T-S9	Steel slag	Kladno	215.38	–23.37	–0.098
T-S10	Ni-slag	Lučenec-Sereď	214.71	8.24	0.040
T-S11	Al-slag	Žiar n/Hronom	202.24	9.22	0.048
		GROUNDS			
T-H4	Bergmeal	Borovany	190.87	–2.15	–0.011
T-H5	Arenac. marl	Nové Strašecí	216.87	23.85	0.124
T-H11	Tephrite	Dubičná	196.00	–10.47	–0.051
T-H12	Trachyte	Valkeřice	198.61	–7.86	–0.038
T-H13	Trachyte	Heřmanov	192.43	–14.04	–0.068
T-H16	Hornfels	Mikulčice	206.16	13.14	0.068
T-H17	Rhyolite	Lehôtka	214.59	8.12	0.039
T-H18	Porfyrite tuff	Vacíkov	218.35	25.33	0.131
		OTHERS			
	Silica fume	Ezanova Šumperk	222.93	25.17	0.127
207	sludge	Lachema	251.03	44.56	0.216
231	Calcin. waste	Cukrspol	13.22	–179.80	–0.932
950	Cinder	Mělník	241.29	–20.23	–0.077

The obtained integrals values represent the amount of evolved heat

$$Q = K\int_0^{\infty} \Delta T \mathrm{d}t \,.$$

The integral application for acquiring of heat flow information follows the general Fourier equation for energy transport

$$\frac{\mathrm{d}Q}{\mathrm{d}t} = k\nabla T \,.$$

In case of stationary experiment geometry the simplified relation

$$\frac{\mathrm{d}Q}{\mathrm{d}t} = k\frac{\mathrm{d}T}{\mathrm{d}x}$$

can be transformed to differential form

$$\frac{\mathrm{d}Q}{\mathrm{d}t} = k\frac{\Delta T}{\Delta x} \text{ and thereafter to } \frac{\mathrm{d}Q}{\mathrm{d}t} = K\Delta T \,.$$

The heat increasing of puzzolanic reactions ΔQ is the difference of heat of the blank cement mixture (clinker with water) Q_c and the same mixture with puzzolan addition Q_p. The relative heat Q_{rel} is comparable each other.

$$Q_{rel} = \frac{Q_p - Q_c}{Q_c} = \frac{\Delta Q}{Q_c}$$

Table I presents the values of reaction heat relative benefit for fluid bed fly ashes, high-temperature fly ashes, slags, grounds and other secondary raw materials. It is evident that the highest additional heat is exhibited in the case of fluid bed fly ashes, in the process the finer portion from filter has higher reactivity. Another factor which may play significant role is the free lime content. The free lime shows in the initial hydration period own hydration heat, but its role in further hydration is more important due to its ability to increase calcium ions concentration in the solution and its contribution to faster start of puzzolanic reactions. And this probably contributes with lower or negative heat values of Hodonín and Ledvice fluid bed fly ashes. High-temperature fly ashes accounts lower activity according to stable high-temperature phases (mullite etc.). Reactivity of these materials is ensured by amorphous glassy phase occurrence. An atypical high activity of Dětmarovice fly ash was recorded. Alit phase was detected in this fly ash except of other phases. On the other hand the Tušimice fly ash exhibited negative value of relative additional reaction heat Q_{rel}. This must be caused by a phase which blocks reactions in the solution, for except it consume calcium ions from solution with low reaction enthalpy or it creates products which prevent solid surface reactions. In the case of slags, there is probably no logical comparison each other due to general diversity of tested slags. Relative high value of the additional heat was measured with Štramberk slag, on the other hand markedly negative value had foundry slag Zetor. Al-slag from Žiar nad Hronom had noticeably retarding effect in spite of positive heat benefit. The measurement results of blast-furnace slags (BFS) were surprising due to strong negative Q_{rel} values. In case of BFSs an alkali activation is needed to reach good puzzolanic and almost hydraulic behavior. Another factor affecting BFS's puzzolanic properties is usage of the portland clinker instead of portland cement. Gypsum present in the portland cement changes over to solution and the sulfate anions play important role in the slag surface activation. So the experimental conditions were not appropriate for measurement of slag puzzolanic activity.

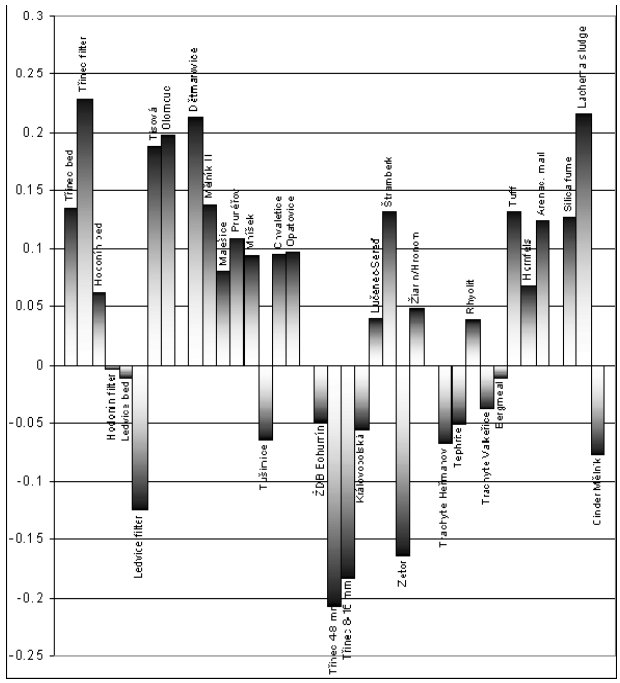

Fig. 1. **column graph of relative heats Q_{rel} of the secondary raw materials**

As expected the addition of grounds had also different effects on hydration process. Trachyte Valkeřice and Heřmanov, tephrite and bergmeal presence exhibited negatively. The first three ones contain a zeolite phases which are stable and probably cause decrease of calcium ions in solution. Bergmeal and hornfels makes rapid retardation of portland cement setting. Hornfels unlike bergmeal has positive heat effect despite of setting time shift. Here probably plays role presence of $SiO_2 \,.\, nH_2O$ phases based on opal which are as crystallic as amorphous. In initial stage these phases can block calcium ions into some CSH forms and after microstructure transformation they can contribute to structure formation. In the case of rhyolite, process is probably started by excitation of glassy phase. Relatively high additional heat of arenaceous marl is interesting. It does not contain any hydraulic active crystalline phases. Porphyryte tuffs from Vacíkov are naturally supposed to have puzzolanic behavior as well as in case of silica fume.

Lachema sludge contains quartz and calcite as major components, but it is probably that some minor constituent can have an activating character. Total blocking of hydra-

tion process by sugars presence in calcination wastes from Cukrspol makes this material unusable in cementitious material.

Conclusions

Conducted calorimetry measurements have reflected processes in first stage of hydration if system does not require any starting material, because rate of reaction is sufficient or starting material is in composition of raw material. Methods must be modified for system, where the reaction rate is low and transport of energy from body is higher then energy given by reaction rate liberated in hydration of puzzolan. In next, attention must be paid to slow processes, because these reactions significantly influence mechanical parameters development. In present time period the method for determination of optimum starting material and its amount is developed.

P24 EFFECT MODELLING OF SHORT- FIBRES ORIENTATION ON STRESS-STATE IN CURVED PARTS OF THIN-WALLED PLASTIC PRODUCTS

OLDŘICH ŠUBA
Tomas Bata University in Zlin, Faculty of Technology, TGM 275, 762 62 Zlin, Czech Republic, suba@ft.utb.cz

Problem of layered cylindrically orthotropic curved wide wall under bending

The superstructure of the injection-moulded part is given by distribution and orientation of short fibres. The resultant structure is an anisotropic and heterogeneous body whose mechanical behaviour may well be significantly different to that of isotropic and homogeneous parts. Growing ratios of R/r of curved-corner areas are accompanied by growing local stresses in comparison to the stress of straight walls. The resultant stress state due to curving are further affected by physical factors for anisotropic and heterogeneous structures.

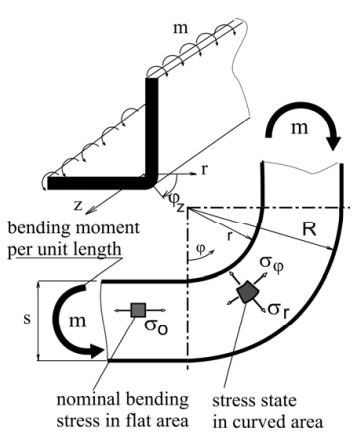

Fig. 1. **Cylindrically symmetric problem of bending of curved wide wall**

Fig. 1. shows a basic case of the bending of highly curved area of the wide wall. Under the loading of the uniform bending moment m (per unit width of the edge), then this has to do with a rotationally symmetrical problem. It follows from the analytic solution of the plane stress problem of cylindrical orthotropy of homogeneous case that the stress problems of cylindrically orthotropic bodies are, apart from the geometric R/r parameter, also the functional parameter $\eta = E_L/E_T$; where E_L and E_T are modules of the elasticity of short-fibre structure in the longitudinal direction of short--fibre orientation (L) and the transversal direction (T).

During the moulding process, the fibres may become oriented in a complex manner. In the component itself, a charakteristic quasi-layered structure is frequently observed. The fibres are oriented in quite different ways according to their location through the thickness of the wall. The polymer melt viscosity and flow rate significantly alter the proportions of the oriented regions. Obviously, for cases of relatively fast injection speeds, the core of the moulding contains fibres mainly aligned perpendicular to the flow direction. Above and below this are regions with the predominant fibre orientation in the flow direction and most of the fibres are lying in planes parallel with the reference plane of the sheet.

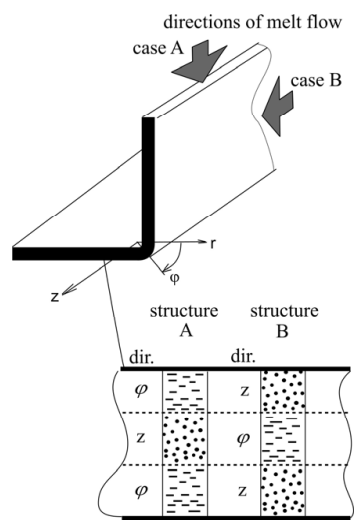

Fig. 2. **Idealised model structures of injection-molded wall**

Selected types of idealised wall structures are shown in Fig. 2. The wall is divided into three layers of identical thicknesses, with different orientation of short fibres 0°, 90°. In case A, it is considered that the short-fibres in skin layers are totally oriented in the direction of the periphery. In case B, the fibres in core are totally oriented in the peripheral direction.

The direction of orientation of the short-fibres in a totally oriented structure gives the axis of a monotropic material in given area. The material characteristics in such a linearly elastic area are given by the set of elastic constants, making up the appropriate matrix of compliance.

Making up the set of effective elastic constants of a 3D monotropic structure on the basis of experimental measurement is virtually impossible. For this reason, the theoretical prediction of these elastic constants is irreplaceable. We have already mentioned the outcomes of the modelling of the elastic behaviour of short-fibre plastic composites at the micro-mechanical level[1]. Here, we used the results achieved to establish the macro-mechanical model of the rounded corner areas of injection-molded part. The elastic constants were determined for the volume fraction of fibres 40 % and the following characteristics of glass reinforcement (1) and polymer matrix (2) as follows: Young's modules : E_1 = 75 000 MPa, E_2 = 1 600 MPa, Poisson's ratios: $\nu_1 = 0.2$, $\nu_2 = 0.4$.

Results and discussion

In order to illustrate the role of the injection-molded structure in the rounded corner areas of wide walls, distributions of stress components of idealised structures of injection wall are compared with stresses of unreinforced polymer, i. e. of isotropic and homogeneous case. The results are shown in the following figures. The relative values of the maximal peripheral stresses σ_φ/σ_0 are shown in Fig. 3., where $\sigma_0 = 6$ m s^{-2} is the nominal bend stress in isotropic and homogenous case at the flat sections.

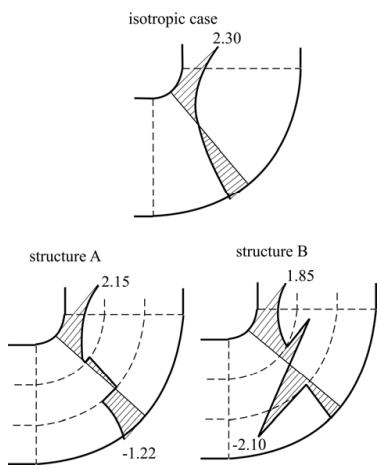

Fig. 3. **Distribution of relative values σ_φ/σ_0 of peripheral stress for unreinforced and short – fibre reinforced injection-molded curved wall (R/r = 5)**

As it follows from the obtained results, bending – peripheral stresses σ_φ reach similar values in material coordinate direction L for both model structures A, B. These values differs not much from max. bending stress of sotropic/ homogenous case. However, a different situation occurs in the transversal material directions T. In case of structure A, the core is strained slightly. Vice versa, structure B shows significant value of relative bending – peripheral stress σ_φ in the direction L. It folows significant disadvantage of this case, because the transversal strength of fibrous structures is generally low, obviously at levels of unreinforced polymer. Similarly, the relative values of the maximal radial stresses σ_r/σ_0 are shown in Fig. 4. As has been demonstrated there is no substantial difference in the values of radial stress. However, in both case A and B, stress components σ_r fall into the material direction T and thus it is necessary to consider these values of stresses when considering the mechanical behaviour in view of the generally low levels for transverse strength of fibrous materials.

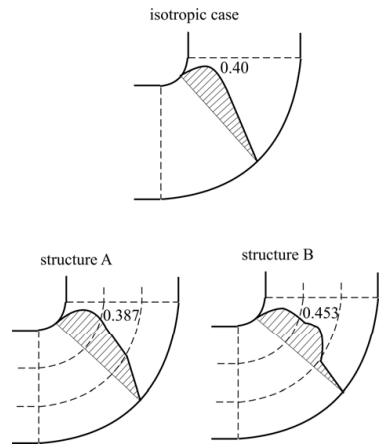

Fig. 4. **Distribution of relative values σ_r/σ_0 of radial stress for unreinforced and short – fibre reinforced injection-molded curved wall (R/r = 5)**

Conclusion

The anisotropy and the heterogenity of mechanical properties caused by short-fibre orientation and distribution in melt flow can influence the macro-mechanical behaviour of injection molded parts. Therefore, it is necessary to pay attention to the design of products exposed to higher mechanical loadings.

This paper was prepared under support of project MSM 708 352 102.

REFERENCES

1. Suba O., Manas M. Proceedings of 16th Annual Meeting: The Polymer Pocessing Society, p. *299*. Shanghai, 2000.

P25 ARENE-IRON COMPLEXES AS INITIATORS FOR PHOTOPOLYMERIZATION

JAN VALIŠ[a], BOHUMIL JAŠÚREK[a]
and TOMÁŠ WEIDLICH[b]
[a]*Department of Graphic Arts and Photophysics, University of Pardubice, Czech Republic,* [b]*Research Institute for Organic Syntheses, Pardubice, Czech Republic*

Introduction

Systems cured by UV radiation, or energy-rich radiation in general, are used in many branches of industry. In the graphic arts industry UV-cured systems has been used for over 20 years. The key driver was the reduction in volatile organic compounds (VOCs), resulting from elimination of solvents[1].

In practice the predominating systems are cured by radical mechanism, for which cheaper and more efficient types of initiators are continuously developed. The cationic systems have begun to win recognition only recently. However, they have certain advantages as compared with the radical initiators, and that is why their applications in practice are becoming more extensive.

The present work deals with a study of photoinitiators of cationic polymerisation of printing inks with the aim of suggesting new initiators for printing inks and transfer inks and testing their properties.

Experimental

Preparation of Photoinitiators

The photoinitiators were prepared by exchanging the ferrocene ligand[2,3,4,5] (Fig. 1.). These initiators were compared with the commercially available initiator (η5-2,4-cyclopentadien-1-yl)[(1,2,3,4,5,6-η)-(1-methylethyl)-benzene]--ferrous hexafluorophosphate under the commercial name Irgacure 261. Rank of initiators of organometallic type have been prepared (Fig. 2.).

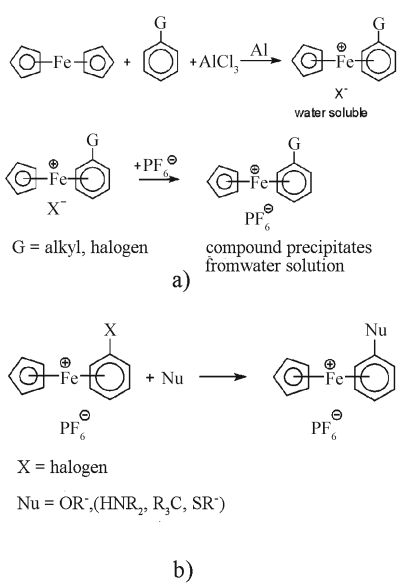

Fig. 1. **a) Preparation of arene-iron cyclopentadienyl (arene--FeCp) complexes from activated aromatic compounds and ferrocene, b) Synthesis of alkoxybenzene-FeCp complexes by nucleophilic substitution reaction**

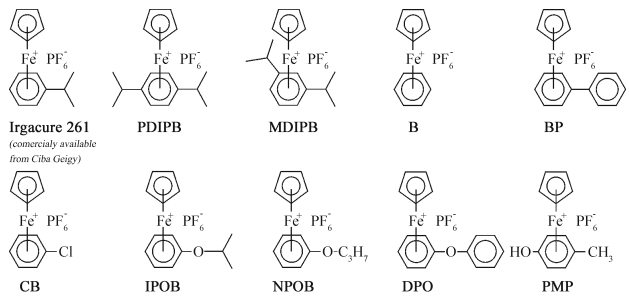

Fig. 2. **Prepared photoinitiators of organometallic type and commercial initiator Irgacure 261**

Experimental apparatus and measurement method

The curing of mixtures was studied by FTIR (spectacular reflectance) and photocalorimetry[6]. IR spectroscopy gives information on chemical groups containing highly polar bonds, or bonds whose dipole moment changes during vibration.

The samples were prepared by coating thin layer of mixture on alluminium foil. The samples were measured by FTIR before exposure and then, after exposure by Green Spot UV Curing System (super pressure mercury lamp), was sample measured in defined time lag. The dosage of UV light per sample was ca 230 mJ cm^{-2}.

The curing process initiated by the above-mentioned initiators was followed using two types of binders: epoxide type, and vinyl ether type. The measured bands for epoxide binder were 1230 cm^{-1} (epoxide group) and 1726 cm^{-1} (carbonyl group as internal standard) and for vinyl ether binder 1617 cm^{-1} (C=C double bond) and 2900 cm^{-1} (C–H bond as internal standard).

The conversion was calculated by following Equation:

$$\text{Conversion} = (A_0 - A_t)/A_0 \qquad (1)$$

Where A_0 is the quotient measured band and internal standard without UV exposure and A_t is the quotient measured band an internal standard after UV exposure and defined time lag.

Results and discussion

The curing process initiated by the above-mentioned initiators was followed using two types of binders: epoxide type, and vinyl ether type. The reaction course was followed for concentration of initiator 3 mass %.

IR spectrums were measured before exposure and then, after exposure by UV light, in time lag 30, 60, 90, 120, 150, 210, 270, 300, 450, 600, 900, 1200 and 1800 seconds. From

these spectrums were calculated conversions using Eq. 1. The conversion curves for epoxide binder are shown in Fig. 3. and for vinyl ether binder in Fig. 4.

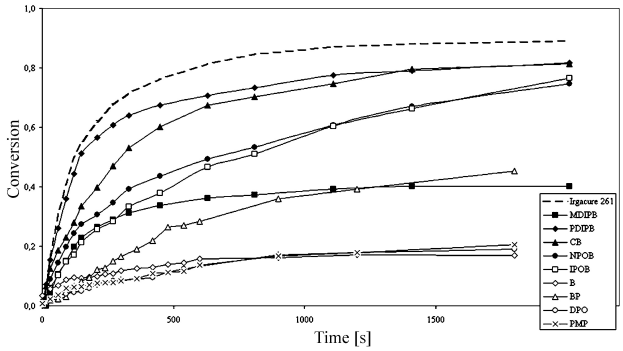

Fig. 3. **The conversion curves for epoxide binder**

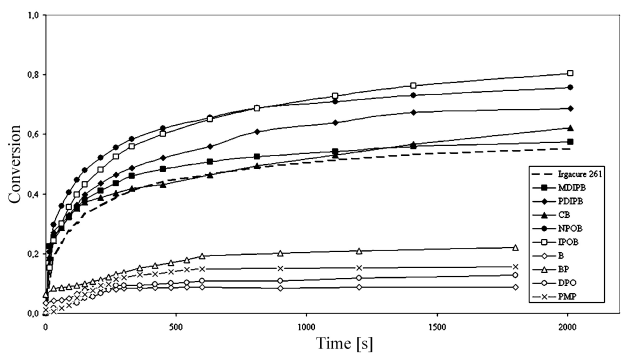

Fig. 4. **The conversion curves for vinyl ether binder**

IR spectra shown, that photoinitiators (exception to B, BP, DPO, PMP) initiated cationic polymerisation in both epoxide and vinyl ether binders. After 3 days the conversion reached in the epoxide binder was higher than in vinyl ether type and was from 93 to 99 %. The conversion reached in the vinyl ether binder was in range from 85 to 90 %.

This work was supported by the Ministry of Education, Youth and Sports of the Czech Republic, project No. MSM 0021627501.

REFERENCES

1. Klang J., Balcerski J.: Ink Maker 80, *September special supplement*, 1 (2002).
2. Valis J., Weidlich T.: Advances in Colour Science and Technology *6*, 73 (2003).
3. Gill T. P., Man K. R. Inorg. Chem. *19*, 3007 (1980).
4. Woods J., Rooney J. M., Coakley M. P.: PCT Internat. Appl. WO 88/02879.
5. Valis J.: *PhD. Degree Thesis*, University of Pardubice, Pardubice, Czech. Rep. 2001.
6. Jasurek B., Valis J., Weidlich T.: *Conference Proceedings of RadTech Europe 2003*, Volume II, 919, Berlin 2003.

P26 THE EFFECTS OF MORPHOLOGY ON THE YIELD BEHAVIOUR OF POLYETHYLENE COPOLYMERS

PETR VESELÝ[a], LADISLAV FIEDLER[a], EVA NEZBEDOVÁ[b] and BOHUMIL VLACH[a]

[a]*Department of Material science and engineering, Brno University of Technology, Faculty of mechanical engineering, Technická 2896/2, 616 69 Brno, Czech Republic, wesa@email.cz,* [b]*Institute of Materials Science, Brno University of Technology, Faculty of Chemistry, Purkyňova 118, 612 00 Brno, Czech Republic, nezbedova@fch.vutbr.cz*

Introduction

The stress/strain behaviour of solid polymers can be categorized into three classes of behaviour: (i) brittle fracture characterised by no yield point, (ii) yield behaviour- characterized by a maximum in the stress/strain curve followed by yielding deformation and (iii) rubber-like behaviour characterized by the absence of a yield point maximum but exhibiting a plateau in an engineering stress/strain curve. Ward[1] shown that all three of these failure types can be seen in a single polymer by variation of either time (rate of deformation) or temperature.

Semi-crystalline polymers such as polyethylene typically display necking behaviour and a yield point in tensile stress/strain curves[2]. Yield points are always associated with a deformation mechanism which absorbs energy. For semi-crystalline polymers this mechanism involves orientation and destruction of micron to colloidal scale semi-crystalline morphologies.

We utilized this result to study the deformation behaviour of several PE types which differed in the SCB and molecular weight[3]. The standard tensile test was used for estimation the yield stress and yield strain of the materials in the study. WAXS technique was applied to observe the re-orientation of lamellae structure as a consequence of changes in deformation rate.

Experimental

Catalyst composition alters placement of comonomer from lower to higher polymer molecular weight fraction together with a certain reduction of broadness MWD. Two polyethylene copolymers from foreign production were chosen, as reference materials (Hostalen and Borealis). The second step was to prepare material with similar molecular structure based on domestic polyethylene copolymer (Liten TB 38). The structural parameters of the basic materials are summarised in Table I.

At first two samples were prepared on the standard S2/Mg (600) catalyst:

S-1, MI = 0.6 g/10min, $\rho = 0.943$ g cm^{-3}

S-2, MI = 0.5 g/10min, $\rho = 0.945$ g cm^{-3}

Another two samples S-3 and S-4 were prepared on the same catalyst but by little bit modify polymeric condition.

Table I
Structural properties of the basic materials

Type	MI [g/10 min]	ρ [g cm^{-3}]	M_W [–]	M_W/M_n [–]	SCB [CH_3/ 1000 C]
TB 38	0.55	0.950	140 400	6.38	3.03
HOSTALEN	0.60	0.944	146 700	6.56	2.35
BOREALIS	0.47	0.942	138 300	4.05	1.90

Tensile test

The specimens were machined from 1 mm thick compression moulded plaques. The shape of specimen was in accord with ČSN EN ISO 527-3. According to this standard the tensile test were carried out on the testing machine ZWICK Z020. The test was done under three speed levels (0.5, 5, 50 mm min^{-1}) and at the temperature of 23 °C. We used extensometer for more accurately estimation of deformation. The following values were estimated:

E modulus (*E*), yield stress (σ_y), deformation at the yield point (ε_y). The results are summarize in Fig. 2.–4.

WAXS (Wide Angle X-ray Scattering)

As quality cannot always be monitored with sufficient reliability, accurate quantitative (and non-destructive) methods of evaluation and characterization can be expected to encounter a fast development. Thus 'wide angle x-ray scattering' (WAXS) techniques are of wide use[4]. The basic principle is shown in Fig. 1. The results are summarized in Fig. 5.–6.

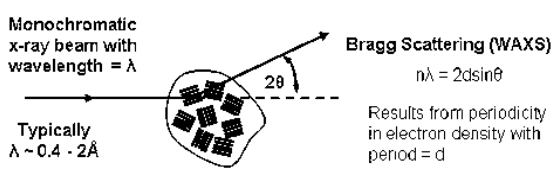

Fig. 1. **WAXS – basic principle[4]**

Visual inspection

We used optical microscop to observe the neck after the standard tensile test for material in the study. Typical examples are shown in Fig. 7.

Results and discussion

Tensile test

The rate dependence of stiffness is demostrated in Fig. 2. Obviously, due to viscoelastic behaviour of polymer, the modulus increases as the deformation rate increases. Material TB38 S-1 and TB38S- 4 devert from this trend. It could be probably due to some heterogeneity in the material.

The most similar stiffness to the reference materials has material marked as TB38 S-3.

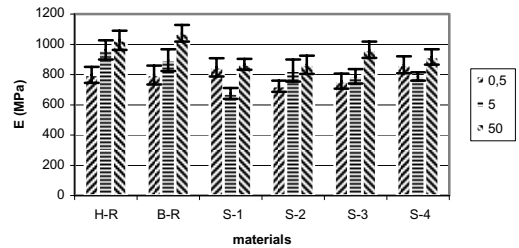

Fig. 2. **E modulus versus materials and deformation speed. H-R = HOSTALEN, B-R = BOREALIS, S-1, S-2, S-3, S-4= = TB38 S-1, TB38 S-2, TB38 S-3, TB38 S-4**

In Fig. 3. the yield stress (σ_Y) as a function of materials and deformation speed is shown. As it was expected the change in σ_Y follows the same trend as was mention above. Materials TB38 S-4 best fit the reference materials. Material TB38 S-1 is also very closed to the reference materials but due to some heterogeneity in *E* modulus we don't prefere it.

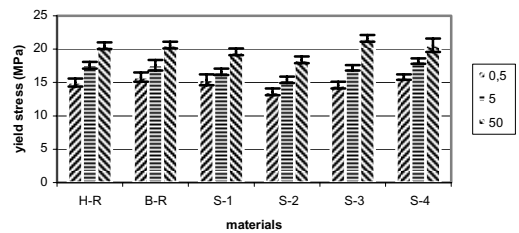

Fig. 3. **Yield stress versus materials and deformation speed**

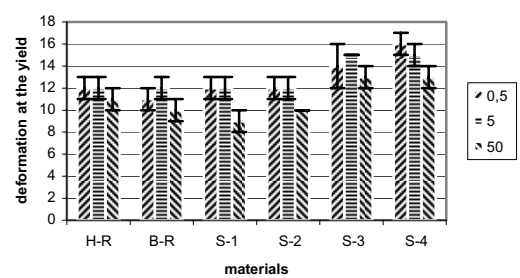

Fig. 4. **Deformation at the yield versus materials and deformation speed**

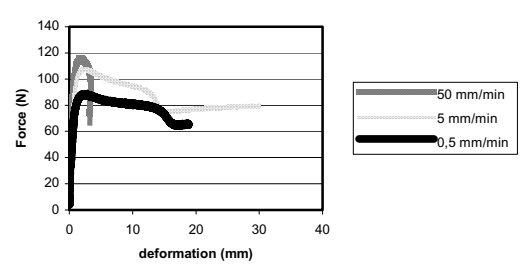

Fig. 5. **Tensile diagram for material TB38 S-1**

In the Fig. 4. the rate dependence of yield deformation for materials in the study is shown. The difference behaviour of materials in dependence on deformation rate is clear from Fig. 5. There are not significant differences among materials; however material S-2 and S-1 best fit the reference materials. In the case that material S-1 would be homogeneous enough than would be the best fits to the the reference materials in all tested values

WAXS (Wide Angle X-ray Scattering)

We used HOSTALEN as an example. Following two graphs (Fig. 6. and 7.) show dependence between intensity (counts/sec) and scattering angle (2 Th). The intensity of referent material (HOSTALEN) after tensile test is lower then the intensity of undeformed material.

This effect is caused by re-orientation of crystalline lamellae after tensile test.

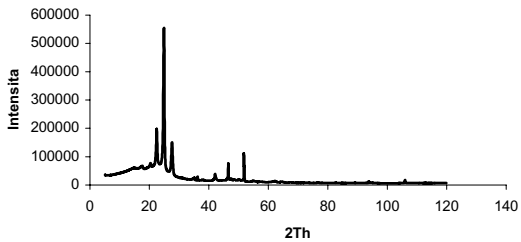

Fig. 6. **HOSTALEN – undeformed state**

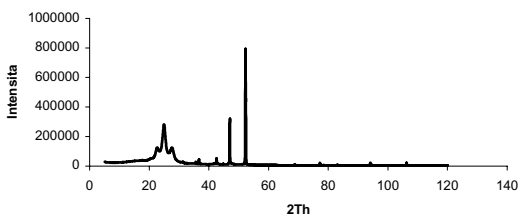

Fig. 7. **HOSTALEN – deformed state**

Visual inspection

In Fig. 8. the examples of different shape of neck are presented.The difference shape of neck give evidence of heterogeneity of materials.

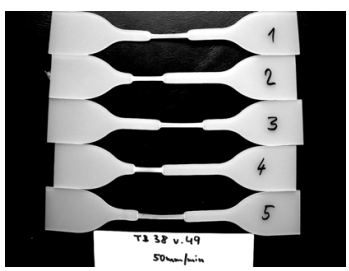

Fig. 8. **The specimens after tensile test. Material TB38 S-3, deformation speed 50 mm min^{-1}**

Conclusion

The results have shown changes in stiffness and yield stress in dependence on deformation speed and type of polyethylene copolymer.

The changes in the deformation at yield point were not significant.

The WAXS analysis (wide-angle X-scattering) confirmed the effect of re-orientation of crystalline lamellae after deformation.

The shape of the neck can tell us about heterogeneity of individual material types.

Modification of catalyst composition enabled to prepare material (S-1) similar to reference materials. Well-balanced rigid and deformation properties are necessary for applications in question i. e. binding tapes.

The research was financially supported by grant No. 101/05/0227 of the Grant Agency of the Czech Republic.

REFERENCE

1. Ward I. M.: *Mechanical properties of solid polymers*. 2nd ed. Willey, New York 1983.
2. Ward I. M.: Plastics rubber and composites *33*, 189 (2004).
3. Brooks N. W., Sirotkin R. O.: Polymer *42*, 3791 (2001).
4. Perrissin-Fabert I., Peix G., Babot D.: Meas. Sci. Technol. *15*, 889 (2004).

P27 PREPARATION OF PE-B-PP AND PE-G-PP COPOLYMERS BY REACTIVE EXTRUSION AND ITS USE IN PP/PE BLENDS

TOMÁŠ VESELÝ
Faculty of Chemistry, Brno University of Technology, Purkyňova 118, 612 00 Brno, Czech Republic,
vesely-t@fch.vutbr.cz

Problem

For the compatibilization of polymer blends have been developed three strategies of: (i) addition of a small quantity of a third component that either is miscible with both phases (co-solvent), or a copolymer whose one part is miscible with one blend's component and the second with another component (0.5–2 wt %, usually block-type, less frequently a graft one, has been used); (ii) addition of a large quantity, ≤35 wt %, of a core-shell copolymer that behaves like a multipurpose compatibilizer-cumimpact modifier; and (iii) reactive compatibilization designed to enhance domain interactions. The reactive blending may be employed to generate in-situ the desired quantities of either block and/or graft copolymer(s).

The third strategy, reactive compatibilization, was found to engender a thick interphase, which shows excellent stability under high stress and strain, such as exists during injection molding[1]. The second method of compatibilization consists of a series of steps that during compounding or processing ensure the presence of chemical reaction(s), capable of generating sufficient amounts of interfacial agents

to compatibilize in situ the system. The compatibilizing copolymer can be produced through an inter-species reaction. The process may be defined as a reaction between two or more polymers to form a copolymer. The five basic chemical processes by which interchain copolymer formation has been achieved in an extruder are summarized in Table I (ref.[2]).

Table I
Chemical processes for interchain copolymer formation in extruder reactors

Type of Chemical Reaction	Type of Obtained Copolymer
Chain cleavage	Block and random copolymers: AAAAABBBBB + AABBBBBAAA + AABBAAABBB, etc.
End-group of 1st polymer reacting with end-group of 2nd polymer	Block: AAAAABBBBB
End-group of 1st polymer reacting with pendant functionality of 2nd polymer	Graft copolymer: A – BBBBB A – BBBBB
Covalent crosslinking: pendant functionality of 1st polymer + pendant functionality of 2nd polymer + main chain of 2nd polymer	Graft copolymer or crosslinked network (crosslinked network)
Ionic bonds formation	Usually graft, frequently crosslinked A B A- - - B

The majority of polymers used to form inter-chain copolymers have nucleophilic end groups such as amine or carbroxylate. These groups can react with suitable electrophilic functionality (e. g., carboxylic acid, cyclic anhydride, epoxide, oxazoline, isocyanate and carbodiimide) leading to copolymer formation. Block copolymers can be formed through reactions between such end groups. Since the probability of two end groups reacting within the residence time in an extruder is low, highly reactive functionality and/or low molecular weight polymers are needed. This type of reaction has been used to couple polypropylene and high density polyethylene too. The procedure was suggested in two steps: 1. the preparation of polyolefine carrying amine functional groups (NAFPO) by addition of diamine with different reactivities of amine groups and 2. the preparation of inter-copolymer in situ from another maleic anhydride functional polyolefine.

Experimental

M a t e r i a l s

1. Maleic anhydride modified PP – Tabond 5007 (product of Silon a. s.) – content of MA 0.7 % wt.
2. Maleic anhydride modified PE – Eltex ADB52 (product of BP Solvay).
3. Epoxy modified PE – E-GMA copolymer Lotader AX8840 (product of Atofina) – content of GMA 8 % wt.
4. Basic type of PP homopolymer – Tiplen H890 (product of TVK, Hungary).
5. 1,3-pentanediamine – Dytek EP (product of DuPont Nylon).

P r e p a r a t i o n o f s a m p l e s

The mixing has been conducted on twin screw extruder Brabender DSE 25 by reactive extrusion. In first step was prepared a amine functionalized polypropylene by reation of MA-PP with 1.5 mole excess of 1,3-pentane diamine to exclude the possibility of cross-linking. The reactivity of the terminal amine group is assumed 100 times more than the ethyl-hindered amine group. For the purpose of the better kneading the viscosity of mixture was increased with the addition of pure polypropylene homopolymer Tiplen H890. In second step was the amine modified polypropylene blended with MA-PE or with E-GMA copolymer to prepare the inter-chain copolymers of PP-PE.

Results and discussion

The complete conversion of anhydride groups of malein anhydride to imide functionality was confirmed by infrared spectroscopy (Fig. 1.).

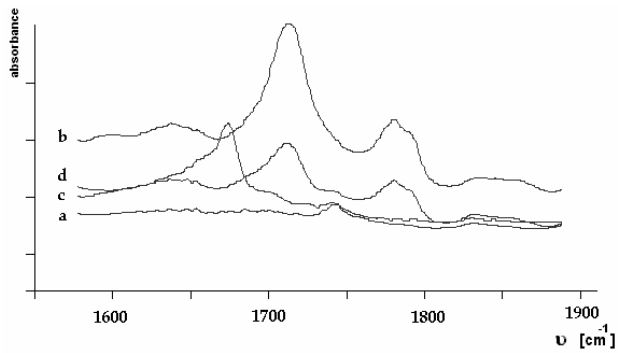

Fig. 1. **IR spectra of PP material in region 1600–1900 cm^{-1} before and after the amine grafting: a – basic type PP (Tiplen H890), b – MA-PP (Tabond 5007), c – mixture of a and b, d – mixture c modified with 1,3-diaminpentane**

The ability of thus prepared copolymers to secure the miscibility of HDPE – PP system depend on the ratio of maleic anhydride functionalized PE to HDPE and amine functionalized PP. This effectiveness can be relatively measured by kinetics of crystallization namely based on isothermal crystallization rates of PP phase in HDPE liquid at various crystallization temperatures. According to[3] the PP crystallization were readily calculated based on the Avrami equation. While the half-times for phase separated blends are similar to the pure PP the half-times for miscible blends are markedly longer and specified half-times serve as a good guide to miscibility of PP by various content and composition of polyethylene part.

Conclusion

Prepared nucleofilic amine functionalized polyolefins are of interest for blending and alloying, and hence the development of new polymeric materials. Beside mentioned use could be apply with other polymers carrying electrofilic group to support better compatibility.

REFERENCES
1. Ajji A., Utracki I. L. A.: Polymer Engineering and Science, *36*, (1996).
2. B. Brown, in *Reactive Extrusion: Principles and Practice*, M. Xanthos Ed., Hanser Pub., Munich (1992).
3. Li J., Shanks R. A., Ollez R. H., Greenway G. R.: Polymer *42*, 7685 (2001).

P28 STUDY OF SECONDARY CRYSTALLIZATION OF ISOTACTIC POLYPROPYLENE VIA PULSED ^{1}H-NMR METHOD

LADISLAV VILČ[a] and JAN KRATOCHVÍLA[b]
[a]*Institute of Materials Chemistry, Faculty of Chemistry, Brno University of Technology, Purkyňova 118, 612 00 Brno, Czech Republic, vilc@fch.vutbr.cz,* [b]*Polymer Institute Brno, Ltd., Brno, Tkalcovská 2, 656 49 Brno, Czech Republic*

Introduction

Application of polymers depends significantly on the ability of their structure to remain unchanged as long as possible. Recrystallization processes as well as changes in amorphous fraction of semicrystalline polymers (such as isotactic polypropylene), induced by ageing, can alter the properties of the basic material. In the case of physical ageing at room temperature, it was found that the main effects were connected with the amorphous phase[1]. It is well known that the form and the portion of a crystalline phase are responsible for mechanical and physical properties of semicrystalline polymers. In this study, the crystallinity was characterised as solid phase content (SPC) measured by pulsed ^{1}H-NMR.

Experimental

The polypropylene in the study was an isotactic polypropylene supplied by Czech company Chemopetrol Litvínov: Mosten 58.412 slot. 432/98 – PP homopolymer (Ziegler-Natta cat.), I.I. = 98.9 %, $MFI_{21\,N,\,230\,°C} = 3.2$ g (10 min)$^{-1}$, $MFI_{49\,N}/MFI_{21\,N} = 4.57$, $T_m = 163.0$ °C, $T_g = 5.4$ °C.

Specimens were injection moulded on Battenfeld (a) BA 750/CD injection moulding machine. Specimens with dimension 4 × 10 × 40 mm were subsequently cooled at –18 °C. The specimens were then isothermally cold crystallised at 23 (room temperature), 30, 40, 50 and 60 °C and stored at given temperature for one year approximately.

Table I
Injection moulding conditions

Melt temperature	200–230 °C
Cavity temperature	40 °C
Packing time	40 s
Injection time	29 %
Packing pressure	50 MPa
Cooling time	10 s

Pulsed ^{1}H-NMR studies were performed on Bruker the minispec mq20 NMR. It was operation at 20 MHz and 0.47 T. Temperature of magnet unit was 40 °C. The instrument conditions used were 25 scans, 18 mm diameter sample tube, spin-spin measurement of 250 points. Free Induction Decay (FID) was detected by software BRUKER – the minispec. FID signal was fitted by experimental Equation 1 (Fig. 1.). The constants were determined by non-linear least – squares curve fitting with Microsoft Excel Solver[2]. The quantity of solid phase content (SPC) was calculated according to Equation 2.

$$y = a.\exp\left(-\frac{t}{\tau_{2s}}\right) + b.\exp\left(-\frac{t}{\tau_{2l}}\right) \quad (1)$$

$$SPC\ [\%] = \frac{a}{a+b}\cdot 100\ , \quad (2)$$

where:
a is solid phase intensity
b is liquid phase intensity
τ_{2s} is spin - spin relaxation time of solid phase
τ_{2l} is spin - spin relaxation time of liquid phase
t is time of decaying.

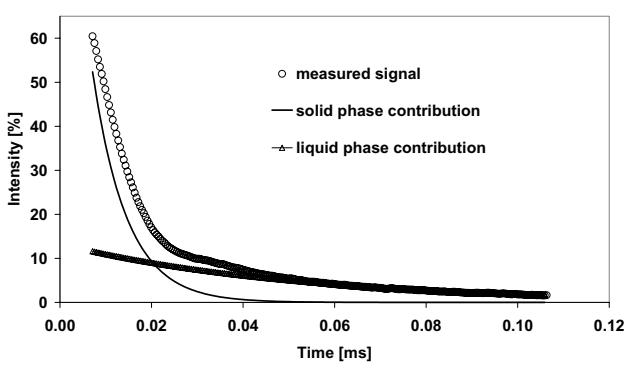

Fig. 1. **Time dependence of intensity of sample magnetisation. Example of free induction decay signal processing**

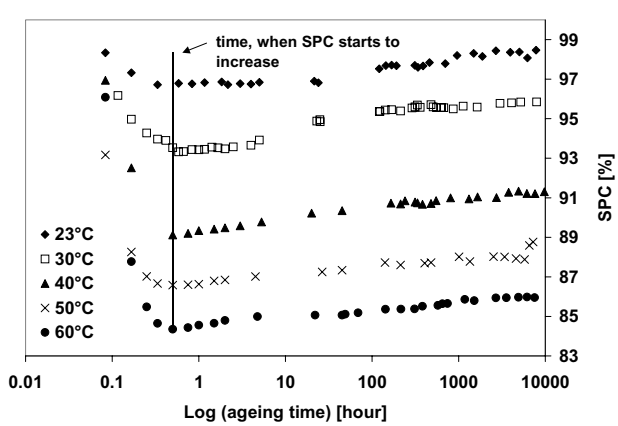

Fig. 2. **SFC plotted versus ageing time for samples aged at 23, 30, 40, 50 and 60 °C**

Results and discussion

Solid phase content

Isotactic polypropylenes show 100 % SPC below T_g. SPC is decreased with temperature[3].

The SPC versus ageing time for specimens aged at 23, 30, 40, 50 and 60 °C, is shown in Fig. 2. A strong decrease with ageing time can be observed at first 30 min for all series. It is due to balancing of temperature in specimens. Then SPC starts to increase. The time dependencies of SPC are linear with high correlation coefficients. Comparison of lines of regression equations for all series is listed in Table II. Line regression equation at 30 °C shows the highest line slope. Consequently, the secondary crystallisation is the fastest at 30 °C.

Table II
Comparison of lines of regression equations after 30 min of ageing

Temperature [°C]	Line of regression equation
23	SPC = 0.46 log t+96.62
30	SPC = 0.72 log t+93.55
40	SPC = 0.52 log t+89.38
50	SPC = 0.41 log t+86.68
60	SPC = 0.38 log t+84.55

Relaxation times

The spin-spin relaxation times (τ_{2s} and τ_{2l}) are plotted in Fig. 3. as a function of ageing time for samples aged at 23, 30, 40, 50 and 60 °C, respectively. Relaxation times of solid phase are independent on ageing time and ageing temperature but relaxation times of liquid phase depend on ageing time and ageing temperature. Our results are in agreement with M. Ito's work[4]. The relaxation time (τ_{2l}) decrease with ageing time for all series, with the exception of τ_{2l} at 23 °C. It is due to fluctuation of room temperature, probably. Relaxation times of liquid phase at 30 °C show the lowest values. This fact corresponds with the fastest secondary crystallisation at 30 °C.

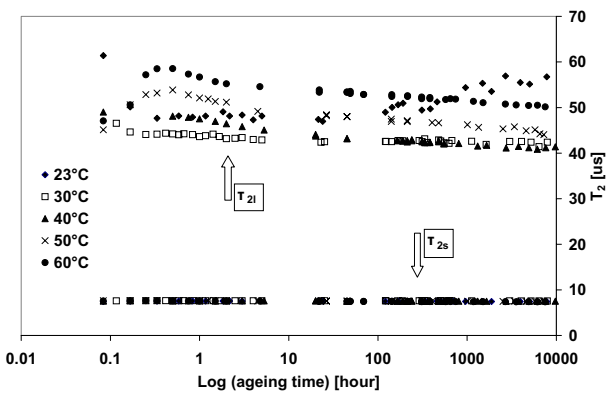

Fig. 3. **The spin – spin relaxation times (τ_{2s} and τ_{2l}) plotted versus ageing time for samples aged at 23, 30, 40, 50 and 60 °C**

This study of relaxation times confirms the fact that amorphous phase of polypropylene is responsible for changes in behaviour of material.

Conclusion

SPC of isotactic polypropylene decreased with temperature. The time dependence of SPC was linear with high correlation coefficient. The fastest secondary crystallisation was observed at 30 °C. Relaxation times of liquid phase depend on ageing time and ageing temperature. Amorphous phase of polypropylene is responsible for changes in behaviour of material.

REFERENCES

1. Dudič D., Djokovič V., Kostoski D.: Polymer Testing, 23, 621 (2004).
2. Harris D. C.: J. Chem. Educ., *75*, 119 (1998).
3. Vilč L., Kratochvíla J.: 11th Inter. Conf. Polymeric Materials 2004, PI-26.
4. Ito M., Serizawa H., Tanaka K.: J. Polym. Sci., *21*, 2299 (1983).

P29 DETERMINATION OF TRACE IMPURITIES IN TITANIUM DIOXIDE BY DIRECT SOLID SAMPLING ELECTROTHERMAL ATOMIC ABSORBTION SPECTROMETRY

BLANKA VOJTKOVÁ[a, b] and BOHUMIL DOČEKAL[a]
[a]Institute of Analytical Chemistry, Czech Academy of Sciences, Veveří 97, 611 42 Brno, Czech Republic, docekal@iach.cz, [b]Institute of Materials Science, Faculty of Chemistry, Brno University of Technology, Purkyňova 118, CZ-61200 Brno, Czech Republic

Introduction

Titanium dioxide plays an important role in various fields of technology. Apart from the mainly use as inorganic pigment in paint production, titanium dioxide becomes important compound in food industry (E 171), pharmacy, cosmetics and in other modern technologies. According to various national and international standards the content of trace toxic impurities As, Cd, Cr, Hg, Pb, Sb and Zn is one of the main characteristics for usability of this material. Consequently, determination of these detrimental impurities is of great importance. However, common analytical wet chemical procedures are inconvenient, time consuming and suffer from necessity to use concentrated hydrofluoric and/or sulfuric acids for sample dissolution[1,2,3]. Therefore, direct solid sampling introduction technique would be preferred. In this work new method for the direct determination of trace impurities in titanium dioxide solid powders by electrothermal atomic absorption spectrometry was developed when using modern dedicated atomic absorption spectrometer equipped with solid sampling system. Behavior of titanium dioxide

Table I
Instrumental parameters and experimental conditions

Element	Slit/nm	Wavelength/nm	Field intensity [T] 2-field	3-field	Temperature [°C] Pyrolysis	Atomization
As	0.5	193.7	0.8		500	1900
Cd	0.8	228.8	0.8		500	1700
Hg	0.5	253.7	1.0		130	1300
Pb	0.8	283.3	0.8	0.8/0.4	500	1800
Sb	0.2	217.6	0.8	0.8/0.5	500	1800
Zn	0.8	213.9	0.8	0.8/0.6	500	1800

matrix in the graphite tube atomizer during the analysis run was investigated. Figures of merit of determination of these detrimental elements are presented.

Experimental

All measurements were preformed with an Analytik Jena Zeenit 60 spectrometer equipped with laterally heated graphite tube atomizer and Zeeman effect background correction system. Hollow cathode lamps for As, Cd, Cr, Hg, Pb and Zn and boosted lamp (SuperLamp, Photron) for Sb were used as specific radiation sources.

Samples of five typical product types of titanium dioxide were obtained from Precheza a.s. (Přerov, Czech Republic). They had a particle size in the range of 0.15−0.40 μm. Doubly distilled water was used for preparation of sample slurries and standard solution. Calibration standards were prepared by dilution of stock standard solutions (Analytica Co., Czech Republic) with a concentration of 1 g dm^{-3}.

Two introduction techniques were used – slurry sampling and true direct solid sampling. Sample slurries were prepared in 25 cm^3 polystyrene vessels by suspending 0.1–1 g of sample in 5–10 cm^3 of water. Before analysis suspensions were treated in an ultrasonic bath for 5 minutes to disintegrate larger particle agglomerates. Typically, 5−20 μl slurry was pipetted onto the graphite boat. For true solid sampling a portion of 0.5−10 mg TiO_2 powder was placed with a spatula directly onto the graphite boat. For all elements standard addition method was used for calibration. Temperature programs and instrumental parameters are summarized in Table I.

Results and discussion

Optimum pyrolysis and atomization temperatures were found from pyrolysis and atomization curves of all analytes for five sample types. The optimum values are given in Table I. When applying high temperature treatment in cleaning step (above 2000 °C) as usually, formation of TiO_2-TiC--liquid phase and its creeping out of the sampling boat was observed. This affected substantially the tube and particularly boat analytical life times to overall approximately 30 runs. Therefore, high temperature cleaning was omitted and a sample residue was removed after atomization step mechanically by pure compressed air with minimum risk of contamination. Maximum applicable atomization temperature was 1900 °C, at which considerable interaction of a sample and graphite is not pronounced.

For calibration, a method of standard additions of aqueous standard solutions to sample slurries was applied. Very good agreement of analytical results with those provided by producer's laboratory was found. Furthermore very good correlation of analytes signal with mass of sample was also observed. It proved that samples once analyzed by wet procedure might be used as internal laboratory standard in subsequent analyses of the same sample type. It also proved that the one very well analyzed sample might serve, when introduced in different sample portions for calibration purposes. For high level analytes concentrations, reduced sensitivity of measurement can be simply achieved by applying lower magnetic field strength (3-field mode). For simultaneous measurement in the most sensitive mode and in the reduced sensitive mode, "3-field dynamic mode" is a measurement technique of choice, which can be performed by the instrument employed. Thus, very wide concentration range can be covered in one run.

Limits of detection of 21, 0.27, 24, 3.9, 6.3 and 1.5 ng g^{-1} were achieved for As, Cd, Cr, Hg, Pb, Sb and Zn respectively. Maximum amount of approximately 10 mg of titanium dioxide sample could be introduced onto the graphite boat in one run is.

Conclusions

Direct solid sampling ETAAS method was developed for the direct determination of traces of As, Cd, Cr, Hg, Pb, Sb and Zn in titanium dioxide powders. It is a simple, rapid, reliable and powerful technique. The sample digestion with hot concentrated acids is not necessary. This method provides very low limits of detection at ppb level.

This work was performed and supported within the Institutional research plan AV0 Z40310501. The authors are grateful to Mrs. A. Glomb (ANALYTIK Jena, Germany) for making available the instrument Zeenit 60 and Mr. J. Balcárek (Precheza comp., Přerov, Czech Republic) for providing powdered samples of TiO_2.

REFERENCES
1. Peng T., Du P., Hu B., Jiang Z.: Analytica chimica acta *421*, 75 (2000).
2. Dong H. M., Krivan V., Welz B., Schlemmer G.: Spectrochimica acta part B – Atomic spectroscopy *52*, 1747 (1997).
3. Wang Z., Ni Z., Qiu D., et al.: Journal of analytical atomic spectrometry *19*, 273 (2004).

P30 SYNTHESIS AND CHARACTERIZATION OF BIOCOMPATIBLE HYDROGELS

LUCY VOJTOVÁ and JOSEF JANČÁŘ
Institute of Materials Chemistry, Faculty of Chemistry, Brno University of Technology, Purkyňova 118, 612 00 Brno, Czech Republic, vojtova@fch.vutbr.cz

Efforts to emulate natural materials, which contain both hydrophilic and hydrophobic properties, have led to the development of amphiphilic biocompatible synthetic polymers[1]. This classification included hydrogels, made by cross-linking (chemical or physical) of polymer chains, which are significant for their special surface and physical properties with the ability to absorb more than 20 % of water in proportion to their total weight[2]. Recently, "smart hydrogels" with the swelling or shrinking ability driven by external stimuli have been prepared. This sensitivity to the ambient environment can be driven by changing the temperature, pH, ionic character, electric field, solvents, pressure, light or strain[3]. Up-to-date, hydrogel-preparing technique is based on "in situ" cross-linking of macromonomers via photopolymerization[4] or phase-transition reaction[5]. In the case of reversible phase-transition process, the resulted physical gel is having reversible sol-gel transition. For this purpose, thermo reversible biodegradable gels based on hydrophilic poly(ethylene glycol) (PEG) and hydrophobic poly(lactic acid) PLA and poly (glycolic acid) PGA have been recently published by Jeong at all[6]. While these thermo reversible gels increase the hydrogel applicability as injectable implants and biodegradable matrix for the controlled drug delivery systems without surgery[7], on the other hand, the reversible physical network, the phase-transition temperature range and low degree of functionality limit the application for other branches.

Therefore, the general goal of the proposed research is synthesis and characterization of well-defined "smart" amphiphilic end-functionalized hydrogels prepared from biodegradable, biocompatible, controlled life-time macromonomers. One possible way is the synthesis of multifunctional copolymers based on the hydrophilic PEG and hydrophobic PLA/PGA copolymers additionally modified by itaconic acid (ITA), which can be gained from renewable resources by pyrolysis of citric acid or by fermentation of polysaccharides[8]. The proposed synthesis consists of three steps (Fig. 1.). The hydrophobic PLA/PGA copolymer is prepared in step 1 via ring-opening polymerization followed by ITA end-capping in step 2. ITA brings reactive double bonds and functional carboxylic acid groups to the end of copolymer resulting in preparation of biodegradable macromonomer. The last step 3 covers esterification reaction of macromonomers with PEG affording PEG-co-PLA/PGA copolymers. Changing the molecular weight and molar ratio of used compounds affects the amphiphilic character of resulted PEG-co-PLA/PGA macromonomers as well as the functional groups separation and also the kinetic of degradation. PEG-co-PLA/PGA macromonomers are pH sensitive and can be cross-linked either by covalent bonding (photopolymerization) or by ionic interaction (physically) in order to produce 3D-hydrogel network Moreover, functional –COOH or –OH groups can be used as coupling sites for increasing hydrogel's biocompatibility, bioinductivity, adhesion or other physical properties and thus might be "tailored" for a certain type of application such as biomedical (e. g. injectable polymer drug delivery systems, tissue implants, resorbable adhesives), agricultural (controlled fertilizer and seed release films), industrial (breathable disposable protective cloth fabric) and environmental (waste-free production).

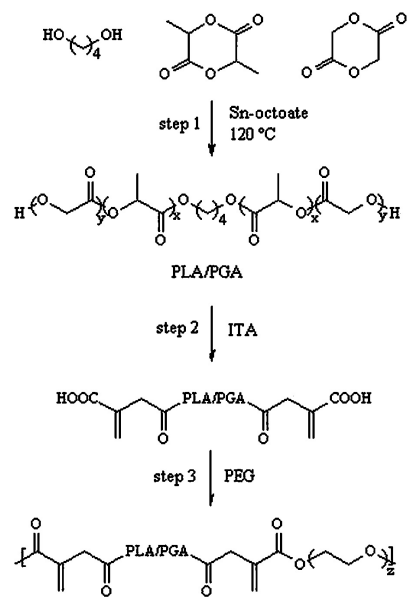

Fig. 1. **The synthesis of multifunctional copolymers of PEG-co-PLA/PGA**

This work was supported by the Ministry of Education of the Czech Republic under research project MSM 0021630501.

REFERENCES
1. Nagata M., Kono Y., Sakai W., Tsutsumi N.: Macromolecules, *32*, 7762 (1999).
2. Brunski A. H., Cooper J. B., Hench S. L., et al.: Biomater. Sci., *37*, 130 (1996).
3. Park H., Park K.: ACS Symp. Ser., *627*, 2 (1996).
4. Hubell J. A.,Pathak C. P., Sawhney A. S., Desai N. P.,

Hossainy S. F. A. (The University of Texas): US patent *5*, 801,033 (Sep.1, 1998).
5. Stile R. A., Burghardt W. R., Healy K. E.: Macromolecules, *32*, 7370 (1999).
6. Jeong B., Kibbey M. R., Birnbaum J. C., Won Y. Y., Glutowska A.: Macromolecules, *33*, 8317 (2000).
7. Jeong B., Kim S. W., Bae Y. H.: Advanced Drug Delivery Reviews, *54*, 37 (2002).
8. Ramos M., Huang S. J.: *Functional Condensation Polymers* (Kluwer Academic), p. *185–198*. New York 2002.

P31 THE HPLC AND GPC CHARACTERIZATION OF THE OZONIZED BEECH PULP

MILAN VRŠKA[a], LÍVIA HAVRILOVÁ[a], MARTIN POLOVKA[a], MICHAL JABLONSKÝ[a], KATARÍNA HROBOŇOVÁ[b], JOZEF LEHOTAY[b] and SVETOZÁR KATUŠČÁK[a]

[a]Department of Chemical Technology of Wood, Pulp and Paper, milan.vrska@stuba.sk, [b]Department of Analytical Chemistry, Faculty of Chemical and Food Technology, Slovak University of Technology in Bratislava, Radlinského 9, 812 37 Bratislava

Introduction

The oxidation reactions of pulp bleaching with ozone lead to the production of complex multi-component mixture of lignins and other degradation products, originating from polysaccharides, present in the liquid phase. Continuing attention has been paid to cellulose degradation processes, occurring during the ozone bleaching. Low-molecular products from ozonization can be effectively determined by means of various methods i. e.: GC, GCMS, NMR or EPR spectroscopy. To characterize the high-macromolecular fractions, mainly UV/VIS, IR/FTIR spectroscopy as well as SEC/GPC and other experimental methods, suitable for the measurement of the changes in optical and morphological structure are frequently used. These experimental methods are usually used separately with the aim to monitor only the specific changes of concrete component of multy-component reaction system.

The aim of this work is the improvement of the complex analysis of low molecular extractive and macromolecular components of ozonized pulps using both HPLC and GPC methods.

Experimental

Sample characterization. Holocellulose from beech, prepared as previously suggested by Wise et al.[1], was used. Before the ozonization procedure, the sample of holocellulose was mixed with 7 cm^3 of H_2SO_4 (30.6 g dm^{-3}) to obtain pH of approximately 2.5–3. Subsequently, the water suspension was ozonized at 40 °C using the ozone flow rate 120 mg of ozone per 20 g of dry holocellulose. The ozonized holocellulose was then wash-out with distilled water. The solid phase was separated from the liquid and analyzed in GPC and HPLC.

HPLC analysis. The sample of ozone-treated holocellulose was analyzed using two different HPLC methods. The first of them was carried out in an order to determine saccharides content. Acetonitrile of HPLC grade (Merck, Germany) and deionized water were used as solvents. Some monosaccharides were used as standards. The samples were pre-concentrated 100 times. The second HPLC method was used in an order to determine the content of organic acids by means of direct injection of the water solution (extract from cellulose) to the analytical column. The analytes were separated by employing the gradient elution. DAD-UV detector, processing sensitive responses at the wavelength of 210 nm was used for the detection. The detected acids were quantified using the external calibration curve.

GPC analysis. The pullulan standards (Fluka, Switzerland) were prepared in two separate solutions containing 0.025 % (w/v) of each standard in DMAc. The samples were dissolved in LiCl–DMAc as described in[2]. To the evaluation of a distribution of molar weights (M_w) of ozonized holocellulose, GPC analysis on Viscogel HR High Resolution Columns was employed under following conditions: inlet volume, 20 µl; eluent flow rate, 0.5 cm^3 min^{-1}; the pressure on columns, 4 MPa; columns temperature, 80 °C; temperature of refractive index detector, 40 °C. The solution of 1% LiCl/DMAc (w/v) was used as eluent.

Results and discussion

During the ozonization process, the holocellulose samples undergo the degradation processes, resulting in the production of low-molecular components, released from the sample progressively in each stage of process. These products were immediately trapped and analyzed after pre-concentration using HPLC (Fig. 1. and 2.). As depicted at Fig. 1b, methyl-D-glucopiranose, D-fructose and glucose

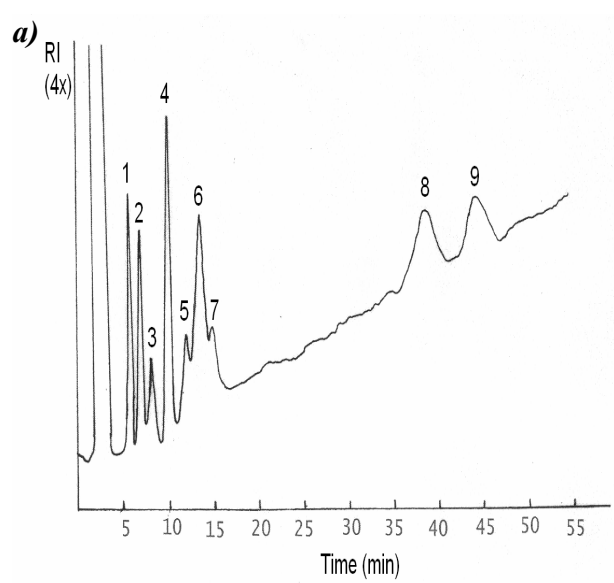

b)

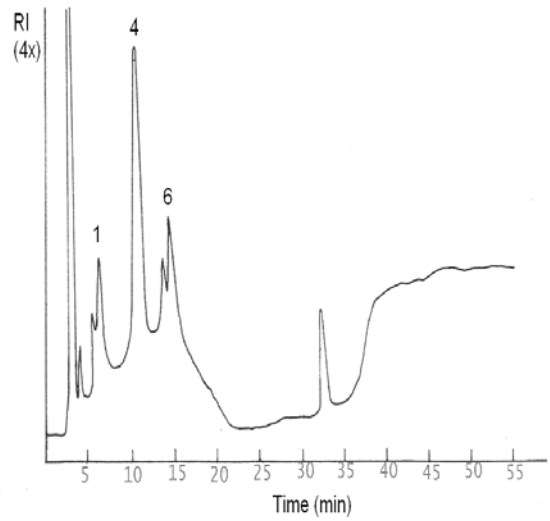

Fig. 1. **The identification of degradation products of holocellulose modified with H_2SO_4 (pH 2.5–3): a) sugar standard solutions containing 5.0 mg cm^{-3} of each: 1 – methyl-D-glucopiranosid, 2 – xylose, 3 – L+D-arabinose, 4 – D -fructose, 5 – D -manose, 6 – glucose, 7 – D -galactose, 8 – cellobiose, 9 – lactose; b) sample of holocelulose solution after the ozonization treatment. HPLC analysis was employed under the following experimental conditions: Separon SGX NH_2 (150 × 3 mm, 5 µm), acetonitrile/water 85/15 (v/v), refractive index detector RI (4×, +polarity), UV detector (210 nm), mobile phase flow rate 0.7 cm^3 min^{-1}, temperature 25 °C, sample loop 20 µl**

were identified as the primary oxidative products. Consecutive secondary reactions cause the destruction of glycosidic bonds accompanied with the decrease of polymerization degree. This is the explanation of the observed arise of the amount of glucogalactones, methylesters, as well as of monomer units of glucose.

In the second HPLC analysis, (Table I), mainly formic, acetic, propionic and butyric acids were determined.

The above described oxidative degradation of glycosidic bonds after ozone treatment causes beside the decrease of the degree of polymerization also the changes in the molecular weights distribution (Fig. 3.) and, finally, influences the parameters of polydispersity (M_w, M_n, M_z). The GPC experiments are in progress nowadays, in an order to verify these facts. Our expectations should be in accord with previously published data for GPC analysis of pullulans or polyurethanes[3,4].

Conclusions

The consistent combination of the HPLC and GPC, as well as of other analytical methods (gravimetry or infrared spectroscopy) provided new valuable information on the low molecular degradation products and on the changes of molecular weight distribution and polydispersity parameters of cellulose.

Table I
The results of HPLC analysis of organic acid content in liquid phase after the ozonization of holocellulose samples

Sample no.	Formic acid [µg cm^{-3}]	Acetic acid [µg cm^{-3}]
1	618	3.3
2	936	176

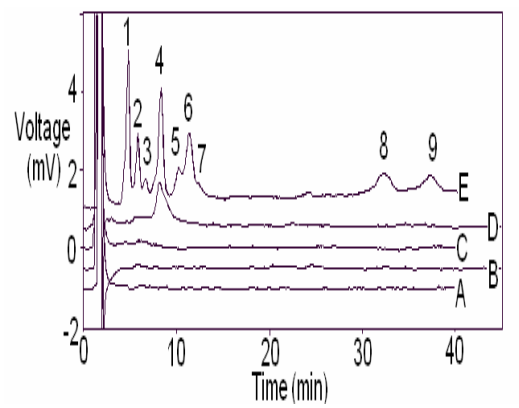

Fig. 2. **HPLC analysis of different extracts from solid phase of: A, B – water/methanol extract of pulps (different conditions of ozonization were used); C – water/methanol/DMAc extract of holocellulose after ozonization; D – water /methanol extract of holocellulose before ozonization; E-sugar standards solution containing 5.0 mg cm^{-3} of each: 1 – methyl-D-glucopiranosid, 2 – xylose, 3 – L+D-arabinose, 4 – D-fructose, 5 – D-manose, 6 – glucose, 7 – D-galactose, 8 – cellobiose, 9 – lactose**

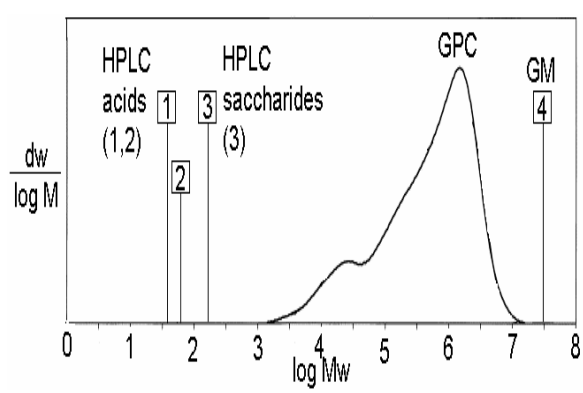

Fig. 3. **The consistent combination of HPLC, GPC and other methods of analysis of holocellulose:**
***HPLC*: 1. Formic acid (M_w = 46 g mol^{-1}); 2. Acetic acid (M_w = 60.05 g mol^{-1}); 3. D-Fructose (M_w = 180.1 g mol^{-1});**
***GPC*: molecular weights distribution. GPC chromatographic conditions: column temperature, 80 °C; PL Mixed A columns; mobile phase, 0.5 % LiCl/DMAc; refractive index detector [3];**
***Gravimetry (GM)* or *FTIR* – insoluble rest of holocellulose, m = 0.00179 g (17,9 % from original mass)**

We thank Slovak Grant Agency (Projects VEGA 1/0061/03 and VEGA 1/2460/05) for its financial support.

REFERENCES

1. Wise L. E., Murphy M., D´Addieco A. A.: Paper Trade J. *122*, 35 (1946).
2. Strlič M., Kolenc J., Kolar J., Pihlar B.: J. Chromatogr. A *964*, 47 (2002).
3. Sjöholm E.: Carbohydr. Polym. *41*, 1 (2000).
4. Katuščák S., Tomáš M., Schiessl O.: J. Appl. Polym. Sci. *26*, 381 (1981).

P32 MICROCOMPOSITE SILICA-POLYNORBORNENE VIA SURFACE INITIATED POLYMERIZATION

PETR ZDÍLNA
Brno University of Technology, Faculty of Chemistry, Department of Chemistry of Materials, Purkynova 118, 612 00 Brno, Czech Republic, zdilna@yahoo.com

Introduction

Controlling of the surface properties is a main effort of numerous research areas and technological processes from biotechnology to microelectronics. One of the methods used to modify surface properties is utilization of polymer brushes. Apart from physisorption method and "grafting to" method is "grafting from" process, facilitating more thick, covalently tethered polymer brushes with a high grafting density than in case of physisorption and "grafting to" processes. Ring-opening metathesis polymerization (ROMP) using 1st generation Grubbs catalyst was applied to the "grafting from" polymerization of norbornene from the silica surface. As a result, hybrid material – silica particles gathered with covalently grafted polynorbornene chains was prepared.

Results

The process of preparation polynorbornene brush modified silica surface via surface initiated ROMP comprise of three subsequent steps.

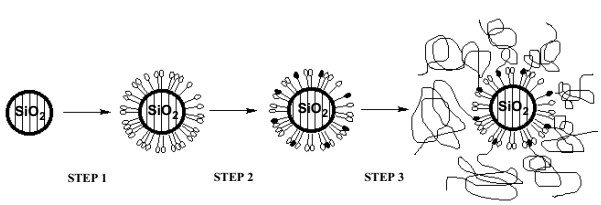

Fig. 1. **Schematic view of polynorbornene brush modified silica preparation**

In the first step is surface of silica modified with norbornenyl ligands necessary for co-production of catalytic active centres in the subsequent step. Typically, silica surface hydroxyl groups undergoes a silanization reaction with

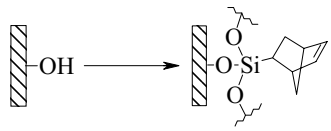

Fig. 2. **Silanization of silica surface with norbornenyltrichlorosilane. Trichlorosilane group reacts with a hydroxyl group**

trichlorosilane groups of bifunctional 5-(bicycloheptenyl)-trichlorosilane, providing so a surface site of norbornenyl ligands, dwelling at the silica surface[1].

The extent of silanization depends on several factors such as concentration of norbornenyltrichlorosilane, polarity of a reaction solvent, concentration of amine catalyst, reaction temperature, duration of silanization and amount of water adsorbed at silica surface. Presence of norbornenyl groups at the silica surface was confirmed by FTIR analysis. The quantitative amount of norbornenyl groups at the silica surface was determined using FTIR and combined with elementar analysis. For following syntheses were used norbornene modified silicas with typically 1.8–2.1 NOR groups nm^{-2}.

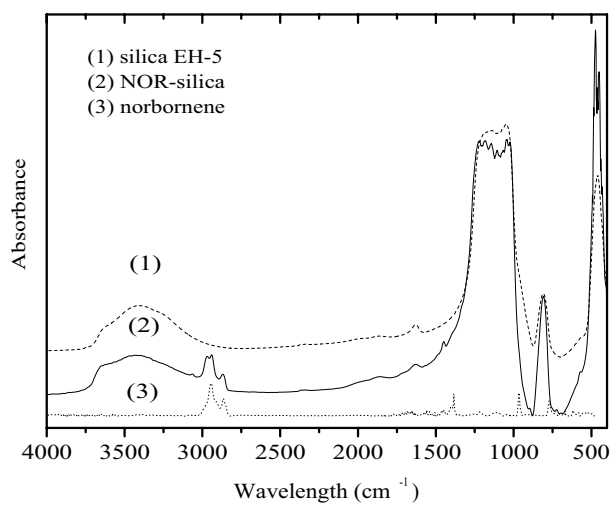

Fig. 3. **FTIR spectra of untreated silica Cab-O-Sil EH-5 (1); silanized silica (2) with norbornenyl groups and norbornene monomer (3)**

Catalytic active centres for polymerization of norbornene monomer are formed in a next step by reaction of silica surface norbornenyl groups with ruthenium catalyst [$(Cy_3P)_2Cl_2Ru$=CHPh, Cy – cyclohexyl]. In fact, this is a initiation reaction of silica surface initiated ROMP.

Progress in initiation reaction was studied by UV-VIS spectroscopy as a decrease of catalyst concentration in a reaction mixture at a wavelength 335 nm, specific for a catalyst molecule[2]. It was observed a second order exponential decrease of a catalyst amount in time during the initiation reaction.

If there are not unbonded free catalyst molecules in a reaction mixture, polymeration is initiated at the silica surface

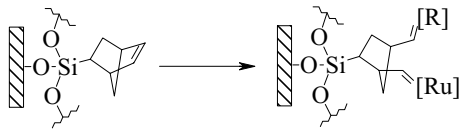

Fig. 4. **Formation of catalytic active centres at silica surface. Catalyst molecule react with a norbornene ligand at silica surface**

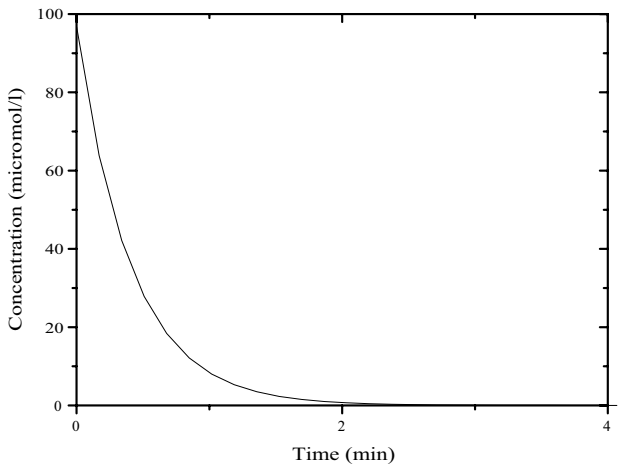

Fig. 5. **Decrease of catalyst amount in reaction mixture in time during active centres formation at silica surface. The typical amount of active centres at silica surface was 0.15 % comparable to norbornenyl groups at silica surface. Initiation is finished after 3 minutes**

and polymer chains grafted by one end to the surface grow from the surface up. Monomer is inserted into active centres, located during all the process at chain ends. Grafting density of polymer brush is directly proportional to the surface density of the active catalyst centres formed while initiation.

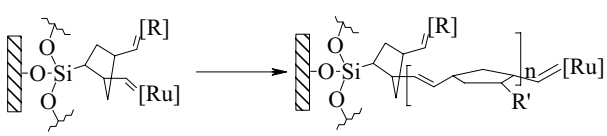

Fig. 6. **Propagation reaction of norbornene polymeration**

Kinetics of polymerization reaction was studied by gravimetric analysis of yielded polymer and compared by dilatometric analysis of polymer shrinkage during polymerization.

To avoid presence of a free, unreacted catalyst molecules in a polymeration mixture, low catalyst concentration are used during polymerization. Growing of polymer chains is stopped by termination with ethylvinylether. For subsequent GPC analysis are polymer molecules cleaved from silica surface by etching the silica by hydrofluoric acid[3].

Discussion

A very crucial circumstances of norbornene polymerization by ROMP from silica surface are: presence of free,

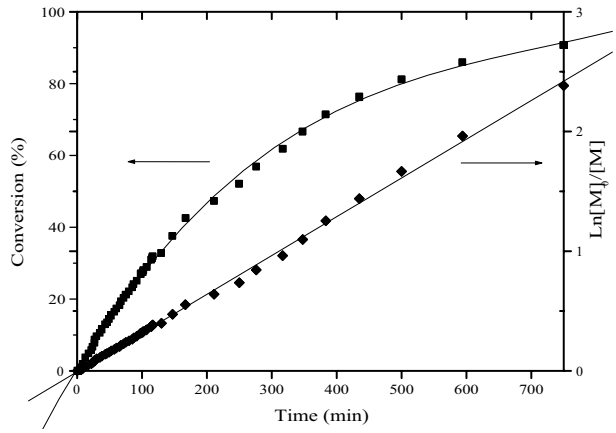

Fig. 7. **Dilatometric analysis of polynorbornene shrinkage during a comparative nongrafting polymerization in solution. During grafting polymerization shrinkage does not occure in such an extent**

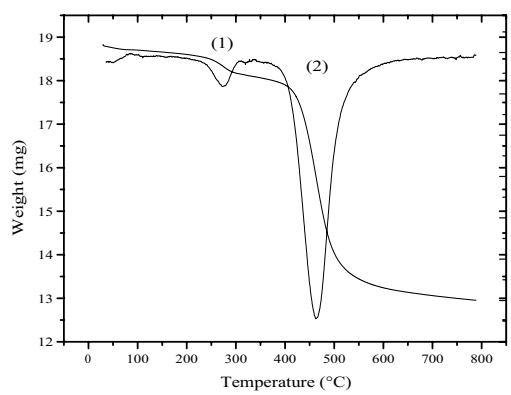

Fig. 8. **TGA analysis of polynorbornene grafted from silica surface. The first decrease in weight corresponds to a unreacted norbornenyl ligands at silica surface, the second decrease in weight corresponds to polynorbornene**

unbound catalyst in a reaction mixture and also critical norbornene concentration in a reaction mixture. When free catalyst is present, polymerization proceeds preferentially in a solution and polynorbornene does not groove from silica surface. In case of critical norbornene concentration, when it is not reached polymerization products are oligomers. To avoid this problems polymerization conditions were tuned.

REFERENCES

1. Mayr B., Buchmeiser, M. R.: Journal of Chromatography *A73*, 907 (2001).
2. Holland M. G., Griffith V. E., France M. B., Desjardins S. G.: J. Polym. Sci., Part A, Polym. Chem. *41*, 2125 (2003).
3. Werne T., Patten T. E.: J. Am. Chem. Soc. *123*, 7497 (2001).

P33 AB INITIO STUDY OF NICKEL MAGNETISM ALONG THE TETRAGONAL AND TRIGONAL DEFORMATION PATHS

MARTIN ZELENÝ[a,b], DOMINIK LEGUT[b], MOJMÍR ŠOB[c,b] and JAROSLAV FIALA[a]
[a]*Faculty of Chemistry, Brno University of Technology, Purkyňova 118, 612 00 Brno, Czech Republic, zeleny@fch.vutbr.cz,* [b]*Institute of Physics of Materials, Academy of Sciences of the Czech Republic, Žižkova 22, 616 62 Brno, Czech Republic,* [c]*Department of Theoretical and Physical Chemistry, Faculty of Science, Masaryk University, Kotlářská 2, 611 37 Brno, Czech Republic*

Introduction

Magnetic thin films and multilayers have recently attracted a lot of interest because of their technological importance in data storage and sensor applications as well as in fundamental research of magnetism. We calculate total energy of nickel along the tetragonal and trigonal deformation paths at various volumes (see Fig. 1.)[1] to identify the stable and metastable phases and to find the phase boundaries between various nickel modifications. The calculated total energies are used to predict lattice parameters and the type of magnetic ordering of nickel overlayers at various (001) and (111) substrates.

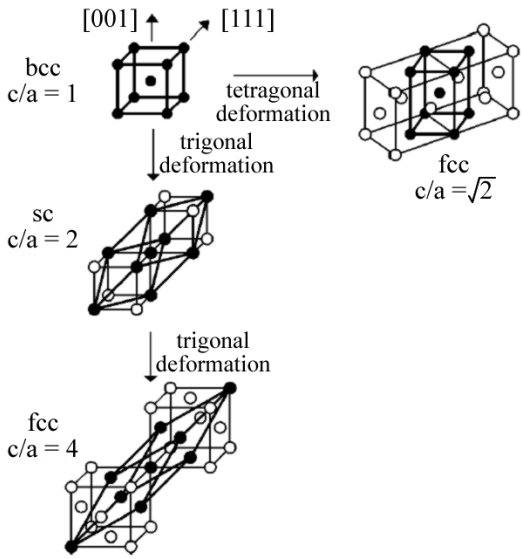

Fig. 1. **High-symmetry structures obtained along the tetragonal and trigonal deformation paths. The c and a are the dimensions of the crystal along the deformation direction and along a perpendicular direction, respectivel**

Material and methods

We calculate the total energy of non-magnetic (NM) and ferromagnetic (FM) nickel above mentioned deformation paths keeping the atomic volume constant. For the total-energy calculations, we employ the full-potential linearized augmented plane waves method incorporated in Wien2k code[2]. The calculations are performed using the generalized gradient approximation (GGA) and local density aproximation (LDA).

The muffin-tin radius of nickel atoms of 2.00 a.u. is kept constant for all calculations, the number of *k*-points in the whole Brillouin zone is equal to 8000, and the product of the muffin-tin radius and the maximum reciprocal space vector, $R_{MT}k_{max}$, is equal to 9. The maximum *l* value for the waves inside the atomic spheres, l_{max}, and the largest reciprocal vector *G* in the charge Fourier expansion, G_{max}, is set to 9 and 16, respectively.

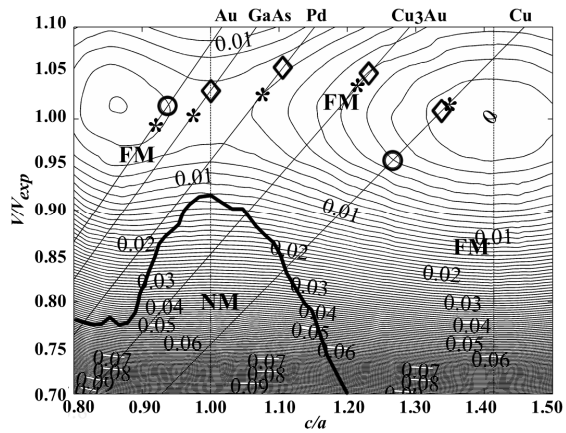

Fig. 2. **Total energy of nickel as a function of c/a and volume along the tetragonal deformation path relative to the FM fcc equilibrium state energy calculated within the GGA. Only states with the minimum energy are shown. The contour interval is 1 mRy/atom**

Table I
The c/a ratio of nickel overlayers on (001) substrates in comparison with theoretically predicted results and calculated magnetic moments. Theoretical results presented in the first four lines (GaAs, Pd, Cu_3Au, Cu) belong to the present work

Substrate	a_{sub} [a. u.]	*c*/*a* (exp)	*c*/*a* (theory)	μ [μ_B] (theory)
GaAs[a]	10.67	1.00	0.98	0.54
Pd[b]	7.34	1.11	1.08	0.56
Cu_3Au[c]	7.08	1.23	1.22	0.61
Cu[d]	6.82	1.34	1.35	0.63
Cu (calc.)[e]	6.82	1.27	1.35	0.63
Au (calc.)[f]	7.69	0.94	0.92	0.55

[a]ref.[3] [b]ref.[4] [c]ref.[5] [d]ref.[6] [e]ref.[7] [f]ref.[8]

Results and discussion

Fig. 2. displays the total energy of nickel as a function of c/a and volume along the tetragonal deformation path relative to the energy of the FM fcc equilibrium state calculated

within the GGA. Thick line shows the FM/NM phase boun--dary. Along the tetragonal deformation path at the experimental atomic volume of the FM fcc nickel of 73.58 a. u.[3] ($V/V_{exp} = 1.0$), only the FM state is stable. The NM state is stable for atomic volumes lower than about $V/V_{exp} = 0.9$ in the neighbourhood of the bcc structure. In the LDA calculation, all extrema on contour plot (global minimum, saddle point and local minum) are shifted to lower volume, $V/V_{exp} = 0.93$. Surprisingly, the position of borderline between NM and FM states is not very different within the GGA and LDA.

The contour plot in Fig. 2. enables us to predict easily the lattice parameters and magnetic states of nickel overlayers at various (001) substrates[9]. Let us suppose that pseudomorphic nickel overlayers adopt the lattice dimensions of the substrate in the (001) plane and relax the interlayer distance (characterized by *c/a*). If the lattice constant of a fcc substrate is equal to asub, then in the coordinates $x = c/a$, $y = V/V_{exp}$, and $z = E - E_0$, the surfaces corresponding to a fixed a_{sub} in the (001) planes are the planes $y = kx$ (straight lines in Fig. 2.), where $k = (\sqrt{2}/8)(a_{sub}^3/V_{exp})$. The configuration and magnetic state of nickel overlayers on a (001) substrate should correspond to the energy minimum constrained to this plane provided that the effect of the substrate/overlayer interface consists primarily in fixing the lattice constant of the Ni overlayer in the (001) plane to asub. For the GaAs substrate with zinc blende structure, we have $k = (1/16)(a_{sub}^3/V_{exp})$. Comparison with experimental data and with other calculations is summarized in Table I. It may be seen that the calculated lattice parameters of Ni(001) thin films on various metallic substrates (represented by asterisks in Fig. 2.) agree well with the experimental values (diamonds) and wit the other calculations (circles). The calculated magnetic moments of nickel overlayers presented in Table I are our theoretical predictions.

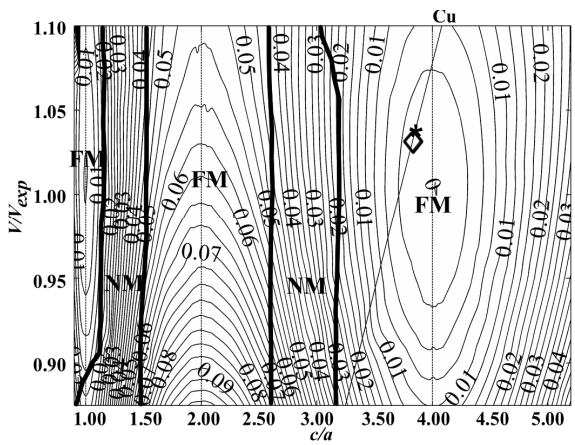

Fig. 3. **Total energy of nickel as a function of c/a and volume along the trigonal deformation path relative to the FM fcc equilibrium state energy calculated within the GGA. Only states with the minimum energy are shown. The contour interval is 2.5 mRy/atom**

Table II
The c/a ratio of nickel overlayers on Cu(111) substrates in comparison with theoretically predicted results

Substrate	a_{sub} [a. u.]	*c/a* (exp)	*c/a* (theory)	μ [μ_B] (theory)
Cu	6.82	3.82	3.84	0.63

Fig. 3. displays total energy of nickel as a function of *c/a* and volume along the trigonal deformation path relative to the energy of the FM fcc equilibrium state calculated within the GGA. The straight line corresponds to constant lateral lattice parameters of the Cu(111) substrate. The meaning of symbols is the same as in the Fig. 2. Along the trigonal deformation path, there are two NM areas for all calculated volumes. The first one is found between $c/a = 1.2$ and $c/a = 1.5$, the second one between $c/a = 2.6$ and c/a = 3.3. In the LDA calculation, all extrema within the contour plot are shifted to lower volumes, $V/V_{exp} = 0.93$, and the position of borderlines between NM and FM states are the same as those obtained within the GGA.

Again, we can use this contour plot to predict the lattice parameters and magnetic states of nickel overlayers on (111) substrates as in the tetragonal case. On the (111) substrate, there are two possible stackings of layers: "ABABAB" giving the hcp structure and "ABCABC" exhibiting trigonally distorted fcc structure. Trigonal deformation path can be used to predict only the parameters of the trigonally distorted fcc overlayers. The configurations of the Ni thin films on the (111) substrates correspond to bound minima of the total energy along the straight lines representing individual subtrates. Again, these straight lines are described by an equation $y = kx$ where $y = V/V_{exp}$, $x = c/a$ and $k = (1/16)(a_{sub}^3/V_{exp})$, analogously to (001) overlayers. We found only one experimental paper regarding Ni overlayers on the Cu(111) substrate[10]. Comparison of our predictions with experimental data is summarized in Table II.

Conclusion

We have calculated the total energies of nickel as a function of volume and tetragonal or trigonal deformation for various magnetic phases and found the phase boundaries between the FM and NM modifications. The calculated contour plots can be used for the understanding and prediction of lattice parameters and magnetic states of Ni(001) and Ni(111) films on various metallic substrates.

This research was supported by the Grant Agency of the Czech Republic (Projects No. 202/03/1351 and 106/05/H008), by the Grant Agency of the Academy of Sciences of the Czech Republic (Project No. IAA1041302), and by the Research Projects AV0Z20410507 and MSM0021622410.

REFERENCES

1. Wang L. G., Šob M.: Phys. Rev. B *60*, 844 (1999).
2. Blaha P., Schwarz K., Madsen G. K. H., Kvasnicka D. and Luitz J.: *WIEN2k, An Augmented Plane Wave + Local Orbitals Program for Calculating Crystal Properties* (Karlheinz Schvarz, Techn. Univerzität Wien, Austria), 2001.
3. Tang W. X. et al., J.: Mag. Mag. Mat. *240*, 404 (2002).
4. Petukhov M., Rizzi G. A., Sambi M., Granozzi G.: Appl. Surf. Sci. *212*, 264 (2003).
5. Braun A., Feldmann B., Wuttig M.: J. Mag. Mag. Mat. *171*, 16 (1997).
6. Yang Z., Gavrilenko V. I., Wu R.: Surf. Sci. *447*, 212 (2000).
7. Wang D., Freeman A. J., Krakauer H.: Phys. Rev. B *26*, 1340 (1982).
8. Luedtke W. D., Landman U.: Phys. Rev. B *44*, 5970 (1991).
9. Friák M., Šob M., Vitek V.: Phys. Rev. B *63*, 052405 (2001).
10. Huang F., Kief M. T., Mankey G. J., Willis R. F.: Phys. Rev. B *49*, 3962 (1994).

P34 DIFFUSION PARAMETERS OF ZINC IN STEELS WITH VARIOUS CHEMICAL COMPOSITION

MARTIN ZMRZLÝ, JOSEF TRČKA
and JAROSLAV FIALA
Faculty of Chemistry, Brno University of Technology, Purkyňova 118, 612 00 Brno, Czech Republic, zmrzly@fch.vutbr.cz

Introduction

Electrolyticaly deposited zinc protective coatings are very often used for corrosion protection of large spectrum of steel parts in engeneering practice. During this wide spread coating technology however a danger of hydrogen embrittlement arises due to the use of electrolyses in water solutions (cathodic hydrogen liberation) and/or due to the pickling in strong inorganic acids prior to zinc deposition. Hydrogen can be safely removed later by short annealing at temperatures at about 300 °C[1].

During annealing the temperature is high enough to increase significantly diffusion of iron and zinc between the coating and substrate. In this way, up to four different Fe-Zn intermetallic compounds can be formed at the interface[2]. These phases are generally much harder as well as brittle than the original layer of zinc coating[3].

From the literature it is well known, that diffusion rate of zinc in steel strongly depends on steel chemical composition[4]. One of the most important factors influencing diffusion rates is the silicon content[5]. Using the diffusion zincing technology (sherardising), it was possible to estimate the activation enthalpy of zinc diffusion in steel[6]. Several papers can be found bringing correlation of activation enthalpy and silicon content in steels[7].

The main goal of the present paper is to observe the growth of intermetallic layers in electrodeposited zinc coatings and theire dependence on steel composition and heat treatment (i. d. annealing time and temperature).

Theoretical

The zinc diffusion from coating into steel can be analytically treated approximately as a diffusion in semi-infinite mass from the surface of constant concentration. The solution of differential equation of The second Fick's law is then an expression:

$$\frac{c - c_0}{c_1 - c_0} = erfc \frac{z}{\sqrt{(4Dt)}}, \qquad (1)$$

where erfc is a complementary error function of (*erfc* $x = 1 - erf\, x$), z is a distance from the surface, D is diffusion coefficient, t is duration of diffusion, c is concentration of difunding element at time t in distance z, c_0 is initial concentration of this element inside the mass and c_1 is concentration of element on the surface of the mass at time t.

Experimental

Four types of steel sheets were studied. Three of them belonging to Czech standards (ČSN) 41 1321, 41 2010, 41 4331 and the fourth was German armour steel WWB 600. Their chemical compositions are shown in Table I.

Sheet samples were electrolyticaly coated by zinc in weak-acid bath. The temperature of bath was 20 °C, current density of 1.5 A dm^{-2}, and DC voltage of 1.5 V. Coatings of thickness 20–40 μm were obtained. These coated samples were annealed in a box furnace. Annealing experiments were carried out as follows:

11 321: 270 °C; 1–15 hrs
12 010: 270 °C; 0.5–15.0 hrs
14 331: 270 °C; 0.5–7.0 hrs
WWB 600: 270 °C; 0.5–7.0 hrs.

Coatings cross sections were prepared using usual metallographical treatment and thicknesses of intermetallic layers were observed and measured by means of light metallographical microscope.

Results and discussion

The growth of the intermetallic phases is evident from plots in Fig. 1. The best fit of the values seems to be parabolic. In the case of steel 11 323 the result obtained after 15 hours should be excluded as false. Then the reliability coefficient R^2 increases to 0.96 from original value of 0.64. Almost linear relationship seems to be very significant in the case of steel 12 010 (power coefficient 0.91). This reflects probably a bit different micromechanism of zinc diffusion in steel of this type with silicon content.

Table I
Compositions of steels used for experiments

Steel	C	Si	Mn	P	S	Cr	Mo	Ni	Al
11321	0.04	0.025	0.18	0.013	0.016				
12010	0.11	0.42	0.73	0.014	0.035	0.12		0.62	
14331	0.32	1.25	1.17	0.017	0.009	0.96			
WWB 600	0.49	1.41	0.58	0.008	0.003	1.03	0.39	1.05	0.046

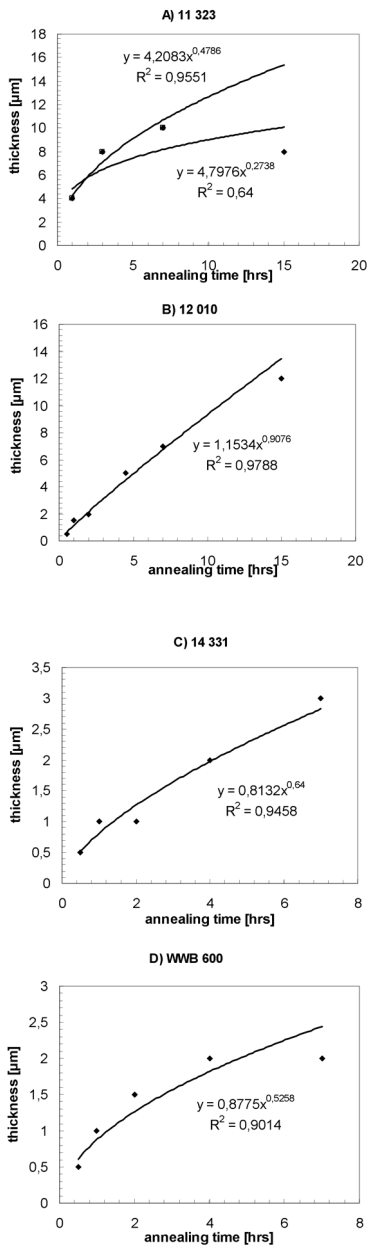

Fig. 1. **Thicknesses of diffusion layers and their dependencies on the duration of annealing at 270 °C. Steel: A) 0.025 pct. Si, lower fit includes the last point, B) 0.42 pct. Si. C) 1.25 pct. Si D) 1.41 pct. Si**

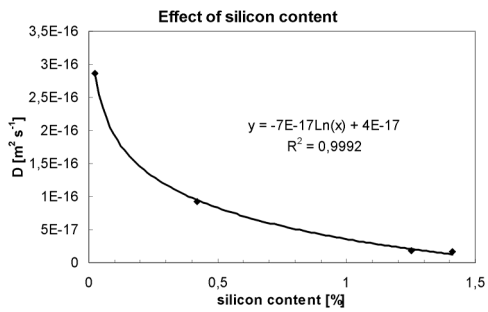

Fig. 2. **Effect of silicon content on diffusion coefficient of zinc in four different types of steels at 270 °C**

Diffusion coefficients were evaluated according to the Equation 1. Since the bottom of diffusion layer was formed by thin layer of zinc solid solution in α-iron of concentration approx. 6pct. (at.), the value c was taken to be 0.06, $c_0 = 0$ and $c_1 = 1$. Then z was a thickness of the diffusion layer after time *t*. Plot of the dependence of diffusion coefficient vs. silicon content is shown in Fig. 2.

The best fit of the experimental values found is logarithmic. Other possible functions could be exponential ($R^2 = 0.98$) and/or power ($R^2 = 0.90$).

Conclusions

The value of zinc diffusion coefficient in steel strongly depends on silicon content in steel; the relationship could be quantitatively described by equation $D = -7.10^{-17}$ ln [Si] + 4.10^{-17}. The growth of interfacial diffusion layer mostly follows the parabolic dependence, with power coefficient of 0.48–0.64, except the case of steel 12 010 (0.42 pct. Si), where the relationship seems to be almost linear (power coefficient 0.91). This result suggests the possibility of different diffusion micromechanism of zinc in steel of particular composition with given content of silicon.

REFERENCES

1. Trčka J., Fiala J., Bucherová L.: Chem. Listy, Symposia, *96*, 221 (2002).
2. Kubaschewski O., Massalski T., editors: *Binary alloy phase diagrams*. Metals Park OH. ASM, 1986, p. 1128.
3. Marder A. R.: The metallurgy of zinc-coated steel, Progress in materials science *45*, 191 (2000).
4. Thomas R., Wallin T.: *Protikorozní ochrana žárovým zinkováním*, AČZ, Prague, 1998.

5. Sandelin R. W.: Wire and Wire products, *15*, 655 (1940).
6. Zmrzlý M., Fiala J.: *Corrosion protection of steel by diffusion zinc coating*, Proceedings of JUNIORMAT 01, FSI VUT Brno 2001, p. 99.
7. Bojda O., Zmrzlý M., Fiala J.: *Steel substrate´s effect on the properties of diffusion zinc coating*, Proceedings of Juniormat 03, FSI VUT Brno. 2003, p. 38.

P35 FRACTURE BEHAVIOUR OF FRACTIONATED PE RESIN

LENKA DIVIŠOVÁ[a] and EVA NEZBEDOVÁ[b]
[a]*Institute of Materials Chemistry, Faculty of Chemistry, Brno University of Technology, Purkyňova 118, 612 00 Brno, Czech Republic, divisova-l@fch.vutbr.cz,* [b]*Polymer Institute Ltd. Brno, Tkalcovská 2, 656 49 Brno, Czech Republic*

PE materials for pipes application break after long time due to the small crack growth (SCG). That is a reason for measurement this limiting state for materials using in the field of water and gas distribution, respectively. Now days there are two laboratory methods, which enable to estimate the resistance against slow crack growth SCG: (i) PENT test – ISO/CD 16241 and (ii) FNCT test – ISO 16770. These tests were used for studies of various pipes materials. It is well known that mechanical response strong depends on the structure of materials, especially for PE materials that are the density of short chain branches and its distribution. Brown and his co-workers[1] confirmed the correlation between the results of PENT and SCB (Fig. 1.). As the results of PENT test the time to rupture (t_f) was estimated.

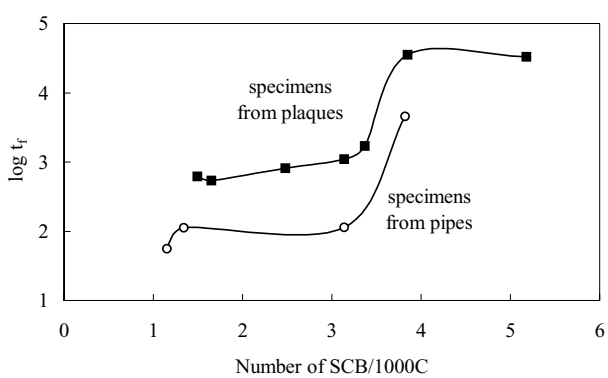

Fig. 1. **Correlation between the SCB and time to fracture for butene copolymers PE**

Nezbedová and her co-workers[2] published the similar results. For estimation the SCB the SIS/DSC technique (Stepwise Isothermal Segregation) was used. Scholtten[3] and also Brown[4] used temperature-rising elution fractionation (TREF) technique for fractionation difference types of ethylene copolymer and estimation the distribution of short chain branching (SCBD). It seemed that placing the chains on the high molecular weight molecules (SCBD) could change the resistance against SCG. To confirm this statement some PENT or FNCT had to be carried out. The problem was that for preparing the PENT or FNCT specimens the amount of material is about 200 g and the amount of fractionated material is only about 0.2 g. This problem can be solved by using so called sandwich specimen. Brown[4] suggested one type of a sandwiched specimen (Fig. 2.).

A gas pipe grade PE with a good resistance to SCG was used as the PE grips. It was suggested that, with the molecular weight distribution that exists in this particular polymer,

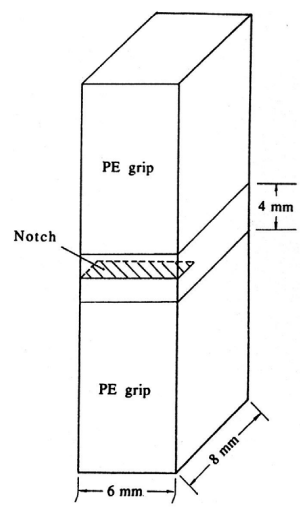

Fig. 2. **Geometry of test specimens. The zone containing the notch consists of about 0.2 g of fractionated resin**

Table I
Typical properties of MB 62 and FB 10

Property	Unit	Typical value MB 62	FB 10	Test method
Melt Flow Rate (190/2,16)	g/10 min	6	0.1	ISO 1133
Melt Flow Rate (190/5)	g/10 min	20	0.55	ISO 1133
Density	kg m^{-3}	960	942	ISO 1183
Yield Stress	MPa	24	22	ISO 527
Tensile Strain at Yield	%	10	6.5	ISO 527
Flexural Modulus	MPa	1100	800	ISO 178
Charpy Notched Impact strenght 23 °C	kJ m^{-2}	6.3	12	ISO 179
Shore Hardness		58	119	ISO 868
Vicat Softening Temperature	°C	122	57	ISO 306

the SCB could be reduced from 4.5 to about 2 SCB/1000C and the resistance to SCG will be excellent if practically all the branches were on $M_W > 1.5 \cdot 10^5$.

We utilised this procedure for preparation similar specimens. As a grip we have used PE 100 material. Two type of polyethylene from Czech Chemical Company (Litvínov) marked as MB 62 and FB 10 were tested. Typical properties are summarised in Table I.

The kinetics of the failure process was observed under a constant nominal stress of 1 MPa and temperature 80 °C. The crack opening displacement, COD, was measured with an optical microscope. The COD was viewed in the middle of the notch and measured at the surface of the specimen. The error of the measurement of the COD was about 2 μm.

For each material a minimum of two specimens were tested. Typical data for brittle fracture are presented in Fig. 3., where the COD is plotted against log (time).

The time to complete fracture (t_f) of MB 62 was 171 min and of FB 10 was 732 min, respectively.

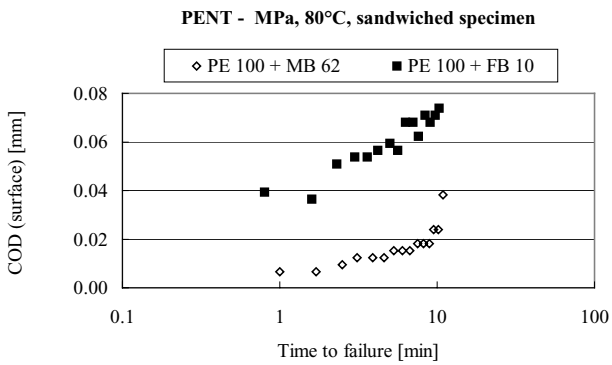

Fig. 3. **Fracture behaviour of two PE matrix**

The results can be summarised in the following way:
Since the diffuse at the interfaced on moulding is very dependent on molecular weight the proper grip resin must be chosen.
The results confirmed the possibility of testing a small amount of material in the similar way as for classical SEN specimen.

The sandwiched type of specimen becomes very imported for study the influence of each fraction on the resistance against SCG. On the other hand those results enable tailoring of material.

The authors gratefully acknowledge the support for this work provided by the Grant Agency of Czech Republic; contract No 1001/05/0227.

REFERENCES

1. Brown N. and Xici Lu: Polym. Eng. Sci., *41*, 1145 (2001).
2. Nezbedová E., Zahradníčková A., Salajka Z.: J. Macromol. Sci.-Physics *B40*, 507 (2001).
3. Scholten F. L. and Rijpkema H. J. M., Proceedings of Plastics Pipes VIII, The plastic and Rubber Indy., London, 1992, C2/4.
4. Xici Lu, Narumi Ishikawa, Brown Norman, J. Polym. Sci. Part B: Polymer Phys. *34*, 1809 (1996).

P36 DETERMINATION OF THE POLYPROPYLENE FIBRES CROSS-SECTION USING OPTICAL MICROSCOPE

IVANA PILÁTOVÁ, LUKÁŠ RICHTERA
and JIŘÍ DVOŘÁK
Faculty of Chemistry, Brno University of Technology, Purkyňova 118, 612 00 Brno, Czech Republic, pilatova@fch.vutbr.cz

Introduction

The growing trend of polypropylene (PP) fibres using for knitting with advantageous properties is noticeable recently. The PP fibres are indifferent to microbes and mildews and are very tolerant to human skin. Wide range of these required properties is possible to modify by fibre cross-section shape changing. In addition to fibres with circular or elliptical cross-section the fibres with trilobal, cross or pentalobal cross-sections are commonly used nowadays. Larger surface of fibres with non circular or non elliptical cross-sections has favourable wetness draining from human skin and better permeability.

The optical microscope is used in practise for fibre cross-section shape determination, the scanning electron microscope (SEM) enables to reach higher resolution possibility and allows to determine other geometrical properties, e.g. the cross-section diameter. Fixation of fibre in tough matrix is usually used to minimize the possibility of fibres damage (Fig. 1., 2.). The microtome is used to cut thin slices from prepared samples. Unfortunately, many of smaller laboratories do not posses of this quite expensive equipment. This study is aimed to use common laboratory equipment like grinder, optical microscope and digital camera for successful solving of this problem and for low-cost, time and instrumental less demanding but sufficient sample preparation.

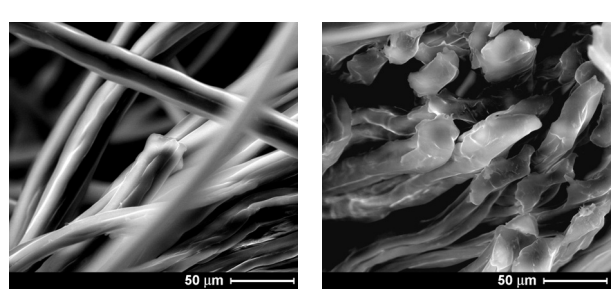

Fig. 1. **Free pentalobal PP fibres (SEM): a) side view, b) front view (deformation of ends after the cut)**

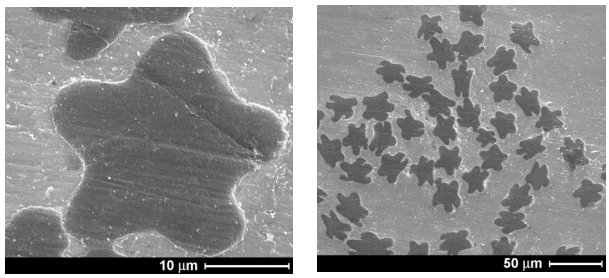

Fig. 2. **Pentalobal PP fibres in matrix (SEM): a) one fibre (magnification 8000×), b) a bundle (magnification 1000×)**

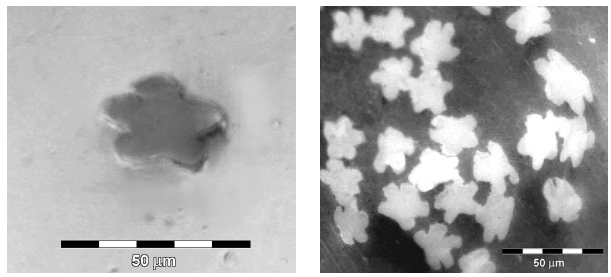

Fig. 4. **Pentalobal PP fibres in matrix (optical microscope, magnification 400×): a) one fibre, b) a bundle**

Experimental

For this purpose the PP fibres from commercial knitting with known pentalobal cross-section shape were used. To minimize the possibility of fibres damage, fixation of fibre in polyester resin was applied. The samples were prepared in two different ways – using the etching technique or abrading. In respect to considerable resistance of PP fibres towards acid, alkali, reducing or oxidizing agents, boiling xylene was used for etching the fibres. However this method was not very useful, xylene etched not only PP fibres, but damaged slightly the resin surface too, and the fibre cross-section was difficult to observe. For that reason further examination was directed only to abrading the samples on metallographic grinder. The surface of the sample was polished to high shine with commercially accessible means. For the high quality of digital photographs and non damaged edges on the cross-section of fibres the thorough polishing is necessary.

Results

The cross-section of fibres was examined with metallographic microscope Neophot 21 with maximal possible magnification 1000× which allows to determine the cross-section diameter comfortably. Photographs of cross-section were taken with digital camera Olympus C-3000Z with optical extension in the magnification of 500× and 1000× on metallographic microscope (Fig. 3.). Optical microscope Olympus BX-50 (maximal magnification 400×) with digital camera Olympus C-4040Z and with optical extension connected to PC with image analysis was successfully used too (Fig. 4.).

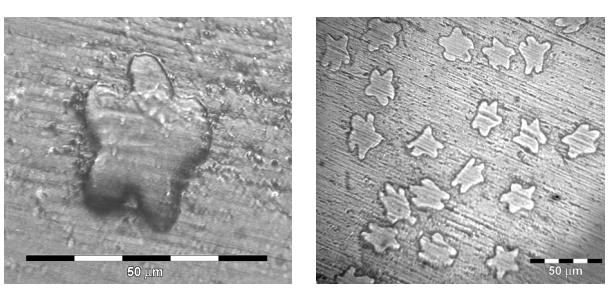

Fig. 3. **Pentalobal PP fibres in matrix (metallographic microscope): a) one fibre (magnification 1000×), b) a bundle (magnification 500×)**

Conclusion

Using easily accessible technique (grinder, optical microscope and digital camera) not only the shape of cross-section was determined but it was possible to determine the cross-section diameter of PP fibres without any problems too (see the figures). This method may be considered as sufficient for full resolving of this problem and a possibility of use of this technique for other textile fibres can be assumed.

REFERENCES

1. Murárová A., Jambrich M., Balogová A.: Vlákna a textil (Fibres & Textiles) *11*, 3 (2004).
2. Kudláček L., Růžička J.: *Struktura a vlastnosti textilních vláken, II. díl*. Skripta VŠCHT, Pardubice 1980.
3. IN 21-108-01/01: *Stanovení geometrických vlastností vláken*. FT TU Liberec.
4. IN 46-108-01/01: *Doporučený postup tvorby příčných řezů*. FT TU Liberec.

P37 METHODS OF HYDRATION OF CEMENTS BASED ON MDF COMPOSITES STOPPING

FRANTIŠEK ŠOUKAL and JAROMÍR HAVLICA
Department of Materials Engineering, Faculty of Chemistry, BUT, Purkyňova 118, 612 00 Brno, Czech Republic, soukal@fch.vutbr.cz

The objective of this work is to study on development of macrodefect-free composites (MDF) structure during hydration. It means composites of water-soluble polymer and cement, which are characterized by extremely low porosity and atypical mechanical properties. The polymer is added into mixture to improve some mechanical properties, especially flexural strength and impact resistance. For example the flexural strength is at least by one period higher than that of ordinary portland cement.

Introduction

Monitoring of the kinetics of MDF composites hydration process according to phase composition requires reactions stopping and evaluation of actual phase composition. Generally there are several ways to stop the hydration of cementitious systems, which may be divided into physical and chemical techniques.

The physical methods lie in water removal from reaction system. It can be done by sample repulping with acetone or ethanol in case of azeotrope composition with 4 % of water is sufficient. According to the water content, methanol is more suitable. On the other hand there are complications with its toxicity and following controlled manipulation. The repulping induces flush of free, unbounded water from the mixture. The water which has participated in hydration is maintained in the solid phase of system in form of hydrates.

There is another variant applicable to stop the hydration process which is drying material in hot-air drier or vacuum desiccator. This method can be used only in case of the long--term increase of temperature do not have kinetics influence. The long term of drying, when the sample is exposed to temperatures about 110 °C in presence of slowly evaporating water, can considerably affect the hydration kinetics.

An alternative of the samples freezing assume hydration process retardation by undercooling to temperatures about –30 °C, when present free water changes into solid state. This strongly retard diffusion processes in the system. But the undercooled sample has damaged macro-structure.

Chemical alternative of hydration stoppage may be an addition of stabilizing or retarding agent. These chemical compounds slow down or stop hydration reactions, but the chemical and phase constitution is disturbed.

The last and furthermore discussed technique is the microwave heating. The principal of this method is similar to hot-air drying, but it is more effective. The sample is heated up in all his volume in the same time and the water is evaporated rapidly faster. Temperature of the sample reaches to 110 °C and most of free water is evaporated through several ten of minutes.

Experimental

Stopping of hydration by microwave heating was chosen for purposes of this work. It was necessary to compare the novel method with an authentic one, then acetone repulping. Therefore an analysis of two parallel made samples of portland cement and water mixture with water ratio w/c = 0.33 was done. Hydration of these samples was stopped in the same stage partly by acetone p. a. repulping and partly by microwave heating. To make better in pores water diffusion, the sample was placed on watch glass in thin layer. The power output of microwave oven was adjusted at 900 W and the sample was heated for 180 s.

Acquired samples were put to x-ray powder diffraction analysis (XRD), termogravimetric analysis (TGA) and differential scanning calorimetry (DSC). XRD was accomplished with diffractometer Philips with copper cathode and monochromator in the range from 0 °2Θ to 120 °2Θ. Chiefly basic portland clinker mineral such as C_3S, C_2S, C_4AF, $CaSO_4 . 2H_2O$ and ettringit were studied. TA Instruments DSC 2920 calorimeter was used for purposes of thermal analysis and the termogravimetric analysis was accomplished with Perkin Elmer TGA 6.

Results and discussion

The X-ray spectrum in Fig. 1. represents sample of PC where the hydration processes were stopped 25 minutes after PC with water mixing with acetone repulping. Monochromator wasn't used within the measurement; therefore the spectrum has natural background. An occurrence of C_3S, C_2S, ettringite and gypsum is apparent. The Fig. 2. stands for spectrum of the acetone repulped sample whose hydration was stopped 60 minutes after mixing and Fig. 3. represents the same sample stopped with microwave heating. If compared spectra of Fig. 1. and Fig. 2., an apparent difference of diffraction intensity at 61 °2Θ, resp. 52 °2Θ can be observed. This diffraction is superposition of C_3S and gypsum diffractions. Comparison shows that when hydration time increases a small decrease of C_3S content is observed. The change gypsum content is more significant. Sample after 25 minutes of hydration is characterized by higher water content, resp. solution content, where the gypsum is mostly solute. With increasing time of hydration free water is consumed by hydration reactions and liquid phase content decreases which leads to gradual gypsum recrystallization. Acetone repulping flushes the solution within the solute gypsum. Therefore the gypsum

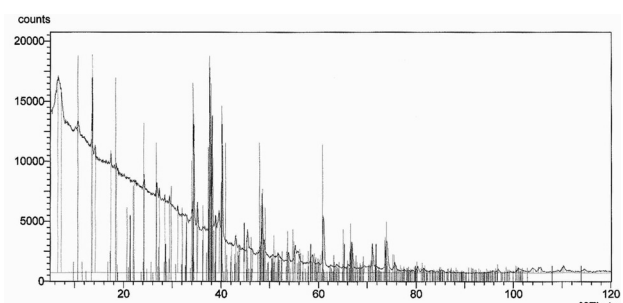

Fig. 1. **XRD spectrum of acetone repulped sample after 25 min. of hydration**

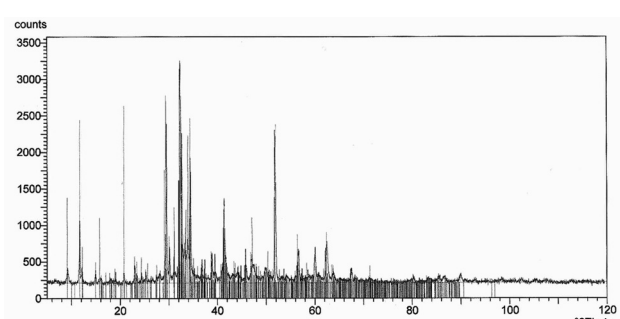

Fig. 2. **XRD spectrum of acetone repulped sample after 60 min. of hydration**

diffraction is higher in spectrum in Fig. 2. than that one in Fig. 1. The samples, where the hydration was stopped with microwave heating, shows the possibility of evaluation of calcium silicates content decrease compared with the initial sample. The lower gypsum diffraction effect was caused by fast dehydration to hemihydrate when temperature increased more above 110 °C after all free water evaporation.

Differential scanning calorimetry results are put on the following figures. The analysis was done with the same samples, where hydration was stopped by acetone repulping after 35 minutes (Fig. 4.), resp. 120 minutes (Fig. 5.) and by microwave heating after 120 minutes of hydration (Fig. 6.). As supposed almost no free water is present in the samples. Primary decrease represents output heat of residual free water evaporation. Then we can observe endothermic effects belonging to ettringite germs disintegration starting about 60 °C following by dehydration of gypsum with generation of calcium sulfate hemihydrate, which dehydrates about 250 °C. Portlandite disintegration endothermic effect was recorded about 600 °C. If compared acetone repulped and microwave heated samples, it shows that microwave heating particularly removed water from calcium sulfate dihydrate.

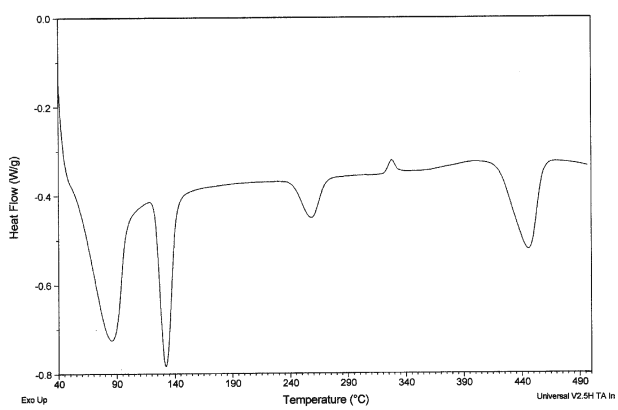

Fig. 4. **DSC record of acetone repulped sample after 35 min. of hydration**

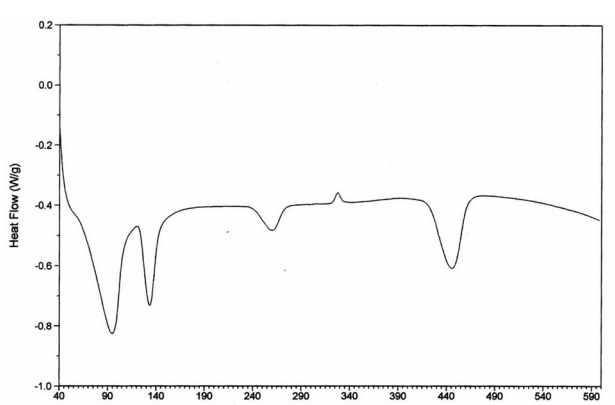

Fig. 5. **DSC record of acetone repulped sample after 120 min. of hydration**

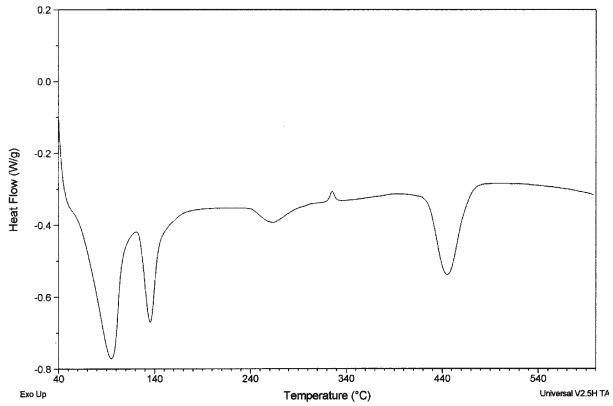

Fig. 6. **DSC record of microwave heated sample after 120 min of hydration**

Conclusion

Both X-ray powder diffraction analysis and differential scanning calorimetry supports the possibility of use of microwave heating to stop hydration processes in cementitious materials for requirement of the calcium silicate phases conversion degree with evidence. Hydration stopping by microwave heating is not suitable for systems where some phases disintegrate at relatively low temperatures.